Title

Analyzing Nuclear Paraspeckle-Dependent Protection of Unphosphorylated microRNAs

Author

Read, Graham H

Publication Date

2023

Peer reviewed|Thesis/dissertation

UNIVERSITY OF CALIFORNIA

Los Angeles

Analyzing Nuclear Paraspeckle-Dependent Protection of Unphosphorylated microRNAs

A dissertation submitted in partial satisfaction of the requirements for the degree Doctor of Philosophy in Molecular Biology

by

Graham H. Read

2023

ABSTRACT OF THE DISSERTATION

Analyzing Nuclear Paraspeckle-Dependent Protection of Unphosphorylated microRNAs

by

Graham H. Read

Doctor of Philosophy in Molecular Biology

University of California, Los Angeles, 2023

Professor Joanne B. Weidhaas, Chair

Mature microRNAs (miRNAs) are typically 22-25 nucleotide-long transcripts that broadly coordinate cellular stress responses by modifying the activity of complementary messenger RNAs (mRNAs). In particular, the miRNA hsa-miR-34 is well characterized as a tumour suppressor- its expression modifies the proliferation, metastasis, and apoptotic responses of cancer cells, and it is both upregulated by the key tumour suppressor p53 after ionizing radiation (IR) and downregulating factors that downregulate p53, resulting in a radiation-responsive feedback loop. *De novo* miRNA production starts by transcribing longer, capped and polyadenylated transcripts before cleavage in the nucleus, export to the cytoplasm, and a second round of processing resulting in the mature-length transcript with a 5' phosphate, which is required for both the activity and stability of mature miRNAs- consequently, mature miR-34 derived from *de novo* transcription and processing is typically observed approximately 6h after IR. However, prior research from our lab has identified a stable population of 5' unphosphorylated miR-34a, which is rapidly phosphorylated in response to IR, resulting in miR-34 activity prior to and independent of *de novo* transcription. Since the 5' phosphate is important

for the stability of mature miRNAs, this work aims to investigate mechanisms responsible for stabilizing and coordinating this unphosphorylated pool of miR-34.

Mass spectrometry of probable interacting partners of unphosphorylated miR-34 identify nuclear paraspeckles as a likely reservoir for unphosphorylated miR-34. Paraspeckles are nuclear subcompartments comprised of several key proteins crosslinked to the long noncoding RNA (lncRNA) NEAT1_2, creating a phase separation that prevents mixing of internal compartments with the rest of the nucleoplasm. We hypothesize that this phase separation maintains the unphosphorylated pool by preventing its interaction with cellular factors responsible for degrading RNAs. This result would align well with prior studies of paraspeckle function, which have been implicated in DNA repair responses and processing of some miRNAs

To study the role of phase separation on the stability and coordination of unphosphorylated miR-34a, we generated Cas9-mediated deletions of the triple helix domain of NEAT1_2, which is required for phase separation. Accordingly, ablation of paraspeckle formation by this method decreased the activity of miR-34 shortly after irradiation without affecting unrelated miRNA species or *de novo* miR-34 transcription or processing. Similarly, cells with intact paraspeckles demonstrate punctate nuclear localization of miR-34a but not other miRNAs, which is lost on deletion of nuclear paraspeckles. Interestingly, contrary to prior reports that IR induces the rapid phosphorylation and cytoplasmic relocalization of unphosphorylated miR-34, IR increased the number of nuclear miR-34 foci observed in both wildtype and paraspeckle-knockdown cells, with no change in nuclear localization of other miRNAs. Reverse transcriptase quantitative polymerase chain reaction of the processing intermediates of miR-34 in irradiated cells implies that these nuclear foci are likely newly-transcribed, p53-dependent pri-miR-34.

These results demonstrate that nuclear paraspeckles interact with unphosphorylated miR-34 mimics and are required for the IR-responsive activity and nuclear localization of the unphosphorylated pool. These results did not extend to other miRNA species shown to lack

unphosphorylated pools, implying a distinct mechanism for regulating miRNA activity and localization. Future work investigating miRNA activity within and around the paraspeckle may reveal novel unphosphorylated miRNAs and mechanisms

The dissertation of Graham H. Read is approved.

Kathrin Plath

Frank Slack

Hilary Ann Coller

Feng Guo

Joanne B. Weidhaas, Committee Chair

University of California, Los Angeles

2023

TABLE OF CONTENTS

ACKNOWLEDGEMENTS

The most important skill a young scientist can learn is the ability to cultivate multiple mentors, personally and professionally- a team of people engaged in the work of training and directing energies in productive directions. I have been fortunate enough to take my academic training in several of those directions, and I am grateful to my many mentors throughout this journey both for their capable guidance and for their willingness to accept my position as a scientist comprehensively. That is to say that this thesis represents not only my doctoral work, but also the time and energy that I and my mentors have put into the entire academic space since I first forayed into research.

I will always be grateful to my first ever research mentor, Professor Mahiri Mwita, of the Princeton Institute for International and Regional Studies. Mwalimu Mwita was willing to take an eighteen-year-old with a shaky grasp on a foreign language halfway around the world and give him enough space to shape a project that both parties cared for deeply. I went into research feeling wholly unprepared in as many ways as it was possible to be unprepared- I had traveled far, felt like I knew little, and was working in subjects that I was excited about but did not feel expert in, working closely with people who I felt had much better knowledge of customs and situations than I had myself. Despite this pressure, Mwalimu Mwita consistently encouraged me to thrive in that discomfort, and refused to dictate exact shapes to our work engaging local communities with educational public health measures. I realized from this experience the profound power of controlled discomfort in an academic space- by recognizing that research spaces are made of people from diverse backgrounds with diverse knowledge, opinions, and experiences, I realized that creation of knowledge is a highly social

process- even when I was ostensibly “leading” a project, I could increase my creativity and productivity by being willing to admit my own position and let others invested in the project move as they saw fit. Ingawa sijarudi pale kwa miaka mingi sana, mimi mwenye majivuno kwamba nchi na watu pale bado wana mahali pa ajabu sana moyoni kwangu, na namshukuru sana Mwalimu na watu wengi wote pale (k.m Fikeni Senkoro, Odu, Liyala, n.k) wameofundisha kuwa mtu anayejua maana ya kupata nguvu ndani ya hofu.

I had the distinct privilege later in my undergraduate career of being trained by a first-rate mentor in Jane Flint, who has continued to aid my scientific journey throughout my career. Again, she was willing to give me considerable slack despite my inexperience- my undergraduate thesis was technically difficult, and those techniques were largely hammered out through a combination of repetition and introspection. Given the complexity of molecular biology, it would have been easy to churn fruitlessly- I am endlessly thankful for Professor Flint’s mentorship, which ably taught me how to take a step back and re-evaluate the pieces of what I was doing. This led directly to the first time I felt like a “real” scientist- I had spent quite some time optimizing a particularly tricky protein purification, when the box holding my Western blot lost power halfway through the run. Since she had taught me to understand the basis of how my experiments worked, I was able to troubleshoot quickly- the buffer was correct, both in composition and temperature. The rig stopped halfway through, so the plates must be fine- the issue was in the rig itself. Borrowing a soldering iron from a friend in Engineering, I repaired the wire running along the bottom of the rig that connects the diodes, which restored current to my gel. The resulting data nearly worked- I was left with an important step towards optimization, bands with a curious jerk in the middle, and

the confidence that I actually knew what I was doing in the lab. I would not be the scientist I am today without the skills and disposition I learned from Professor Flint during my undergraduate years.

I don't think I could possibly write words sufficient to thank Aparna Kesarwala for her sustained efforts in guiding my scientific journey. My time in the Kesarwala lab fully transformed me from somebody who felt like I was expected to consume and reproduce information to somebody who was supposed to produce information- a scientist in my own right. This came in large part through Dr. Kesarwala's sustained and capable efforts. I am endlessly thankful for Aparna's willingness to let me explore- I felt and believed that I was supposed to build expertise in the subjects I studied, with my progress aptly guided in productive directions. More than productivity, I also learned that science is done in a community. The few "friendly introverts" who comprised that small group at the NIH remain close friends and scientific advisors, and I thank both Aparna and the rest of the Kesarwala lab for their fundamental work in shaping my scientific identity.

My graduate studies have been capably stewarded by Joanne Weidhaas and the team at the Weidhaas Lab, spanning both the immediate lab space and her broader collaborations. I am thankful that my insistence on picking a project somewhat against the grain of the usual lab's work characterizing miRNA-related single nucleotide polymorphisms was met with enthusiasm and support. I extend my warmest thanks to my PI. This work also could not have begun without the help of David Salzman, a former postdoc in the lab whose work uncovered unphosphorylated miR-34 and whose input helped guide the project substantially. I am also endlessly grateful for the constant

help of Emily Rietdorf, both in her capacity as lab manager keeping the project well supplied and for her considerable effort in making the lab a welcoming workplace. I am also thankful for the continued and valuable efforts of my entire thesis committee, whose expertise in diverse fields and commitment to mentorship proved invaluable in the development of complicated projects.

Much as I have been guided by excellent mentors, I have also been privileged to have excellent mentees. There is something especially powerful about helping somebody else achieve their goals, and I am thankful for the considerable brainpower and significant hours contributed to this project by the many undergraduates who have worked on this project alongside me. Above all else, I am proud of how well this project served as something in which the students could find agency- mentees in this lab have had diverse interests and goals for their future, and we have done a capable job designing projects that are both interesting to all parties and good training for their futures. I extend both my sincerest thanks and my most fervent hopes for a strong future to Cynthia Tsang, Ihsan Turk, Ethan Pak, Swetha Ampabathina, Lubna Abdulrahman, Sabrina Chriqui, Jennifer Lathrop, Tiffany Yang, and Hanny Issawi.

My identity as a scientist has been one of an educator as much as a researcher- to this end, I am extraordinarily grateful for the many resources at UCLA that have developed me on both fronts. Firstly, the professors who helped me through my TAships- Amander Clark, Nat Prunet, and Hilary Coller, both for their guidance and their willingness to give flexibility in instructional design. This flexibility was potentiated well by an excellent program in TA training at UCLA, which both taught me how to feel confident in the classroom and gave me a structure to develop my personal pedagogy-

a method of TA training which later became a significant part of my own career as I progressed into teaching that same TA training class. Lastly, I have been grateful for UCLA's vibrant ecosystem for education research, which, while outside the scope of this dissertation, occupies a significant part of my current and ongoing research interests. I am endlessly grateful to my many mentors in education research, including Rachel Kennison, Katie Dixie, Leigh Harris, Rachel Prunier, K. Supriya, and the wider CIRTL community. I would also like to thank my "students" in Teaching-as-Research-exceptional TAs from departments around campus whose significant experience and insight into their own teaching informed much of my own development as a teacher and provided me with the means and confidence to pursue education research.

Considerable thanks during this project must also go to an unidentified attendee of the 2019 Keystone Symposium on Biomolecular Condensates and RNA-Protein interactions, who correctly identified the strong enrichment of nuclear paraspeckle proteins in our mass spectrometry dataset. This serves as an ample testament to the power of collaboration and collegiality in advancing science, since neither I nor my direct coworkers had even heard of paraspeckles prior to this moment. My thanks, both to this stranger and to the organizers for planning a joint meeting that placed the relevant expertise in the proper place. We would not easily have shifted paradigms away from direct RNA-protein interactions without this critical support.

All of this is a very long way to say that a scientific journey is not just made of data and pipettes- science is done by scientists, and it's much easier to figure out where you want to go with a more complete sense of who you are. Many people have taught me many valuable things, but the most precious contributions I have received have

been the ones that taught me how to walk the world like myself- to meet challenges ably, reconsider orthodoxies, consider the community, and emerge from these trials more like myself than I was when I entered. None of this is possible without sustained effort and a willingness to persist, and I am endlessly grateful to the many people who have walked with me.

The work presented here was made possible by the generous and timely support of the California Tobacco Related Diseases Research Program, which funded the project from 2019-2022. I am grateful to the program and its officers, both for their funding of the work and for their constructive feedback during review periods.

VITA

EDUCATION

University of California, Los Angeles, Los Angeles, CA September 2017 - Present
PhD Candidate — Gene Regulation, Epigenomics, and Transcriptomics
Adviser: Joanne Weidhaas, MD, PhD, MSM

Princeton University, Princeton, NJ September 2011 - June 2015
A.B. — Molecular Biology
Adviser: S. Jane Flint, PhD, Emeritus Professor
Senior Thesis: Substrate Identification of the Adenovirus E3 Ubiquitin Ligase

RESEARCH EXPERIENCE

Weidhaas Lab, UCLA June 2018 - Present
PhD Candidate

Kesarwala Lab, National Institutes of Health September 2015 - September 2017
Postbaccalaureate Cancer Research Training Award Fellow

Flint Lab, Princeton, NJ April 2014 - June 2015
Undergraduate Senior Thesis

TEACHING EXPERIENCE

University of California, Los Angeles

John-Eiserling-Lengyel Teaching Excellence Award	September 2021
GRAD PD 496B: Teaching as Research	Winter 2021
LS 495: Preparation for College Level Teaching in the Life Sciences	Fall 2020
MCDB 165a: Molecular Biology of the Cell	Fall 2019, Spring 2020
MCDB 144: Molecular Biology of Cellular Processes	Fall 2018

Princeton University

APC 151: Problem Solving in Mathematics	June - August 2014
POL 245: Visualizing Data	June - August 2013

PROFESSIONAL EXPERIENCE

UCLA Department of Life Sciences September 2020 – December 2021
Teaching Assistant Consultant

UCLA Undergraduate Research Center June 2019 – September 2023
Graduate Research Mentor

UCLA Department of Molecular, Cell and Developmental Biology September 2018-June 2020

Teaching Assistant

Freshman Scholars Institute QuantLab June-August 2013, 2014

LEADERSHIP EXPERIENCE

UCLA Biosciences Student Advisory Committee June 2018 - Present
Mental Health Subcommittee

UCLA Biosciences Diversity, Equity and Inclusion (DEI) Committee August 2020- Present

FUNDING AWARDED

Tobacco Related Diseases Research Program Predoctoral Fellowship (T30DT0811)
2019-2022

NIH T32 Training Grant (#CA009056) (Declined)
2019-2020
Tumor Cell Biology Training Program

Publications:

Lewis BL, Supriya K, **Read GH**, Ingraham-Dixie KL, Kennison R, Friscia AR. Effects of Popular Science Writing Instruction on General Education Student Attitudes Towards Science: A Case Study in Astronomy. *Astronomy Education Journal*, 2023 August 5. https://doi.org/10.32374/AEJ.2023.3.1.049ra

Gunatilaka AB, Marco N, **Read GH**, Sweeney M, Regan G, Tsang C, Abdulrahman L, Ampabathina S, Spindler A, Lu SS, Schink E, Gatti R, Ingersoll C, Telesca D, Weidhaas JB. Viral burden and clearance in asymptomatic COVID-19 Patients, *Open Forum Infectious Diseases*, 2022 Mar 14. doi:10.1093/ofid/ofac126.

Read GH, Miura N, Carter JL, Kines KT, Yamamoto K, Devasahayam N, Cheng JY, Camphausen KA, Krishna MC, Kesarwala AH. Three-dimensional alginate hydrogels for radiobiological and metabolic studies of cancer cells. Colloids Surf B Biointerfaces. 2018 Nov 1;171:197-204. doi: 10.1016/j.colsurfb.2018.06.018. Epub 2018 Jun 18. PMID: 30031304; PMCID: PMC6261367.

Reviews:

Read GH*, Bailleul J*, Vlashi E, Kesarwala AH. Metabolic response to radiation therapy in cancer. Mol Carcinog. 2021 Dec 27. doi: 10.1002/mc.23379. Epub ahead of print. PMID: 34961986.

Malhotra P*, **Read GH*,** Weidhaas JB. Breast Cancer and miR-SNPs: The Importance of miR Germ-Line Genetics. Noncoding RNA. 2019 Mar 20;5(1):27. doi: 10.3390/ncrna5010027. PMID: 30897768; PMCID: PMC6468861.

*These authors contributed equally to this work.

Chapter 1: Introduction

Radiation Biology, miRNA Regulation, and Liquid-Liquid Phase Separation

Introduction

MiRNAs have been widely studied in cancer and stress responses for their ability to downregulate specific transcripts and transcriptional programs [1, 2]. Notably, miR-34 regulates DNA repair and apoptosis in irradiated cancer cells, and is strongly upregulated after ionizing radiation (IR) in a p53-dependent manner [3, 4], regulating DNA repair [5, 6] and apoptosis [7]. Uniquely among miRNAs, hsa-miR-34 maintains a stable pool of fully-processed miRNA lacking a 5' phosphate in the nucleus of lung cancer cells [8], even though the 5' phosphate is necessary for Ago2-mediated stabilization[9],[10] and targeting to downregulated mRNAs .. This unphosphorylated miR-34 pool is rapidly phosphorylated shortly after irradiation, resulting in measurable miR-34 activity and Ago2 loading [8]. While our prior research has shown that the unphosphorylated pool is inactive before IR, its inability to bind Ago2 implies a novel mechanism for stabilizing fully-processed, unphosphorylated miR-34.

This chapter will summarize the relevant background in radiation biology, miRNA biology, and the stress responses relevant to studies of unphosphorylated miR-34. Since prior literature on unphosphorylated miRNAs is scarce[8], much of this information will talk about the dynamics of miRNAs and their related stress responses, paired with hypotheses about the functional relevance of unphosphorylated miRNAs.

Anatomy of a microRNA

MicroRNAs (miRNAs) are ~20-25nt-long RNA transcripts implicated in downregulation of specific messenger RNA (mRNA) transcripts. While predictive algorithms often incorporate binding from flanking base pairs during target prediction

[11, 12], the main determinant of specificity appears to be governed by nucleotides 2-8 from the 5' end of a mature miRNA that form a seed sequence that base pairs with perfect or near-perfect complementarity with regulatory sites on target RNAs, most often in the 3'UTR of those mRNAs[11, 13]. Prior to Ago2 binding, mature miRNAs exist as a duplex with a passenger miRNA that may or may not have function, often termed the miR*[14, 15]. The active miRNA may derive from either the 5' or 3' arm of the pre-miRNA, and may also be termed similarly- for the sake of clarity, miR-34a-5p in this work will refer to active miR-34 with a 5' phosphate group, which also happens to be derived from the 5' arm of pre-miR-34a. Much of this work will study unphosphorylated miR-34a, which is the same sequence as miR-34a-5p, but lacks a 5' phosphate group. For this reason, this work will only use "5p" to refer to the chemical composition of the miRNA rather than its origin, with active and passenger miRNAs instead referred to without reference to their origin (e.g. miR-34a and miR-34a*, respectively).

Mature miRNAs carry few chemical modifications- canonical miRNAs possess a 5' phosphate group established during Dicer cleavage[16] that is necessary for Ago2 binding [17, 18]. The 3' end of a mature miRNA contains no chemical modifications- the PAZ domain on Ago2 binds to two overhanging nucleotides directly[19]. Non-templated modifications and additions, largely added to the 3' end of mature miRNAs, may have significant effects on miRNA stability[20-22], and have been implicated in target-directed degradation [23, 24].

Mechanisms of miRNA Turnover and Processing Regulation in Animals

Steady-state populations of miRNAs can be expressed as a balance between miRNA synthesis rates and turnover rates. Processing of miRNAs after transcription by RNA Polymerase II (Pol II) is a two-step process split between the nucleus and cytoplasm and involving a complex array of key proteins interacting with a wide array of cofactors, eventually resulting in fully processed, ~20-25nt long transcripts primarily localized to the cytoplasm. [25, 26].

Since miRNAs are initially transcribed by Pol II, transcriptional regulation of miRNAs by a variety of transcription factors are capable of significantly regulating the expression of miRNAs by controlling the rate of *de novo* transcription. Transcriptional regulation of miR-34, the primary subject of this work, is well characterized- the miR-34 family is transcribed from two separate loci on chromosomes 1 and 11, encoding for miR-34a and miR-34b/c, respectively. This study will focus predominantly on miR-34a, which is widely expressed- miR-34b and c are expressed more specifically in the lungs, brain, and testes [27]. Baseline transcription of miR-34a is low, though individual Ago2-associated miR-34 transcripts may persist for as long as 48h after transcription[28]. *De novo* transcription and processing of miR-34 occurs slowly at baseline in most cell types, but is strongly upregulated after IR, especially in cells expressing p53[29, 30].

Several mechanisms exist to control the stability of transcribed, mature miRNAs, including target-dependent mechanisms and the addition of nontemplated nucleotides to mature transcripts [24, 31, 32]. While tailing and trimming affect miRNA in plants and affect the stability of animal piRNAs and other small RNAs, significant tailing and trimming of animal miRNAs has not been observed[32].

Instead, stability of animal miRNAs is largely a function of the fidelity of Ago2's interactions with the 3' end[24, 33]. A high degree of base pairing past the seed sequence induces steric clashes on the miRNA that can disengage the PAZ domain from the 3' end, exposing the 3' end of the miRNA to solvent. This 3' end can then recruit the E3 ubiquitin ligase ZSWIM8, which polyubiquitinates Ago2 on lysine 493, causing proteasome-mediated degradation of Ago2 via target-directed miRNA degradation (TDMD) [33, 34]. Since TDMD is mediated by the degree of complementarity between the miRNA and the target, the rate of TDMD is a function of both the identity of the miRNA and its complementary transcript- downregulation or knockout of highly-complementary transcripts can prevent ZSWIM8-mediated Ago2 ubiquitination and miRNA turnover [35].

Given the poor half-life of miRNAs that are not bound to Ago2[9, 25], it is plausible that the decreased half-life of miRNAs targeted by this pathway is primarily a function of local loss of Ago2 rather than fundamental changes to the chemistry of the miRNA. Accordingly, this pathway is unlikely to significantly affect the stability of unphosphorylated miRNAs, since interaction with the Ago2 MID domain is mediated by the 5' phosphate of the miRNA[17].

While the turnover rate of mature, Argonaute-bound miRNAs is often on the order of 24-48h[28], several stimuli can induce rapid degradation of target miRNAs[36-38], and loss of Ago2 expression significantly decreases the half-life of many miRNA species [9, 39], implying Ago2 binding is important for the half-life of mature miRNAs. Importantly, Ago2 binding is not the sole determinant of miRNA stability- miRNAs with fast turnover, including miRNA* species, associate with Ago2 prior to induction of their

rapid degradation [39]. Interestingly, studies of rapid miRNA degradation have found subpopulations of mature miRNA that are broadly unaffected by stimuli regulating degradation, implying alternative localization or regulation of specific miRNA subpopulations [40].

The miR-34 Family

miR-34 is a widely studied miRNA with diverse roles in regulating cancer progression and stress response. It is transcribed from two loci, expressing three miRNAs (miR-34a and miR-34 b/c).

Considerable research has demonstrated that miR-34 functions as a tumour suppressor oncomiR, largely due to its interplay with p53[6, 7, 41-43]. In brief, p53 activity transcriptionally upregulates miR-34 expression, and miR-34 itself targets the E3 ubiquitin ligase Mdm2, which is responsible for ubiquitinating and downregulating p53 expression, creating a feedback loop that amplifies both miR-34 and p53 expression [44, 45]. (Figure 1.1). miR-34 also targets several other pathways important to cancer cells, including pathways governing cancer stemness [43], apoptosis [46, 47], epithelial-to-mesenchymal transition[48, 49], cell cycle arrest [30, 50], and DNA repair[46].

Within the miR-34 family, miR-34a is ubiquitously expressed[51] and miR-34b/c are expressed predominantly in lung and testes tissues and tumours [51, 52]. Similarly, miR-34 is expressed in a variety of tumour types, though CpG methylation at the miR-34a promoter often outcompetes p53-dependent expression [53]. Interestingly, ablation and overexpression of miR-34a does not have an identical phenotype to modulation of

miR-34b/c- while the species share seed sequences, only about a fifth of miR-34a targets are also targeted by miR-34b/c [54].

Several studies have characterized the phenotypic effects of miR-34 overexpression or knockout. While deletion of miRNAs is usually phenotypically mild, simultaneous deletion of the entire miR-34 family and related miR-449 family results in aberrant development through cell cycle inhibition, leading to postnatal mortality in mouse models[55]. Accordingly, high baseline expression of miR-34 in tumours correlates with increased patient survival[56].

In terms of cancer biology, miR-34 expression can have significant effects on cancer phenotype. Notably, since miR-34 directly targets several factors involved in epithelial-to-mesenchymal transition (EMT) (e.g. SNAIL1, SLUG, and ZEB2) [57]cells with lower miR-34 expression tend to be more metastatic[58, 59]. Decreased expression of miR-34 similarly promotes apoptosis and senescence, since miR-34 targets direct regulators of apoptosis like Bcl2 [60] and coordinates DNA repair through modulation of p53, Rad51, and p21[60].

Unphosphorylated miR-34

Currently, miR-34 is the only miRNA known to maintain an unphosphorylated, radiation-responsive pool[8]. Following an observation that IR-responsive miR-34 activity often increased prior to *de novo* transcription, Salzman and colleagues hypothesized that a fully processed but inactive pool of miR-34 was being activated by IR, enabling activation of miR-34-dependent stress responses faster than would be allowed by *de novo* transcription and processing[8].

Accordingly, luciferase miRNA activity reporter assays paired with RT-PCR demonstrated an increase in miR-34 activity but not expression shortly after IR, consistent with the activity of a miRNA's dependence on the 5' phosphate, while RT-PCR uses primers that bind to the 3' terminus. Pairing this experiment with 36h-long siRNA-mediated knockdown of Dicer and Drosha revealed that activation of this early responsive pool was independent of *de novo* processing and occurred even in cells without expression of factors necessary for miRNA processing.

To assess the status of the 5' phosphate in the inactive, pre-IR pool, Northern blotting for miR-34 was paired with treatment with the 5' RNA phosphatase CIP. This experiment demonstrated a 1-nucleotide shift in apparent miR-34 weight, consistent with changes to the charge of the molecule imparted by the phosphate group, in cells after IR but not before. Notably, CIP-treated miR-34 migrated at the same mass as pre-IR miR-34, indicating that the inactive pool lacked a 5' phosphate. Similarly, since the 5' phosphate is required for Ago2 loading[17], miR-34 did not pull down with Ago2 before IR, but did afterwards, indicating that this pool is inactive before IR and active shortly after.

Since activation of the unphosphorylated pool seems to occur shortly after IR, the team next investigated the role of stress response pathways often implicated in IR in activating the unphosphorylated pool. Accordingly, cells with siRNA-mediated knockdowns of the master radiation response kinase ATM lost IR-dependent activation of the unphosphorylated pool without a loss of *de novo* p53-dependent transcription. This activation was also shown to be dependent on the RNA-directed kinase hClp1. Interestingly, both of these factors are nuclear, unlike mature miRNAs, which typically

colocalize with Ago2 in the cytoplasm [61, 62]. RT-PCR on fractionated lysates confirmed that the unphosphorylated pool is nuclear before IR, demonstrating a change in miR-34 localization from the nucleus to the cytoplasm after IR.

This work demonstrated the existence of an IR-dependent unphosphorylated pool of miR-34, enabling activation of miR-34 faster than allowed by *de novo* transcription after IR. This pool localizes to the nucleus before IR, where uncharacterized interactions with ATM and hClp1 enable phosphorylation, cytoplasmic localization, and Ago2 loading of miR-34 derived from the unphosphorylated pool. While this study characterized the existence, localization, and activation of the unphosphorylated pool, it did not show how the unphosphorylated pool is synthesized or maintained, nor did it offer specific hypotheses for which ATM-dependent downstream effects were responsible for activation of the unphosphorylated pool.

Radiation and Radiation Therapy

Ionizing radiation causes cellular stress through multiple modalities on different time scales- in light of this, a thorough understanding of the effects of miR-34 activation in irradiated cells over time must be placed in the proper context of the effects of radiation on the cell.

Ionizing Radiation

Ionizing radiation (IR) refers to electromagnetic radiation or subatomic particles that deposit energy sufficient to remove electrons from biologically meaningful structures, most notably DNA and fatty acid chains. Light made of high-energy

ultraviolet radiation, x-rays, and gamma rays are capable of ionizing biological structures, as are particulate sources of radiation such as alpha and beta particles or neutrons (Figure 1.2)

IR damages biological structures through either direct or indirect ionization- in the former, energy is transferred from the radiation source directly into the biological structure- for example, removing electrons directly from a DNA backbone to induce breaks. Direct ionization is typical of “heavier” sources of radiation that deposit energy more frequently, more commonly derived from particulate sources such as alpha particles [63]. By contrast, indirect ionization involves the radiation source interacting with sources of reducing agents, most typically oxygen-containing molecules, in the area around the ionizing event to produce local free radical species [63-65]. These free radical species can then themselves ionize surrounding biomolecules, attacking the phosphate backbone of DNA to both break the strand and induce the formation of bulky adducts that make repair more difficult [66-68]. Similarly, adduct formation generated by different radiation modalities vary, which may have significant effects on the speed and capacity for DNA repair in damaged cells [69].

Cellular Responses to IR

IR generates biologically meaningful damage on multiple biomolecules, most notably DNA and fatty acids. This results in a rapid reconfiguration of cellular phenotypes into a variety of well-characterized stress responses, including changes to many metabolic pathways [70, 71] and engagement of DNA repair pathways[72]. Repair of IR-induced phenotypes fall into multiple distinct phases, with early radiation response

focused on maintaining cell viability and repairing the majority of DNA double strand breaks (DSBs), followed by a protracted period of slower DSB repair and potential activation of senescence or apoptosis pathways[73-75]. A brief summary of the relevant pathways is provided below.

Rates of cell survival after IR vary significantly by cell type, accumulated dose, and environmental conditions [76-78]. Briefly, survival after IR is typically measured using clonogenic assays, which capture both direct cell death and radiation-induced senescence [76, 79]. Under this model, cell survival typically displays a “two-hit” curve, with low radiation doses inducing relatively little cell death per increasing dose. This “shoulder” is largely a function of cellular ability to repair sublethal damage [77, 80]- accordingly, IR-induced cell death increases at a logarithmic rate at higher cell doses, when IR-accumulated damage supersedes cellular capacity for repair[81, 82]

DNA Repair

IR induces both single- and double-strand breaks on nuclear DNA, either by direct or indirect ionization of the DNA backbone, as described above. While IR-induced single strand breaks are numerous[83], efficient and low-error base excision repair (BER) and nucleotide excision repair (NER) pathways[84] tend to mitigate the biological impact of IR-induced single strand breaks relative to the biological damage caused by DSBs.

Two distinct pathways exist to repair double strand breaks- homologous recombination (HR) and nonhomologous end joining (NHEJ). While all cells are capable of utilizing the more error-prone NHEJ pathway, homologous recombination is only

possible for cells with a homology donor chromosome- that is to say, cells that are in the S or G2 phase of the cell cycle, after DNA has already been replicated[85].

Both mechanisms of DNA repair start with recognition of the site of double strand breaks. Early recognition of the sites of DSBs is often performed by the MRN complex, consisting of MRE11, Rad50, and NBS1, which recruit the kinase Ataxia Telangiectasia Mutated [86] to DSB sites [87, 88]. ATM autophosphorylates, enabling phosphorylation of marker proteins (e.g. γ-H2AX and Rad51)[89, 90] responsible for recruitment of DNA repair effector proteins, as well as second messengers responsible for activation of broader DNA repair programs (e.g. Chk1/2)[91-93].

Homologous recombination begins with a presynaptic step in which DNA ends are resected by MRE11 and CtIP to generate ssDNA, which is then coated with Rad51[94, 95]. Recruitment of BRCA1/2 to polymerized Rad51 at the site of a DSB[95]. Exonucleases resect strands at the site of the break to generate flexible overhangs, at which point the homologous strand of an undamaged chromosome is brought in to the site of the double strand break. The donor strand and the overhang strand from the damaged chromosome are both used as templates to synthesize a copy of the damaged region, followed by either resolution of the DNA back into the original chromosome or crossing-over between the donor and recipient chromosome[96]. The newly-replicated strands are then ligated, generating two chromosomes lacking double-strand breaks[97]. The repaired strand will incorporate any DNA present on the donor strand in between the sites of double strand breaks, which may result in gain or loss of content on the damaged strand, depending on the nature of the homology donor- a fact that has been productively leveraged by Cas9-mediated gene editing by providing

homology donors on plasmids incorporating the desired edits, paired with site-specific DSBs specified by the sgRNA used by Cas9[98].

While HR is higher fidelity, the majority of IR-induced DSBs are repaired by NHEJ[99]. Unlike HR, NHEJ does not use DNA around the DSB compared to a homologous template to ensure fidelity to the original sequence- instead, broken DNA ends are resected and ligated together irrespective of sequence[100]. Briefly, DNA around the site of the DSB is bound by KU70/80, a heterodimer that recruits further repair factors[101, 102]. DNA-PKcs and Artemis are recruited by KU- DNA-PKcs acting as a kinase to potentiate repair and Artemis resecting overhanging ends. Once both strands are resected to compatible lengths, the DNA ligase XRCC4 ligates the strands together[103] (Figure 1.3).

The timing of IR-induced DNA damage and repair have significant biological implications, especially in the context of timing of stress responses. Briefly, IR-induced DNA double strand breaks resulting from both direct and indirect ionization happen within nanoseconds[76], with repair complexes forming in less than a minute[73]. The resolution of these repair complexes happens on a variable time scale depending on cellular context, but generally, the majority of double strand breaks resolve within a few hours of damage, with the residual DSBs resolving slowly over hours to days[74].

miR-34 in Radiation Response

Expression of miR-34 has a significant impact on cellular DNA damage repair, both due to its interactions with p53 and its ability to affect expression of DNA repair factors[1]. Since p53 is strongly activated by IR [104, 105] and mIR-34 is both a direct

transcriptional target of p53 and capable of upregulating p53 by inhibition of MDM2, IR strongly induces *de novo* expression of miR-34[106], although IR-dependent upregulation of miR-34 is not entirely p53-dependent[107]. Active miR-34 expression has significant effects on DNA repair- notably, cells expressing miR-34 show fewer markers of DNA damage and increased expression of a broad panel of DNA repair factors[108, 109], consistent with decreased IR-induced apoptosis relative to cells that do not express miR-34. Accordingly, depletion of miR-34 significantly radiosensitizes cancer cells *in vitro* as well as animal models[106], consistent with impaired rapid repair of DNA damage in these systems. Interestingly, several studies have also demonstrated decreased radiosensitivity in miR-34 depleted models[110], or increased radiosensitivity in models overexpressing miR-34[3, 111]. This is likely due to a separation between apoptotic and reproductive cell death- early activity of miR-34 may be especially relevant to promote repair of DNA damage immediately after IR to prevent apoptotic death[3, 112, 113], while inhibition of apoptosis during later repair increases reproductive cell death [107, 109, 114].

Since DNA damage after IR strongly upregulates p53, IR similarly upregulates miR-34 expression shortly after irradiation. Interestingly, this leads to increased radiosensitivity in cells that overexpress miR-34 [111] and cells that underexpress miR-34 [115], through increased vulnerability to apoptotic or reproductive death after IR, respectively. This may imply that the timing of miR-34 signaling is particularly important- studies of the kinetics of DNA repair after IR have shown that the vast majority of lesions repair within four hours after initial challenge [73], with the remaining repair happening slowly until the next cell division [74, 75]. Since radiation-induced apoptotic

death can occur prior to and independent of cell division[116], IR-induced apoptotic cell death is significantly influenced by early DNA repair[75, 117], with reproductive cell death more significantly influenced by DNA repair up to the point of the next cell division[118, 119].

Given the timing of DNA repair and IR-dependent stress responses in irradiated cells, this raises interesting questions about miR-34, which has been shown to have differential effects on radiosensitivity through different pathways[3, 110]. Since miR-34 increases the expression and fidelity of early DNA repair[108, 109], could early expression of active miR-34 prior to *de novo* transcription improve the fidelity of DNA repair shortly after IR, when the majority of lesions are repaired? While the present work does not directly investigate the phenotype imparted by the unphosphorylated pool, future work into how the timing of miR-34 activation affects phenotypes after IR could be an attractive avenue for research.

miR-34 Therapeutics

Given the importance of the miR-34 tumor suppressor network and its notable interactions with p53, significant work has attempted to re-introduce miR-34 into tumours to inhibit cancer cell proliferation. Liposomal introduction of miR-34 (MRX34) proceeded through clinical trials (NCT01829971) and demonstrated significant capacity to regulate target genes after injections [120, 121] but did not progress to Phase II due to adverse events[122].

To have efficacy as an efficient therapeutic agent, a miRNA delivery system needs to have certain characteristics common to other pharmaceuticals- in particular, these therapeutics ought to mitigate side effects (including stimulation of the immune

system), be functional at a concentration amenable to administration, and provide sufficient bioavailability, uptake, and biological half-life to maximize time between doses[123]. These factors are impacted both by the carrier, as discussed above, and by the RNA itself, with recent studies demonstrating increased tolerability and efficacy using chemically modified miR-34 analogues. [124]

Despite these setbacks, several vehicles have shown greater therapeutic utility in recent years. Mrx34, the only therapeutic in this class to have attempted a clinical trial, used anionic lipids to introduce miR-34 to cancer cells [122, 125, 126]. Other studies have similarly investigated the potential of miR-34 transfection with different carriers, including diamond [127] or gold [128] nanocarriers and conjugated folates [129].

Paraspeckle Structure and Function

Paraspeckles are phase separated subnuclear organelles organized by several critical proteins and the long noncoding RNA NEAT1_2 [136, 143], which is itself stabilized by a triple helix motif in lieu of a poly(A) tail [133, 139] (Figure 1.4A). On average, cells have between 5 and 20 paraspeckles per nucleus [144], though it is not clear what factors predict the number of paraspeckles per cell. Notably, levels of NEAT1_2 expression do not predict number of paraspeckles formed- increased NEAT1_2 expression instead causes significant swelling of existing paraspeckles into oblate, “sausagelike” shapes [145, 146]. Both typical and swollen paraspeckles have an average diameter of 500nm-1um[146], determined by the internal structure of the compartment.

NEAT1_2 is made of several distinct domains with important implications in processing and paraspeckle function (Figure 1.4B). While NEAT1_2 is a core structural

component of the paraspeckle, paraspeckles, similar to other phase separations, are largely held together by multivalent interactions involving both the RNA and a set of obligate RNA binding proteins [133, 147, 148]. Both the 5' and 3' end of NEAT1_2 localize to the outermost regions of the paraspeckle, with the middle of the NEAT1_2 transcript forming the core of the paraspeckle [149]. Accordingly, the middle of the NEAT1_2 transcript contains repeat motifs amenable to binding several obligate paraspeckle proteins, in addition to other sites nearer the termini that coordinate RNA binding proteins [150].

Paraspeckle proteins preferentially localize to either the core or shell of the paraspeckle, in addition to distinct patchlike localization throughout the structure (Figure 1.4C) [151]. Notably, while a subset of proteins are required for paraspeckle formation [152], these proteins do not localize exclusively to the paraspeckle, and can often be found in proteomic datasets for other nuclear subcompartments [146, 153], especially since paraspeckles themselves often localize near perinucleolar caps[154]. Likewise, specific RNA subsets localize to paraspeckles- most notably, adenine deamination to inosine by ADAR proteins stimulates paraspeckle localization[155]. Several studies have implicated NEAT1_2 in sponging miRNAs independent of paraspeckle formation[156-158], including one study arguing that NEAT1_2 contains a site complementary to miR-34 in the middle of the transcript that sequesters miR-34[159]. While this work did not investigate deamination of miR-34, nor has previous work on deaminated transcripts retained by paraspeckles investigated miRNAs[155], miR-34 is deaminated by a similar mechanism to the studied mRNAs[160]. Importantly, since phase separations are often organized by multiple weak interactions rather than

distinct motifs, organization of internal contents in phase separations often happens at superstoichiometric levels [161]- while base pairing between NEAT1_2 and miR-34 is plausible, sequestration of miR-34 within paraspeckles need not depend on such sequence-specific interactions.

Paraspeckles have been implicated in several stress responses, including immune activation [162], hypoxia[163], physiological stress in animals[164], and retention of deaminated transcripts[165]. From a miRNA perspective, paraspeckles regulate the processing of several pri-miRNA species by binding the pri-miRNA processing enzyme Drosha [166], though the miRNAs regulated by this mechanism did not include miR-34a. Importantly, phase separation by nuclear paraspeckles prevents mixing of internal components with the rest of the nucleoplasm, likely including RNAses and exosome complexes[167-169], which may provide a mechanism that protects sequestered RNAs from degradation.

Phase Separation and Condensate Formation

Biomolecular condensates are complex, concentration-dependent cellular subcompartments responsible for coordinating diverse cellular chemistry [137]. While several different chemistries can drive biomolecular condensation, shared properties include fusion on contact with other condensates, capacity to wet against membranous surfaces, and the concentration-dependent accumulation of interacting factors into micron-scale, membraneless structures from diffuse solution [137, 168, 169]. While the formation of concentration-dependent phase separations do not preclude the presence of phase-separating chemicals in the dilute phase[170, 171], phase separations have

been shown to prevent biochemical interactions by sequestration of key components within an inaccessible condensed phase[172-174].

In light of paraspeckles' ability to coordinate diverse stress responses and separate internal contents from the rest of the nucleoplasm, we propose that paraspeckles could both sequester unphosphorylated miR-34 and coordinate the chemistry necessary to activate the unphosphorylated pool after IR. The present study will demonstrate that paraspeckles are required for the activity and punctate nuclear localization of unphosphorylated miR-34. Future studies could leverage interactions between paraspeckles, unphosphorylated miRNAs, and radiation stress response pathways to further investigate both paraspeckle-coordinated stress responses and the kinetics of unphosphorylated miRNAs.

Interactions between DNA repair machinery and paraspeckles

Previous work has demonstrated that phosphorylation of unphosphorylated miR-34a is dependent on activation of the master regulator of DNA double strand break repair, Ataxia Telangiectasia Mutated [86]**.** While the present work demonstrates that paraspeckles localize and coordinate the activation of unphosphorylated miR-34a, we have not demonstrated a connection between the unphosphorylated pool's dependency on ATM after IR, nor is an interaction between paraspeckles and ATM present in existing literature. Confirmation that ATM directly or indirectly affects paraspeckle function within a timescale relevant to the proposed mechanism would provide good evidence that paraspeckles not only store unphosphorylated miR-34a, but contribute to its activity and regulation.

ATM is a well-studied kinase responsible for phosphorylating many effectors of double strand break repair after IR [72, 89], including the obligate paraspeckle protein FUS [132, 175]. FUS is phosphorylated at several residues by both ATM and DNA-PKcs, leading to distinct downstream phenotypes[175]. Many of these phosphorylated tyrosines fall within a prionlike domain in FUS, which is required for phase separation [176].

While interactions between ATM and FUS are well established in general, we are not aware of evidence in the literature for interactions between ATM and FUS in the context of the paraspeckle. Furthermore, while FUS has been shown to change the structure of other phase separated condensates [176, 177], there has been comparably little investigation into the role of FUS phosphorylation in maintaining or altering the structure or contents of nuclear paraspeckles. Since paraspeckles have been shown to dynamically regulate their cargoes in response to stimulus [152, 178, 179], a molecular mechanism linking those stimuli to changes within the paraspeckle would provide important insight into how paraspeckles regulate diverse responses, including phosphorylation of IR-responsive unphosphorylated miRNAs.

Importantly, some preliminary evidence makes it plausible that ATM and paraspeckle-associated FUS could interact after IR. As stated above, ATM and FUS are well established to interact in general, with ATM phosphorylating FUS at several residues after IR. Importantly, ATM also establishes punctate localization after IR, both at the sites of DSBs and near the nucleolus [180]. Paraspeckles similarly alter their localization in response to stimuli, moving to the nucleolus in a similar time frame to ATM after IR or exposure to UV light[181]. Future studies investigating IR-responsive

colocalization of ATM and paraspeckles, paired with activation of paraspeckle-resident FUS, could provide an important framework for understanding paraspeckle-dependent stress responses after IR.

Summary of Chapters

Here, we will characterize current knowledge in the field covering unphosphorylated miR-34. First, we will demonstrate that nuclear paraspeckles are required for the nuclear localization and IR-dependent activation of unphosphorylated miR-34, but not necessary for coordinating other miRNAs. A mass spectrometry approach using 3' biotinylated miRNA mimics and RNAse A incubation will demonstrate that nuclear paraspeckles are plausible interactors with unphosphorylated miR-34, and are specific to both the sequence and phosphorylation status of the probe. Following a hypothesis that phase separation by nuclear paraspeckles sequesters unphosphorylated miR-34 from the rest of the nucleoplasm, a Cas9-mediated deletion of the triple helix motif (NEAT1 dTH) of the critical paraspeckle structural lncRNA NEAT1_2 was generated and validated, showing minimal phenotypic consequences at baseline, durable loss of paraspeckle formation, and significant knockdown of NEAT1_2 without loss of the shorter NEAT1_1 isoform, which is not required for paraspeckle formation. Paired RT-PCR and dual luciferase reporter assays to assess the expression and activity of IR-responsive miR-34 showed a loss of early miR-34 activity in NEAT1 dTH lines relative to wildtype lines, but no change in early radiation-responsive dynamics of other miRNAs known to lack an unphosphorylated pool. Primary and precursor miR-34 levels were also similar in both lines, implying no global loss in miR-34 processing and implying the above difference in activity shortly after IR was due to

loss of the unphosphorylated pool. Lastly, *in situ* hybridization for miR-34 shows that it localizes to the nucleus in a paraspeckle-dependent manner, while other miRNAs' nuclear localization occurs independent of paraspeckle formation. This chapter concludes that the nuclear localization and radiation-responsive activity of unphosphorylated miR-34 is dependent on paraspeckle formation maintained by the lncRNA NEAT1_2.

Since little literature describing unphosphorylated miRNAs currently exists, several novel experimental approaches were attempted to characterize the unphosphorylated pool- these approaches are detailed in Chapter 3. Briefly, Chapter 3 describes an initial alternative hypothesis for interactors with unphosphorylated miR-34, investigating hypothesis based on the high-confidence mass spectrometry hits Rbm3 and NUDT21. This chapter also details several approaches directed at nuclear paraspeckles that did not generate usable data, including alternative methods for disrupting paraspeckle formation *via* siRNA-mediated knockdown of critical paraspeckle proteins or chemical disruption of phase separation by hexanediols. We will also describe attempts to colocalize miR-34 and nuclear paraspeckles by *in situ* hybridization paired with immunofluorescence or ISH for NEAT1_2, as well as attempts to colocalize nuclear paraspeckles and the two factors known to activate the unphosphorylated pool after IR, hClp1 and ATM. Lastly, this chapter will discuss attempts to ascribe phenotypic consequences to loss of the unphosphorylated pool via ablation of nuclear paraspeckles.

Chapter 4 will discuss the significant potential for future studies of unphosphorylated miRNAs, including alternative approaches to address important gaps

in understanding described above. We will discuss the overall significance of the data presented in this work, as well as hypotheses for valuable future directions. This will include electron microscopy-based approaches to demonstrate direct colocalization and quantification of paraspeckle-associated miR-34, as well as methods to investigate mechanisms responsible for synthesis of unphosphorylated miRNAs and identification of other paraspeckle-associated miRNAs. This chapter will also discuss methods to demonstrate paraspeckles as broader coordinators of cellular response to ionizing radiation, which may provide significant new mechanistic insights into the regulation and utility of nuclear phase separations.

Figures

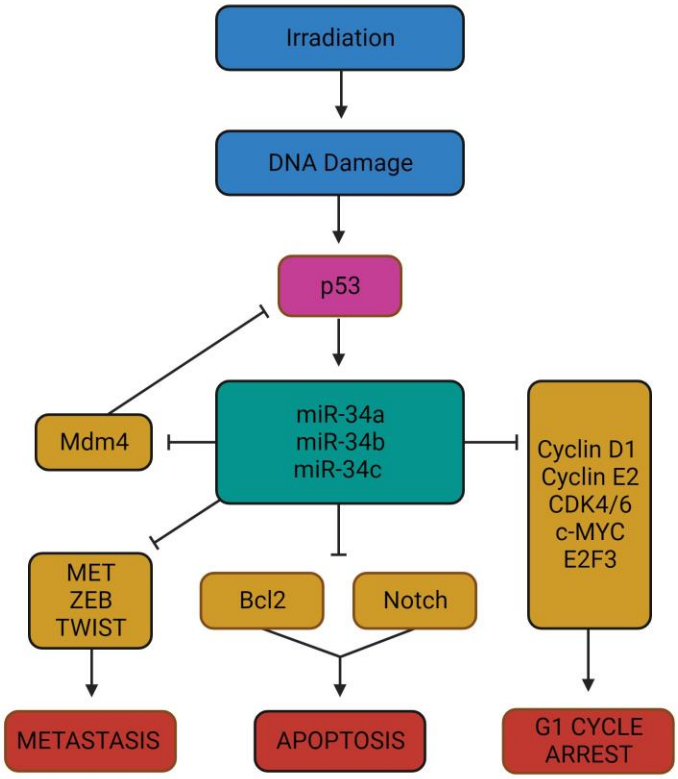

Figure 1.1- IR-responsive activation of miR-34 transcription and downstream pathways implicated in cancer progression. The mir-34 family is well characterized both for its roles in cancer cell radiosensitivity and as a tumor suppressor- miR-34 is upregulated after IR by p53 and downregulates the p53 ubiquitin ligase Mdm4, causing a positive feedback loop. Activity of miR-34 modulates cell cycle arrest, metastasis, and apoptosis via multiple downstream targets.

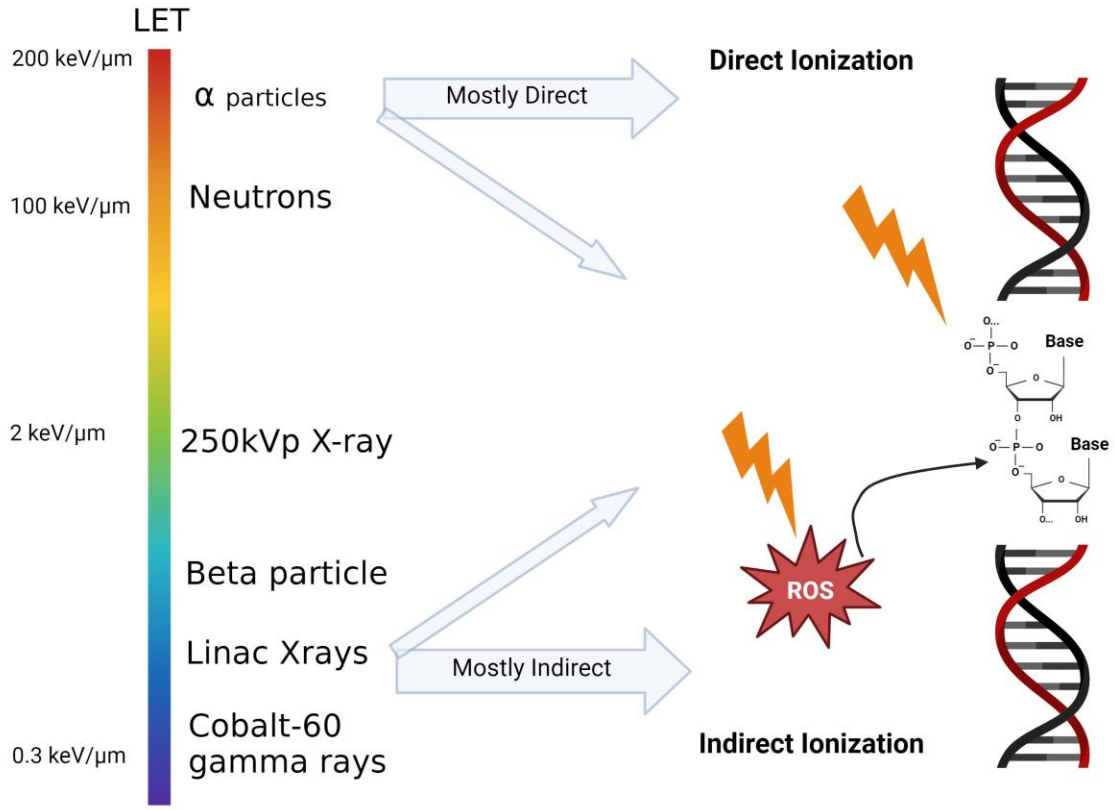

Figure 1.2- Radiation modalities and their relative effects. Ionizing radiation is capable of damaging biologically relevant structures either through direct or indirect ionization. Direct ionization involves the radiation source ionizing high-energy bonds directly, while indirect ionization involves the creation of reactive species that can then ionize the bonds. While all forms of radiation are capable of both mechanisms, higher linear energy transfer (LET) modalities, which deposit more energy per unit length traveled, are more capable of direct ionization than “softer” radiation sources. This work uses 300kV X-rays.

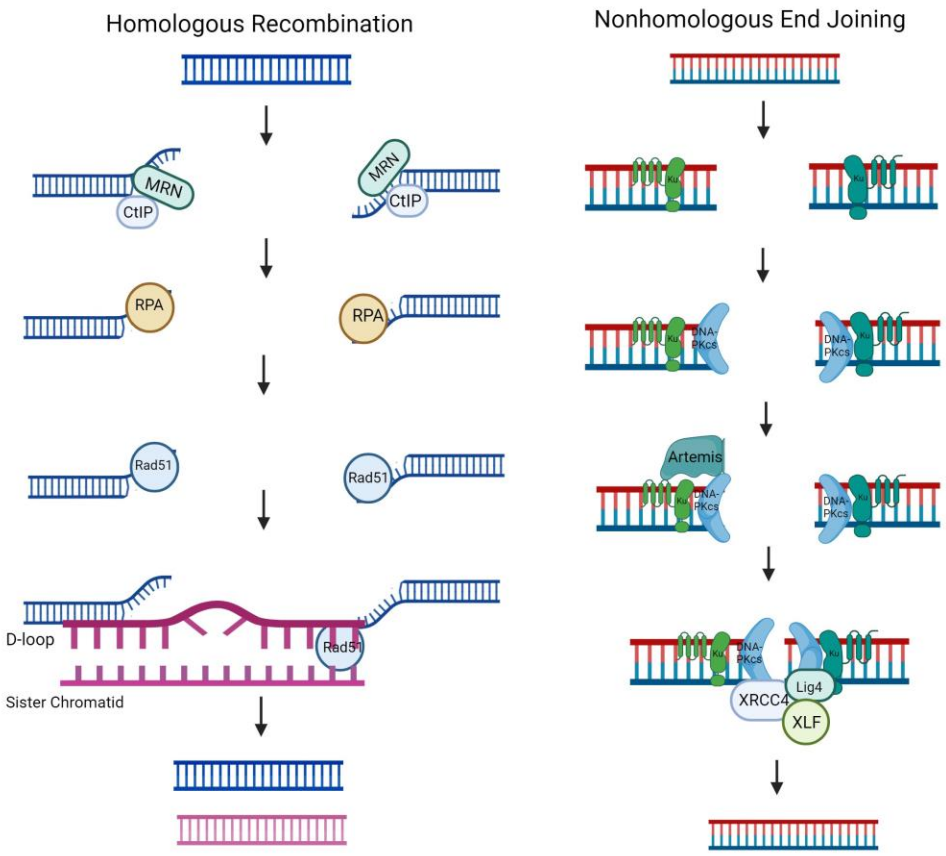

Figure 1.3- A general model of homologous recombination and nonhomologous end joining DNA repair, which are responsible for double strand break repair after ionizing radiation. Homologous recombination creates high-fidelity repair with decreased risk of loss or alteration of damaged sequences by copying damaged sequences using a repair template, typically the sister chromatid. Nonhomologous end joining resects overhangs created by DNA damage and ligates strands together, which may result in loss or alteration of intervening sequences.

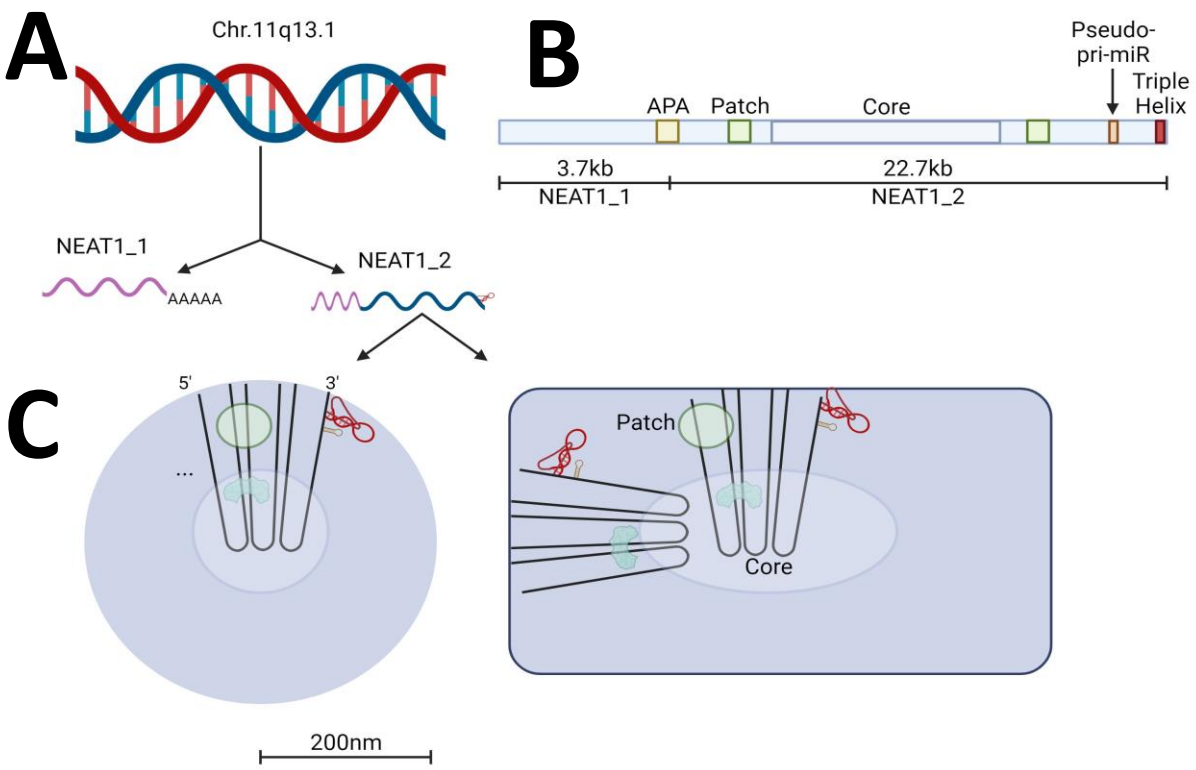

Figure 1.4- Anatomy and molecular mechanisms of NEAT1 and nuclear paraspeckles. A) NEAT1 is transcribed as two distinct transcripts from a locus on chromosome 11- the shorter isoform, NEAT1_1, is polyadenylated and dispensible for paraspeckle formation. The longer isoform, NEAT1_2, is required for paraspeckle formation. B) Domains of the NEAT1_2 transcript. The alternative polyadenylation site responsible for NEAT1_1 production (APA), patch and core regions responsible for protein localization, pri-miRNA-like sequence, and triple helix are highlighted in the same colours as in (C).B) Paraspeckles form into circular or "sausagelike" nuclear phase separations, with the 5' and 3' end of NEAT1_2 localized to the periphery. Associated proteins preferentially localize to core or patch regions within the paraspeckle, corresponding to different locations along the NEAT1 transcript. A triple helix motif (red) and pseudo-pri-miR (brown) localize to the 3' end of the transcript.

References

1. Metheetrairut, C. and F.J. Slack, *MicroRNAs in the ionizing radiation response and in radiotherapy.* Curr Opin Genet Dev, 2013. **23**(1): p. 12-9.
2. Leung, A.K. and P.A. Sharp, *MicroRNA functions in stress responses.* Mol Cell, 2010. **40**(2): p. 205-15.
3. Lacombe, J. and F. Zenhausern, *Emergence of miR-34a in radiation therapy.* Crit Rev Oncol Hematol, 2017. **109**: p. 69-78.
4. Kato, M., et al., *The mir-34 microRNA is required for the DNA damage response in vivo in C. elegans and in vitro in human breast cancer cells.* Oncogene, 2009. **28**(25): p. 2419-2424.
5. He, L., et al., *A microRNA component of the p53 tumour suppressor network.* Nature, 2007. **447**(7148): p. 1130-4.
6. Chang, T.C., et al., *Transactivation of miR-34a by p53 broadly influences gene expression and promotes apoptosis.* Mol Cell, 2007. **26**(5): p. 745-52.
7. Raver-Shapira, N., et al., *Transcriptional activation of miR-34a contributes to p53-mediated apoptosis.* Mol Cell, 2007. **26**(5): p. 731-43.
8. Salzman, D.W., et al., *miR-34 activity is modulated through 5'-end phosphorylation in response to DNA damage.* Nat Commun, 2016. **7**: p. 10954.
9. Zamudio, J.R., T.J. Kelly, and P.A. Sharp, *Argonaute-bound small RNAs from promoter-proximal RNA polymerase II.* Cell, 2014. **156**(5): p. 920-934.
10. Zamudio, J.R., T.J. Kelly, and P.A. Sharp, *Argonaute-bound small RNAs from promoter-proximal RNA polymerase II.* Cell, 2014. **156**(5): p. 920-34.
11. Peterson, S.M., et al., *Common features of microRNA target prediction tools.* Front Genet, 2014. **5**: p. 23.
12. John, B., et al., *Human MicroRNA Targets.* PLOS Biology, 2004. **2**(11): p. e363.

13. Bartel, D.P., *Metazoan MicroRNAs.* Cell, 2018. **173**(1): p. 20-51.

14. Kawamata, T. and Y. Tomari, *Making RISC.* Trends Biochem Sci, 2010. **35**(7): p. 368-76.

15. Schwarz, D.S., et al., *Asymmetry in the assembly of the RNAi enzyme complex.* Cell, 2003. **115**(2): p. 199-208.

16. Ando, Y., et al., *Two-step cleavage of hairpin RNA with 5' overhangs by human DICER.* BMC Molecular Biology, 2011. **12**(1): p. 6.

17. Elkayam, E., et al., *The Structure of Human Argonaute-2 in Complex with miR-20a.* Cell, 2012. **150**(1): p. 100-110.

18. Boland, A., et al., *Crystal structure and ligand binding of the MID domain of a eukaryotic Argonaute protein.* EMBO Rep, 2010. **11**(7): p. 522-7.

19. Lingel, A., et al., *Nucleic acid 3'-end recognition by the Argonaute2 PAZ domain.* Nat Struct Mol Biol, 2004. **11**(6): p. 576-7.

20. D'Ambrogio, A., et al., *Specific miRNA stabilization by Gld2-catalyzed monoadenylation.* Cell Rep, 2012. **2**(6): p. 1537-45.

21. Gutiérrez-Vázquez, C., et al., *3' Uridylation controls mature microRNA turnover during CD4 T-cell activation.* Rna, 2017. **23**(6): p. 882-891.

22. Baccarini, A., et al., *Kinetic analysis reveals the fate of a microRNA following target regulation in mammalian cells.* Curr Biol, 2011. **21**(5): p. 369-76.

23. Yang, A., et al., *AGO-bound mature miRNAs are oligouridylated by TUTs and subsequently degraded by DIS3L2.* Nature Communications, 2020. **11**(1): p. 2765.

24. Han, J., et al., *A ubiquitin ligase mediates target-directed microRNA decay independently of tailing and trimming.* Science, 2020. **370**(6523).

25. Winter, J. and S. Diederichs, *Argonaute proteins regulate microRNA stability: Increased microRNA abundance by Argonaute proteins is due to microRNA stabilization.* RNA Biol, 2011. **8**(6): p. 1149-57.

26. Ha, M. and V.N. Kim, *Regulation of microRNA biogenesis.* Nature Reviews Molecular Cell Biology, 2014. **15**(8): p. 509-524.

27. Wu, J., et al., *Two miRNA clusters, miR-34b/c and miR-449, are essential for normal brain development, motile ciliogenesis, and spermatogenesis.* Proceedings of the National Academy of Sciences, 2014. **111**(28): p. E2851-E2857.

28. Marzi, M.J., et al., *Degradation dynamics of microRNAs revealed by a novel pulse-chase approach.* Genome Research, 2016. **26**(4): p. 554-565.

29. Krell, J., et al., *TP53 regulates miRNA association with AGO2 to remodel the miRNA-mRNA interaction network.* Genome research, 2016. **26**(3): p. 331-341.

30. Tarasov, V., et al., *Differential regulation of microRNAs by p53 revealed by massively parallel sequencing: miR-34a is a p53 target that induces apoptosis and G1-arrest.* Cell Cycle, 2007. **6**(13): p. 1586-93.

31. Chatterjee, S. and H. Grosshans, *Active turnover modulates mature microRNA activity in Caenorhabditis elegans.* Nature, 2009. **461**(7263): p. 546-9.

32. Han, J. and J.T. Mendell, *MicroRNA turnover: a tale of tailing, trimming, and targets.* Trends in Biochemical Sciences, 2023. **48**(1): p. 26-39.

33. Jones, B.T., et al., *Target-directed microRNA degradation regulates developmental microRNA expression and embryonic growth in mammals.* Genes Dev, 2023. **37**(13-14): p. 661-674.

34. Shi, C.Y., et al., *The ZSWIM8 ubiquitin ligase mediates target-directed microRNA degradation.* Science, 2020. **370**(6523).

35. Cazalla, D., T. Yario, and J.A. Steitz, *Down-Regulation of a Host MicroRNA by a Herpesvirus saimiri Noncoding RNA.* Science, 2010. **328**(5985): p. 1563-1566.

36. Avraham, R., et al., *EGF decreases the abundance of microRNAs that restrain oncogenic transcription factors.* Sci Signal, 2010. **3**(124): p. ra43.

37. Zhu, Y., et al., *MicroRNA-26a/b and their host genes cooperate to inhibit the G1/S transition by activating the pRb protein.* Nucleic Acids Res, 2012. **40**(10): p. 4615-25.

38. Rissland, O.S., S.J. Hong, and D.P. Bartel, *MicroRNA destabilization enables dynamic regulation of the miR-16 family in response to cell-cycle changes.* Mol Cell, 2011. **43**(6): p. 993-1004.

39. Guo, Y., et al., *Characterization of the mammalian miRNA turnover landscape.* Nucleic Acids Res, 2015. **43**(4): p. 2326-41.

40. Krol, J., I. Loedige, and W. Filipowicz, *The widespread regulation of microRNA biogenesis, function and decay.* Nat Rev Genet, 2010. **11**(9): p. 597-610.

41. Bommer, G.T., et al., *p53-Mediated Activation of miRNA34 Candidate Tumor-Suppressor Genes.* Current Biology, 2007. **17**(15): p. 1298-1307.

42. Corney, D.C., et al., *MicroRNA-34b and MicroRNA-34c Are Targets of p53 and Cooperate in Control of Cell Proliferation and Adhesion-Independent Growth.* Cancer Research, 2007. **67**(18): p. 8433-8438.

43. Li, W.J., et al., *MicroRNA-34a: Potent Tumor Suppressor, Cancer Stem Cell Inhibitor, and Potential Anticancer Therapeutic.* Front Cell Dev Biol, 2021. **9**: p. 640587.

44. Cao, L., et al., *A feedback circuit of miR-34a/MDM4/p53 regulates apoptosis in chronic lymphocytic leukemia cells.* Transl Cancer Res, 2020. **9**(10): p. 6143-6153.

45. Okada, N., et al., *A positive feedback between p53 and miR-34 miRNAs mediates tumor suppression.* Genes Dev, 2014. **28**(5): p. 438-50.

46. Gupta, S., D.A. Silveira, and J.C.M. Mombach, *ATM/miR-34a-5p axis regulates a p21-dependent senescence-apoptosis switch in non-small cell lung cancer: a Boolean model of G1/S checkpoint regulation.* FEBS Lett, 2019.

47. Shao, T., et al., *The long noncoding RNA HOTAIR serves as a microRNA-34a-5p sponge to reduce nucleus pulposus cell apoptosis via a NOTCH1-mediated mechanism.* Gene, 2019. **715**: p. 144029.

48. Siemens, H., et al., *miR-34 and SNAIL form a double-negative feedback loop to regulate epithelial-mesenchymal transitions.* Cell Cycle, 2011. **10**(24): p. 4256-71.

49. Yu, G., et al., *miRNA-34a suppresses cell proliferation and metastasis by targeting CD44 in human renal carcinoma cells.* J Urol, 2014. **192**(4): p. 1229-37.

50. Sun, F., et al., *Downregulation of CCND1 and CDK6 by miR-34a induces cell cycle arrest.* FEBS Lett, 2008. **582**(10): p. 1564-8.

51. Liang, Y., et al., *Characterization of microRNA expression profiles in normal human tissues.* BMC Genomics, 2007. **8**: p. 166.

52. Kim, J.S., et al., *MiR-34a and miR-34b/c have distinct effects on the suppression of lung adenocarcinomas.* Exp Mol Med, 2019. **51**(1): p. 1-10.

53. Lodygin, D., et al., *Inactivation of miR-34a by aberrant CpG methylation in multiple types of cancer.* Cell Cycle, 2008. **7**(16): p. 2591-600.

54. Navarro, F. and J. Lieberman, *miR-34 and p53: New Insights into a Complex Functional Relationship.* PLoS One, 2015. **10**(7): p. e0132767.

55. Otto, T., et al., *Cell cycle-targeting microRNAs promote differentiation by enforcing cell-cycle exit.* Proc Natl Acad Sci U S A, 2017. **114**(40): p. 10660-10665.

56. Serviss, J.T., et al., *An antisense RNA capable of modulating the expression of the tumor suppressor microRNA-34a.* Cell death & disease, 2018. **9**(7): p. 736-736.

57. Siemens, H., et al., *miR-34 and SNAIL form a double-negative feedback loop to regulate epithelial-mesenchymal transitions.* Cell Cycle, 2011. **10**(24): p. 4256-71.

58. Yang, S., et al., *MicroRNA-34 suppresses breast cancer invasion and metastasis by directly targeting Fra-1.* Oncogene, 2013. **32**(36): p. 4294-303.

59. Daugaard, I., et al., *The association between miR-34 dysregulation and distant metastases formation in lung adenocarcinoma.* Exp Mol Pathol, 2017. **102**(3): p. 484-491.

60. Gupta, S., D.A. Silveira, and J.C.M. Mombach, *ATM/miR-34a-5p axis regulates a p21-dependent senescence-apoptosis switch in non-small cell lung cancer: a Boolean model of G1/S checkpoint regulation.* FEBS Letters, 2020. **594**(2): p. 227-239.

61. Lee, R.C., R.L. Feinbaum, and V. Ambros, *The C. elegans heterochronic gene lin-4 encodes small RNAs with antisense complementarity to lin-14.* Cell, 1993. **75**(5): p. 843-54.

62. Gebert, L.F.R. and I.J. MacRae, *Regulation of microRNA function in animals.* Nat Rev Mol Cell Biol, 2019. **20**(1): p. 21-37.

63. Holley, W.R. and A. Chatterjee, *Clusters of DNA Damage Induced by Ionizing Radiation: Formation of Short DNA Fragments. I. Theoretical Modeling.* Radiation Research, 1996. **145**(2): p. 188-199.

64. Biaglow, J.E., et al., *Nonprotein thiols and the radiation response of A549 human lung carcinoma cells.* Int J Radiat Biol Relat Stud Phys Chem Med, 1983. **44**(5): p. 489-95.

65. Toburen, L.H., *Ionization and charge-transfer: basic data for track structure calculations.* Radiat Environ Biophys, 1998. **37**(4): p. 221-33.

66. Cucinotta, F.A., et al., *Biological effectiveness of high-energy protons: target fragmentation.* Radiat Res, 1991. **127**(2): p. 130-7.

67. Nakano, T., et al., *Radiation-induced DNA–protein cross-links: Mechanisms and biological significance.* Free Radical Biology and Medicine, 2017. **107**: p. 136-145.

68. Ewing, D., *The oxygen fixation hypothesis: a reevaluation.* Am J Clin Oncol, 1998. **21**(4): p. 355-61.

69. Hada, M. and A.G. Georgakilas, *Formation of clustered DNA damage after high-LET irradiation: a review.* J Radiat Res, 2008. **49**(3): p. 203-10.

70. Read, G.H., et al., *Three-dimensional alginate hydrogels for radiobiological and metabolic studies of cancer cells.* Colloids Surf B Biointerfaces, 2018. **171**: p. 197-204.

71. Read, G.H., et al., *Metabolic response to radiation therapy in cancer.* Mol Carcinog, 2022. **61**(2): p. 200-224.

72. Canman, C.E., et al., *Activation of the ATM Kinase by Ionizing Radiation and Phosphorylation of p53.* Science, 1998. **281**(5383): p. 1677-1679.

73. Kochan, J.A., et al., *Meta-analysis of DNA double-strand break response kinetics.* Nucleic Acids Res, 2017. **45**(22): p. 12625-12637.

74. Shibata, A., et al., *Factors determining DNA double-strand break repair pathway choice in G2 phase.* Embo j, 2011. **30**(6): p. 1079-92.

75. Jo, G.H., et al., *Radiation-induced autophagy contributes to cell death and induces apoptosis partly in malignant glioma cells.* Cancer Res Treat, 2015. **47**(2): p. 221-41.

76. Puck, T.T. and P.I. Marcus, *Action of x-rays on mammalian cells.* J Exp Med, 1956. **103**(5): p. 653-66.

77. Phillips, R.A. and L.J. Tolmach, *Repair of potentially lethal damage in x-irradiated HeLa cells.* Radiat Res, 1966. **29**(3): p. 413-32.

78. Ngo, F.Q., et al., *Sequential exposures of mammalian cells to low- and high-LET radiations. II. As a function of cell-cycle stages.* Radiat Res, 1988. **115**(1): p. 54-69.

79. Franken, N.A., et al., *Clonogenic assay of cells in vitro.* Nat Protoc, 2006. **1**(5): p. 2315-9.

80. Elkind, M.M. and H. Sutton, *X-ray damage and recovery in mammalian cells in culture.* Nature, 1959. **184**: p. 1293-5.

81. Puck, T.T., et al., *Action of x-rays on mammalian cells. II. Survival curves of cells from normal human tissues.* J Exp Med, 1957. **106**(4): p. 485-500.

82. Yamada, M. and T.T. Puck, *Action of radiation on mammalian cells. IV. Reversible mitotic lag in the S3 HeLa cell produced by low doses of x-rays.* Proc Natl Acad Sci U S A, 1961. **47**(8): p. 1181-91.

83. Buatti, J.M., L.R. Rivero, and T.J. Jorgensen, *Radiation-induced DNA single-strand breaks in freshly isolated human leukocytes.* Radiat Res, 1992. **132**(2): p. 200-6.

84. Abbotts, R. and D.M. Wilson, 3rd, *Coordination of DNA single strand break repair.* Free Radic Biol Med, 2017. **107**: p. 228-244.

85. Brandsma, I. and D.C. van Gent, *Pathway choice in DNA double strand break repair: observations of a balancing act.* Genome Integrity, 2012. **3**(1): p. 9.

86. Pongsavee, M., et al., *The BRCA1 3'-UTR: 5711+421T/T_5711+1286T/T genotype is a possible breast and ovarian cancer risk factor.* Genet Test Mol Biomarkers, 2009. **13**(3): p. 307-17.

87. Uziel, T., et al., *Requirement of the MRN complex for ATM activation by DNA damage.* Embo j, 2003. **22**(20): p. 5612-21.

88. Warren, C. and N.P. Pavletich, *Structure of the human ATM kinase and mechanism of Nbs1 binding.* Elife, 2022. **11**.

89. Burma, S., et al., *ATM phosphorylates histone H2AX in response to DNA double-strand breaks.* J Biol Chem, 2001. **276**(45): p. 42462-7.

90. Bakr, A., et al., *Involvement of ATM in homologous recombination after end resection and RAD51 nucleofilament formation.* Nucleic Acids Res, 2015. **43**(6): p. 3154-66.

91. Salminen, A., et al., *NEMO shuttle: a link between DNA damage and NF-kappaB activation in progeroid syndromes?* Biochem Biophys Res Commun, 2008. **367**(4): p. 715-8.

92. Cheng, Q., et al., *ATM activates p53 by regulating MDM2 oligomerization and E3 processivity.* Embo j, 2009. **28**(24): p. 3857-67.

93. Smith, J., et al., *The ATM-Chk2 and ATR-Chk1 pathways in DNA damage signaling and cancer.* Adv Cancer Res, 2010. **108**: p. 73-112.

94. Sartori, A.A., et al., *Human CtIP promotes DNA end resection.* Nature, 2007. **450**(7169): p. 509-14.

95. Mazón, G., E.P. Mimitou, and L.S. Symington, *SnapShot: Homologous recombination in DNA double-strand break repair.* Cell, 2010. **142**(4): p. 646, 646.e1.

96. Sung, P., *Catalysis of ATP-dependent homologous DNA pairing and strand exchange by yeast RAD51 protein.* Science, 1994. **265**(5176): p. 1241-3.

97. Morrical, S.W., *DNA-pairing and annealing processes in homologous recombination and homology-directed repair.* Cold Spring Harb Perspect Biol, 2015. **7**(2): p. a016444.

98. Jinek, M., et al., *RNA-programmed genome editing in human cells.* eLife, 2013. **2**: p. e00471.

99. Beucher, A., et al., *ATM and Artemis promote homologous recombination of radiation-induced DNA double-strand breaks in G2.* Embo j, 2009. **28**(21): p. 3413-27.

100. Budman, J. and G. Chu, *Processing of DNA for nonhomologous end-joining by cell-free extract.* Embo j, 2005. **24**(4): p. 849-60.

101. Smider, V., et al., *Restoration of X-ray resistance and V(D)J recombination in mutant cells by Ku cDNA.* Science, 1994. **266**(5183): p. 288-91.

102. Taccioli, G.E., et al., *Impairment of V(D)J recombination in double-strand break repair mutants.* Science, 1993. **260**(5105): p. 207-10.

103. Grawunder, U., et al., *DNA ligase IV is essential for V(D)J recombination and DNA double-strand break repair in human precursor lymphocytes.* Mol Cell, 1998. **2**(4): p. 477-84.

104. Gudkov, A.V. and E.A. Komarova, *The role of p53 in determining sensitivity to radiotherapy.* Nat Rev Cancer, 2003. **3**(2): p. 117-29.

105. Lee, C.L., J.M. Blum, and D.G. Kirsch, *Role of p53 in regulating tissue response to radiation by mechanisms independent of apoptosis.* Transl Cancer Res, 2013. **2**(5): p. 412-421.

106. Weidhaas, J.B., et al., *MicroRNAs as potential agents to alter resistance to cytotoxic anticancer therapy.* Cancer research, 2007. **67**(23): p. 11111-11116.

107. Kato, M., et al., *The mir-34 microRNA is required for the DNA damage response in vivo in C. elegans and in vitro in human breast cancer cells.* Oncogene, 2009. **28**(25): p. 2419-24.

108. Zeng, H., et al., *MicroRNA 34a promotes ionizing radiation-induced DNA damage repair in murine hematopoietic stem cells.* Faseb j, 2019. **33**(7): p. 8138-8147.

109. Kofman, A.V., et al., *microRNA-34a promotes DNA damage and mitotic catastrophe.* Cell Cycle, 2013. **12**(22): p. 3500-11.

110. Kato, M., et al., *The mir-34 microRNA is required for the DNA damage response in vivo in C. elegans and in vitro in human breast cancer cells.* Oncogene, 2009. **28**(25): p. 2419-24.

111. Cortez, M.A., et al., *In Vivo Delivery of miR-34a Sensitizes Lung Tumors to Radiation Through RAD51 Regulation.* Mol Ther Nucleic Acids, 2015. **4**(12): p. e270.

112. Derry, W.B., A.P. Putzke, and J.H. Rothman, *Caenorhabditis elegans p53: role in apoptosis, meiosis, and stress resistance.* Science, 2001. **294**(5542): p. 591-5.

113. Yamakuchi, M., M. Ferlito, and C.J. Lowenstein, *miR-34a repression of SIRT1 regulates apoptosis.* Proc Natl Acad Sci U S A, 2008. **105**(36): p. 13421-6.

114. Weidhaas, J.B., et al., *A Caenorhabditis elegans tissue model of radiation-induced reproductive cell death.* Proc Natl Acad Sci U S A, 2006. **103**(26): p. 9946-51.

115. Liu, C., et al., *MiR-34a in age and tissue related radio-sensitivity and serum miR-34a as a novel indicator of radiation injury.* Int J Biol Sci, 2011. **7**(2): p. 221-33.

116. Sheard, M.A., S. Uldrijan, and B. Vojtesek, *Role of p53 in regulating constitutive and X-radiation-inducible CD95 expression and function in carcinoma cells.* Cancer Res, 2003. **63**(21): p. 7176-84.

117. De Zio, D., V. Cianfanelli, and F. Cecconi, *New insights into the link between DNA damage and apoptosis.* Antioxid Redox Signal, 2013. **19**(6): p. 559-71.

118. Gewirtz, D.A., *Autophagy and senescence in cancer therapy.* J Cell Physiol, 2014. **229**(1): p. 6-9.

119. Burki, H.J., *Mammalian cells: damage in late replicating DNA as the most efficient cause of reproductive death.* Exp Cell Res, 1974. **87**(2): p. 277-80.

120. Adams, B.D., C. Parsons, and F.J. Slack, *The tumor-suppressive and potential therapeutic functions of miR-34a in epithelial carcinomas.* Expert Opin Ther Targets, 2016. **20**(6): p. 737-53.

121. Diener, C., A. Keller, and E. Meese, *Emerging concepts of miRNA therapeutics: from cells to clinic.* Trends in Genetics, 2022. **38**(6): p. 613-626.

122. Hong, D.S., et al., *Phase 1 study of MRX34, a liposomal miR-34a mimic, in patients with advanced solid tumours.* Br J Cancer, 2020. **122**(11): p. 1630-1637.

123. Lipinski, C.A., et al., *Experimental and computational approaches to estimate solubility and permeability in drug discovery and development settings.* Advanced Drug Delivery Reviews, 1997. **23**(1): p. 3-25.

124. Abdelaal, A.M., et al., *A first-in-class fully modified version of miR-34a with outstanding stability, activity, and anti-tumor efficacy.* Oncogene, 2023. **42**(40): p. 2985-2999.

125. Ling, H., M. Fabbri, and G.A. Calin, *MicroRNAs and other non-coding RNAs as targets for anticancer drug development.* Nat Rev Drug Discov, 2013. **12**(11): p. 847-65.

126. Trang, P., et al., *Systemic delivery of tumor suppressor microRNA mimics using a neutral lipid emulsion inhibits lung tumors in mice.* Mol Ther, 2011. **19**(6): p. 1116-22.

127. Abate, M., et al., *Fluorescent nanodiamonds as innovative delivery systems for MiR-34a replacement in breast cancer.* Mol Ther Nucleic Acids, 2023. **33**: p. 127-141.

128. Papasani, M.R., G. Wang, and R.A. Hill, *Gold nanoparticles: the importance of physiological principles to devise strategies for targeted drug delivery.* Nanomedicine, 2012. **8**(6): p. 804-14.

129. Orellana, E.A., et al., *FolamiRs: Ligand-targeted, vehicle-free delivery of microRNAs for the treatment of cancer.* Sci Transl Med, 2017. **9**(401).

130. Naganuma, T. and T. Hirose, *Paraspeckle formation during the biogenesis of long non-coding RNAs.* RNA Biol, 2013. **10**(3): p. 456-61.

131. Nakagawa, S., et al., *Paraspeckles are subpopulation-specific nuclear bodies that are not essential in mice.* The Journal of cell biology, 2011. **193**(1): p. 31-39.

132. Naganuma, T., et al., *Alternative 3'-end processing of long noncoding RNA initiates construction of nuclear paraspeckles.* The EMBO journal, 2012. **31**(20): p. 4020-4034.

133. Wilusz, J.E., et al., *A triple helix stabilizes the 3' ends of long noncoding RNAs that lack poly(A) tails.* Genes Dev, 2012. **26**(21): p. 2392-407.

134. Clemson, C.M., et al., *An architectural role for a nuclear noncoding RNA: NEAT1 RNA is essential for the structure of paraspeckles.* Mol Cell, 2009. **33**(6): p. 717-26.

135. Cardinale, S., et al., *Subnuclear localization and dynamics of the Pre-mRNA 3' end processing factor mammalian cleavage factor I 68-kDa subunit.* Mol Biol Cell, 2007. **18**(4): p. 1282-92.

136. Fox, A.H. and A.I. Lamond, *Paraspeckles.* Cold Spring Harbor perspectives in biology, 2010. **2**(7): p. a000687-a000687.

137. Banani, S.F., et al., *Biomolecular condensates: organizers of cellular biochemistry.* Nat Rev Mol Cell Biol, 2017. **18**(5): p. 285-298.

138. Yap, K., T.H. Chung, and E.V. Makeyev, *Hybridization-proximity labeling reveals spatially ordered interactions of nuclear RNA compartments.* Mol Cell, 2022. **82**(2): p. 463-478.e11.

139. Yamazaki, T., T. Yamamoto, and T. Hirose, *Micellization: A new principle in the formation of biomolecular condensates.* Front Mol Biosci, 2022. **9**: p. 974772.

140. Yamazaki, T., et al., *Paraspeckles are constructed as block copolymer micelles.* Embo j, 2021. **40**(12): p. e107270.

141. Fay, M.M. and P.J. Anderson, *The Role of RNA in Biological Phase Separations.* J Mol Biol, 2018. **430**(23): p. 4685-4701.

142. Naganuma, T., et al., *Alternative 3'-end processing of long noncoding RNA initiates construction of nuclear paraspeckles.* Embo j, 2012. **31**(20): p. 4020-34.

143. Andersen, J.S., et al., *Directed proteomic analysis of the human nucleolus.* Curr Biol, 2002. **12**(1): p. 1-11.

144. Shav-Tal, Y., et al., *Dynamic sorting of nuclear components into distinct nucleolar caps during transcriptional inhibition.* Mol Biol Cell, 2005. **16**(5): p. 2395-413.

145. Hirose, T., et al., *NEAT1 long noncoding RNA regulates transcription via protein sequestration within subnuclear bodies.* Molecular Biology of the Cell, 2013. **25**(1): p. 169-183.

146. Zhang, Y., et al., *lncRNA Neat1 Stimulates Osteoclastogenesis Via Sponging miR-7.* Journal of Bone and Mineral Research, 2020. **35**(9): p. 1772-1781.

147. He, Z., et al., *NEAT1 promotes colon cancer progression through sponging miR-495-3p and activating CDK6 in vitro and in vivo.* J Cell Physiol, 2019. **234**(11): p. 19582-19591.

148. Yan, H., et al., *Long noncoding RNA NEAT1 sponges miR-125a-5p to suppress cardiomyocyte apoptosis via BCL2L12.* Mol Med Rep, 2019. **19**(5): p. 4468-4474.

149. Ji, Y., et al., *The Long Noncoding RNA NEAT1 Targets miR-34a-5p and Drives Nasopharyngeal Carcinoma Progression via Wnt/β-Catenin Signaling.* Yonsei medical journal, 2019. **60**(4): p. 336-345.

150. Paul, D., et al., *A-to-I editing in human miRNAs is enriched in seed sequence, influenced by sequence contexts and significantly hypoedited in glioblastoma multiforme.* Sci Rep, 2017. **7**(1): p. 2466.

151. Elguindy, M.M. and J.T. Mendell, *NORAD-induced Pumilio phase separation is required for genome stability.* Nature, 2021. **595**(7866): p. 303-308.

152. Imamura, K., et al., *Long noncoding RNA NEAT1-dependent SFPQ relocation from promoter region to paraspeckle mediates IL8 expression upon immune stimuli.* Mol Cell, 2014. **53**(3): p. 393-406.

153. Choudhry, H., et al., *Tumor hypoxia induces nuclear paraspeckle formation through HIF-2α dependent transcriptional activation of NEAT1 leading to cancer cell survival.* Oncogene, 2015. **34**(34): p. 4482-90.

154. Kukharsky, M.S., et al., *Long non-coding RNA Neat1 regulates adaptive behavioural response to stress in mice.* Transl Psychiatry, 2020. **10**(1): p. 171.

155. Hirose, T., et al., *NEAT1 long noncoding RNA regulates transcription via protein sequestration within subnuclear bodies.* Mol Biol Cell, 2014. **25**(1): p. 169-83.

156. Adriaens, C., et al., *p53 induces formation of NEAT1 lncRNA-containing paraspeckles that modulate replication stress response and chemosensitivity.* Nat Med, 2016. **22**(8): p. 861-8.

157. Idogawa, M., et al., *Long non-coding RNA NEAT1 is a transcriptional target of p53 and modulates p53-induced transactivation and tumor-suppressor function.* Int J Cancer, 2017. **140**(12): p. 2785-2791.

158. Wang, Y.-L., et al., *DNA damage-induced paraspeckle formation enhances DNA repair and tumor radioresistance by recruiting ribosomal protein P0.* Cell Death & Disease, 2022. **13**(8): p. 709.

159. Jiang, L., et al., *NEAT1 scaffolds RNA-binding proteins and the Microprocessor to globally enhance pri-miRNA processing.* Nature structural & molecular biology, 2017. **24**(10): p. 816-824.

160. Kilgore, H.R., et al., *Distinct chemical environments in biomolecular condensates.* Nature Chemical Biology, 2023.

161. Forman-Kay, J.D., et al., *What are the distinguishing features and size requirements of biomolecular condensates and their implications for RNA-containing condensates?* Rna, 2022. **28**(1): p. 36-47.

162. Kilgore, H.R. and R.A. Young, *Learning the chemical grammar of biomolecular condensates.* Nat Chem Biol, 2022. **18**(12): p. 1298-1306.

163. Adriaens, C. and J.-C. Marine, *NEAT1-containing paraspeckles: Central hubs in stress response and tumor formation.* Cell cycle (Georgetown, Tex.), 2017. **16**(2): p. 137-138.

164. Modic, M., et al., *Cross-Regulation between TDP-43 and Paraspeckles Promotes Pluripotency-Differentiation Transition.* Molecular Cell.

165. Brown, J.A., et al., *Formation of triple-helical structures by the 3′-end sequences of MALAT1 and MENβ noncoding RNAs.* Proceedings of the National Academy of Sciences, 2012. **109**(47): p. 19202-19207.

166. Clark, M.B., et al., *Genome-wide analysis of long noncoding RNA stability.* Genome Res, 2012. **22**(5): p. 885-98.

167. Fox, A.H., C.S. Bond, and A.I. Lamond, *P54nrb forms a heterodimer with PSP1 that localizes to paraspeckles in an RNA-dependent manner.* Mol Biol Cell, 2005. **16**(11): p. 5304-15.

168. Putnam, A., L. Thomas, and G. Seydoux, *RNA granules: functional compartments or incidental condensates?* Genes Dev, 2023.

169. Putnam, A. and G. Seydoux, *Cell-free reconstitution of multi-condensate assemblies.* Methods Enzymol, 2021. **646**: p. 83-113.

170. Seim, I., et al., *Dilute phase oligomerization can oppose phase separation and modulate material properties of a ribonucleoprotein condensate.* Proceedings of the National Academy of Sciences, 2022. **119**(13): p. e2120799119.

171. Mittag, T. and R.V. Pappu, *A conceptual framework for understanding phase separation and addressing open questions and challenges.* Molecular Cell, 2022. **82**(12): p. 2201-2214.

172. Decker, C.J. and R. Parker, *P-bodies and stress granules: possible roles in the control of translation and mRNA degradation.* Cold Spring Harb Perspect Biol, 2012. **4**(9): p. a012286.

173. Li, H., et al., *Sequestration and inhibition of Daxx-mediated transcriptional repression by PML.* Mol Cell Biol, 2000. **20**(5): p. 1784-96.

174. Lester, E., et al., *Tau aggregates are RNA-protein assemblies that mislocalize multiple nuclear speckle components.* Neuron, 2021. **109**(10): p. 1675-1691.e9.

175. Gardiner, M., et al., *Identification and characterization of FUS/TLS as a new target of ATM.* Biochemical Journal, 2008. **415**(2): p. 297-307.

176. Carey, J.L. and L. Guo, *Liquid-Liquid Phase Separation of TDP-43 and FUS in Physiology and Pathology of Neurodegenerative Diseases.* Front Mol Biosci, 2022. **9**: p. 826719.

177. Qamar, S., et al., *FUS Phase Separation Is Modulated by a Molecular Chaperone and Methylation of Arginine Cation-π Interactions.* Cell, 2018. **173**(3): p. 720-734.e15.

178. Choudhry, H., et al., *Tumor hypoxia induces nuclear paraspeckle formation through HIF-2alpha dependent transcriptional activation of NEAT1 leading to cancer cell survival.* Oncogene, 2015. **34**(34): p. 4482-90.

179. Sawyer, I.A., J. Bartek, and M. Dundr, *Phase separated microenvironments inside the cell nucleus are linked to disease and regulate epigenetic state, transcription and RNA processing.* Semin Cell Dev Biol, 2019. **90**: p. 94-103.

180. Alexander, A. and C.L. Walker, *Differential localization of ATM is correlated with activation of distinct downstream signaling pathways.* Cell Cycle, 2010. **9**(18): p. 3685-6.

181. Moore, H.M., et al., *Quantitative proteomics and dynamic imaging of the nucleolus reveal distinct responses to UV and ionizing radiation.* Molecular & cellular proteomics : MCP, 2011. **10**(10): p. M111.009241-M111.009241.

Chapter 2:

Nuclear Paraspeckles are Required for Localization and Activity of 5'OH miR-34a

Abstract

MicroRNAs are processed post-transcription by two rounds of cleavage, resulting in a ~22nt-long transcript with a 5' phosphate group required for Argonaute binding and targeting. Work from our group has identified a steady-state pool of processed miR-34 in human lung cancer cells lacking a 5' phosphate and unbound by Ago2. In response to radiation-induced cellular stress, this pool of miR-34 is rapidly phosphorylated in a mechanism dependent on ATM and the nucleotide kinase Clp1, enabling Ago2-mediated gene repression. This work identifies nuclear paraspeckles as necessary for the radiation-responsive activation and nuclear localization of this unphosphorylated pool, which may imply direct coordination of the pool. Mass spectrometry of binding partners of unphosphorylated miR-34 mimics was used to identify candidate binding partners of unphosphorylated miR-34. Following identification of probable binding partners, immunoprecipitation was used to confirm interaction with miR-34, identifying significant enrichment of proteins localizing to nuclear paraspeckles. Based on this, we hypothesize that phase separation sequesters unphosphorylated miR-34 in unstressed lung cancer cells. Expression and activity of miR-34 after irradiation was tested in cells lacking paraspeckles due to siRNA-mediated knockdowns of necessary paraspeckle proteins or Cas9-mediated deletion of the NEAT1 triple helix domain. Consistent with prior reports of radiation-responsive activity derived from unphosphorylated miR-34, IR induced a rapid activation of miR-34 in wildtype cells, but not in cells lacking paraspeckles**.** Additionally, cells lacking paraspeckles failed to organize punctate nuclear miR-34 foci, which were observed in wildtype cells. These phenotypes were not observed in miRNAs known to lack an unphosphorylated pool. The levels and dynamics of pri- and pre-miR-34 were similar between wildtype cells and those lacking

paraspeckles, which may imply that paraspeckles do not contribute to the transcription or processing of 5'OH miR-34. Our study demonstrates that paraspeckles are necessary for the activity and punctate nuclear localization of unphosphorylated miR-34.

Introduction

Canonical microRNA (miRNA) regulation is a two-step process occurring in multiple cellular compartments- miRNAs are transcribed as long, hairpinned transcripts, processed by the Microprocessor complex, exported to the cytoplasm, and processed again by Dicer to generate a ~22-25 nucleotide-long transcript with a 5' phosphate[1, 2]. This 5' phosphate is required for binding to Argonaute (Ago2), which is required both for stabilizing the miRNA and directing it to target mRNAs[3].

The tumor suppressor miRNA miR-34 has been implicated in several key pathways in cancer cells, including metastasis, apoptosis, cell cycle regulation, and DNA repair [4, 5]. To this end, miR-34 is well characterized as a tumour suppressor [6, 7], with higher miR-34 expression correlating with improved patient survival[8] and increasing interest in miR-34 delivery as a therapeutic[6, 9, 10]. Ionizing radiation (IR) induces *de novo* miR-34 expression in a p53-dependent manner[11]- accordingly, miR-34 has been well described as an important determinant of cancer cell radiosensitivity[5, 12].

Uniquely among miRNAs, miR-34 has been shown to maintain a fully-processed unphosphorylated pool in the nucleus, which is rapidly phosphorylated after IR, causing an increase in miR-34 activity prior to *de novo* transcription and processing[13]. While the

existence and activation of unphosphorylated miR-34 has been characterized, mechanisms governing the nuclear localization and stabilization of unphosphorylated miR-34 have not yet been described.

This work demonstrates for the first time that nuclear paraspeckles are necessary for the stability and localization of unphosphorylated miR-34. Paraspeckles are formed by several critical proteins bound to the long noncoding RNA (lncRNA) NEAT1_2[14], which is stabilized by a triple helix motif in lieu of polyadenylation[15-17]. Binding between NEAT1_2 and these proteins generates a membraneless sub-organelle capable of phase separation, which prevents mixing between internal contents and the rest of the nucleoplasm[18, 19]. Accordingly, paraspeckles have been implicated in several stress response pathways for their ability to sequester target factors[20-22]. Here, we show that deletion of the NEAT1_2 triple helix motif causes a loss of early IR-responsive miR-34 activation without significantly affecting miR-34 transcription and processing, suggesting that paraspeckles are necessary for the activity, but not the production of unphosphorylated miR-34. Similarly, *in situ* hybridization for miR-34 shows paraspeckle-dependent punctate localization in the nucleus for miR-34, but not for other miRNAs known to lack an unphosphorylated pool. This study proposes formation of nuclear paraspeckles as necessary for the activity and punctate nuclear localization of unphosphorylated miR-34.

Materials and Methods

Cell Culture

A549 lung adenocarcinoma cells (ATCC) were cultured in F12K media supplemented with 10% fetal bovine serum and 1% streptomycin/penicillin at 37^{o}C with 5% CO2.

Cas9 editing

For Cas9-mediated modification of paraspeckle proteins, cells were passaged into 6-well plates at 50% confluency. 24 hours after plating, cells were transfected with 1ug per well of Cas9 donor and sgRNA plasmids (See Table S1**)** and 5uL Lipofectamine 2000 (Thermo Scientific). 24h after transfection, cells were trypsinized, counted, and serial diluted to 5 cells per mL. 200uL of cell stock were transferred to 96 well plates and cultured for approximately six weeks. Confirmed single colonies were trypsinized, genotyped by PCR, and maintained as described above.

Deletion of the NEAT1 triple helix motif was performed by direct lipofection of Cas9 (IDT #1081058) conjugated to Alt-R CRISPR-Cas9 sgRNAs (see Table S1). RNP complexes were assembled *in vitro* using 1uM sgRNA and 1uM Cas9 enzyme and reverse transfected into 40,000 cells per well for 48h. Successful editing was confirmed by PCR and sequencing (see Table S1), and loss of paraspeckle formation was confirmed by *in situ* hybridization against a sequence in the middle of the NEAT1_2 transcript (Stellaris SMF-2037-1) and immunofluorescence for PSF (Sigma-Aldrich P2860).

Mass Spectrometry

A549wt cells were cultured on 10cm plates in triplicate for each condition as described above. Protein was extracted by scraping plates into 300uL cold RIPA buffer (Thermo #89900). Triplicates were pooled and mixed 1:1 with 2x TENT buffer (20mM Tris pH 8.0, 2mM EDTA, 500mM NaCl, 1% Triton X-100) with protease inhibitor (Thermo A32965). Lysates were cleared by incubating overnight with 100uL agarose streptavidin (Vector SA-5010). In parallel, 100uL agarose streptavidin beads were incubated with 600pmol 3'biotinylated miRNA probe[23] in 1x TENT buffer at 4 degrees Celsius overnight. Cleared lysates were incubated with probe-conjugated streptavidin beads in 1x TENT at 4 degrees overnight. Beads were washed three times in 1x TENT without inhibitors and eluted by adding 10ug RNAse A to each tube for 1h at room temperature.

ESI-FTICR MS/MS was performed on eluted samples and flowthroughs at the Pasarow Mass Spectrometry facility, UCLA. Candidate proteins were determined by identifying proteins unique to eluates from 5'OH miR-34a 3'biotin-incubated beads with scores above 20. After initial curation, candidate proteins were cross-referenced with RBPDP [24]. Identification of paraspeckle proteins was performed by Gene Ontology analysis of candidate proteins for cellular components[25, 26].

Luciferase assay

Dual luciferase plasmids were created using the Promega PsiCHECK-2 platform as previously described[27]. To create plasmids for measuring the expression of the indicated miRNAs, seed sequences complementary to the target miRNA were edited into the 3'UTR of Renilla luciferase. Briefly, the psiCHECK2 backbone was cut with XhoI and NotI, followed by

insertion of oligonucleotides containing the indicated seed sequence. Seed sequences were accessed from miRBase[28], and control sequences were generated using the inverse of the wildtype sequence.

Cells were cultured in 60mm plates at 50% confluency in triplicate and transfected with 1ug PsiCHECK-2 plasmid and 5uL Lipofectamine-2000 per condition. 12h after transfection, triplicate plates were pooled and split onto 60mm plates. 24h after transfection, cells were irradiated with a single 6 Gy dose at a rate of 1.15Gy/min.

At the indicated time points, cells were washed twice in PBS and lysed using 750uL 1x Passive Lysis Buffer (Promega). 20uL of unclarified lysate was added to a white-walled 96 well plate and measured on a multiwell plate reader (SpectraMax iD3) in duplicate with a two second read time and no delay according to the Promega DualGLO protocol (Promega #E1980).

Relative miRNA activity was calculated according to manufacturer specifications. Briefly, raw luminescence from four readings for each condition were averaged, background luminescence subtracted, and the ratio of luminescence from the Renilla to the firefly luciferase reporter was taken. To assess miRNA-responsive activity, the ratio of parallel transfections of PsiCHECK plasmids containing wildtype miRNA seed sequences or scrambled seed sequences was taken and normalized to unirradiated controls. Error bars represent pooled standard error of the mean of three repeats. * = $P < 0.05$.

RNA extraction and RT-PCR

Confluent plates were split into 60mm plates at 50% confluency and irradiated with a single 6 Gy dose 24h after passaging. At the indicated time points after a single 6 Gy dose, plates

were scraped into cold PBS, pelleted, and resuspended in 300uL QiaZOL lysis reagent for RNA purification using the miRNEasy Mini Kit (Qiagen #217004).

Total cDNA was synthesized according to manufacturer specifications (Thermo Fisher TaqMan miRNA). Briefly, 20ng of input RNA was mixed 1:1 with a master mix containing random primers to generate whole-genome cDNA for quantification of mRNA transcripts. miRNA transcript cDNA was synthesized using transcript-specific hairpin primers- 10ng of input RNA was mixed with 5x TaqMan miRNA probes for each target and master mix. Synthesized cDNA for all targets was quantified using TaqMan amplification on a QuantStudio 3, per manufacturer instructions. Transcript expression was normalized to endogenous U6 expression. Data represents three independent replicates of three samples each.

Fluorescence Microscopy

22mm square coverslips (Thermo Fisher #102222) were ethanol-sterilized and coated with poly(L) lysine for 30 minutes at room temperature, then seeded with 100,000 cells per condition. 24h after plating, cells were either irradiated for time course experiments or fixed for all other experiments.

miRNA in situ hybridization was performed as previously described [29] with modifications. Briefly, cultured cells were affixed to slides as described above, and desiccation, proteinase K incubation, and acetylation steps were omitted. TSA amplification and hybridization using 2pmol 5' DIG-labelled Qiagen miRcury mimics were performed as described, with hybridization at 45 degrees Celsius (miR-34 and let-7) or 50 degrees (miR-17). Streptavidin incubation was performed using 5:100 TexasRed-Streptavidin (Sigma-Aldrich #189738).

NEAT1 ISH and sequential immunofluorescence-ISH were performed using Stellaris FISH probes [30]. Briefly, formaldehyde-fixed coverslips were permeabilized with Triton X-100 and incubated with 1:50 anti-PSF primary antibody (Sigma #P2860) followed by fluorophore-conjugated secondary antibody (Thermo Fisher **A32723**). Slides were washed and incubated overnight at 37 degrees Celsius with 1uL 12.5uM (12.5pmol) Stellaris FISH probe in 100uL Stellaris hybridization buffer. Coverslips were washed and mounted on slides with 15uL VectaShield mounting media with DAPI (Vector Laboratories #H-1000).

All coverslips were imaged using a Zeiss LSM700 confocal microscope at 100x magnification. Images represent maximum intensity projections of Z-stacks collected on cell nuclei. To ensure verifiable nuclear localization of foci, quantification of nuclear foci was performed on individual slices, with only foci colocalized with DAPI signal and distinct from cytoplasmic signal from neighbouring cells were counted.

Results

Paraspeckle proteins interact with unphosphorylated miR-34a

Since rates of miR-34a transcription in A549s are low at baseline[31] and the unphosphorylated pool is detectably large [13], we hypothesized that unphosphorylated miR-34 must be stabilized within cells at steady-state conditions. To detect proteins responsible for stabilizing the unphosphorylated pool, we incubated sonicated whole-cell lysates with 3' biotinylated mimics of miR-34a with either a 5' phosphate or 5' hydroxyl[32]. Since other miRNAs do not appear to have unphosphorylated pools, we also included a 5'OH 22-nucleotide

RNA containing the sequence of miR-34 with the seed sequence inverted to demonstrate sequence specificity of identified proteins.

Interacting proteins were isolated and purified by conjugating miRNA mimics to streptavidin beads and incubating with sonicated whole-cell lysates. Mass spectrometry on unsonicated lysates did not recover significant proteins above background (Data not shown), consistent with the nuclear localization of unphosphorylated miR-34a [13]. Given the high affinity between biotin and streptavidin, we eluted proteins by incubating with RNAse A to degrade the linker RNA between the beads and the target proteins (Figure 2.1A)

Mass spectrometry of eluted proteins was then processed to identify significantly-enriched proteins unique to the 5'OH miR-34 sample (Figure 2.1B). Briefly, proteins were analyzed for significant enrichment in the mass spectrometry dataset, presence in three independent replicates, and presence of a canonical RNA binding domain[24]. We identified 199 proteins unique to the 5'OH miR-34 sample, representing 49.8 percent of all proteins identified in that sample (Figure 2.1C). Overlap between samples was common, implying many of these proteins bound to the sequence, backbone, or 3' termini of the probes- 109 proteins were detected binding to all RNA probes, and 61 bound to any miR-34 mimic independent of 5' phosphorylation status. Gene Ontogeny (GO) analysis[25] on cellular compartments for the 199 significant proteins isolated uniquely in the 5'OH miR-34 sample showed strong enrichment of nuclear paraspeckle proteins, presenting a hypothesis that paraspeckles interact with 5'OH miR-34 (Figure 2.1E). While this set is not entirely comprised of paraspeckle proteins, it isolated 52.5% of all known paraspeckle proteins and 85.7% of all proteins required for paraspeckle

formation[33]. Western blotting was performed to confirm isolation of specific proteins in the MS/MS data set (Figure 2.1D). A complete list of isolated proteins is shown in Table 2.2.

Cas9-mediated deletion of paraspeckle formation

To investigate the effect of paraspeckle loss on the unphosphorylated pool, we designed Cas9-mediated deletion of the triple helix motif of the lncRNA NEAT1_2 (NEAT1 dTH), which is responsible for stabilizing the transcript and maintaining the structure of paraspeckles (Figure 2.2A). Since the triple helix motif is required for the stability of the longer NEAT1_2 isoform but not the shorter NEAT1_1 (Figure 2.2A), and NEAT1_2 is necessary for paraspeckle formation and phase separation (Figure 2.2B), deletion of the triple helix motif causes loss of paraspeckle formation, consistent with prior reports describing deletion of the NEAT1_2 triple helix motif [15].

RT-PCR for both NEAT1_2 and total NEAT1, including NEAT1_1, showed a significant decrease in NEAT1_2 levels and a moderate decrease in total NEAT1 levels, confirming destabilization of the longer isoform (Figure 2.2C). *In situ* hybridization for middle regions of NEAT1_2 alongside immunofluorescence for the paraspeckle marker protein PSF showed colocalization in wildtype A549 cells, with punctate signal for both targets lost upon deletion of the NEAT1_2 triple helix motif (Figure 2.2E, quantified in Figure 2.4C). Consistent with prior reports that loss of NEAT1_2 is phenotypically mild [15, 34], dTH cells show no morphological differences (data not shown) and no difference in viability or rate of growth (Figure 2.2D).

Loss of paraspeckle formation disrupts unphosphorylated miR-34 activity

To assess the activity of radiation-responsive miRNAs, dual-luciferase reporters were used to quantify relative capacity for miRNAs to bind to repressive 3'UTR elements as previously described [13] (Figure 2.3A-B). These data were paired with RT-PCR for mature miRNA sequences to assess relative expression of miRNAs after IR. Since prior work demonstrated that miR-34a activity less than 6h after IR originates from phosphorylation of the unphosphorylated pool rather than *de novo* transcription and processing[13], we hypothesized that loss of paraspeckle formation would eliminate this unphosphorylated pool and result in loss of early miR-34 activity after IR.

Accordingly, the activity of miR-34a after a single 6 Gy dose increased rapidly in A549wt cells, including a spike in activity 1h after irradiation that was not detected in A549 dTH cells (a 37% increase relative to baseline in WT ($p = 0.0002$) and a 4% decrease in dTH cells ($p=0.12$) (Figure 2.3C). Both wildtype and dTH cells demonstrated an increase in miR-34 activity at later time points after IR – activity of miR-34a began increasing 6h after IR in both cell lines (42.2% and 11%, respectively). 24h after IR, activity had increased 86% relative to baseline in wildtype cells, and 46% in dTH cells. While dTH cells showed lower activity and expression at all time points tested, the difference in increased activity between cell lines was only significant 1h after IR ($p=0.02$) prior to *de novo* transcription [13]. Additionally, RT-PCR for pri- and pre-miR-34 showed little difference between WT and dTH cells (Figure 2.3D), implying that paraspeckles are not necessary for *de novo* transcription and processing of the total miR-34 population- although without relative quantification of the size of the unphosphorylated and total pools, it is difficult to conclude whether the unphosphorylated pool is processed in a paraspeckle-dependent manner. Loss of paraspeckle formation did not significantly affect the activity or expression of

the unrelated miRNAs miR-17 and let-7 (Figure 2.5A), which are known to lack unphosphorylated pools[13].

Paraspeckles are required for nuclear localization of miR-34

To assess the effects of paraspeckle formation on miR-34a localization, we performed *in situ* hybridization (ISH) against miR-34a in WT and dTH cells. Prior reports have demonstrated that mature-length unphosphorylated miR-34a resides in the nucleus [13], in contrast to more typical cytoplasmic localization of Ago2-associated miRNAs. Accordingly, ISH against miR-34a in WT cells showed punctate nuclear localization in addition to typical cytoplasmic localization. Deletion of paraspeckle formation in dTH cells caused a significant decrease in punctate nuclear localization ($p<0.01$) with no detectable effect on cytoplasmic miR-34a (Figure 4). ISH for miRNA species known to lack an unphosphorylated pool showed occasional nuclear foci that were not affected by deletion of nuclear paraspeckles (Figure 4b,c). While nuclear localization of miRNA ISH targets could be explained by pri-miRNAs, the loss of nuclear miR-34a foci specifically in dTH cells with no change in other miRNA species, paired with past observations of a nuclear population of fully-processed, unphosphorylated miR-34a, implies that paraspeckles coordinate nuclear localization of unphosphorylated miR-34a.

Since IR activates the unphosphorylated pool and directs its loading onto Ago2, we hypothesized that the nuclear localization as detected by tyramide-amplified ISH would show a loss of punctate nuclear signal in irradiated cells with intact paraspeckles. Surprisingly, ISH performed at 1h and 3h after a single 6 Gy dose showed an increase in nuclear miR-34 foci that becomes more pronounced over time (Figure 4D). Given that this increase occurs in both WT

and dTH A549s, it is likely that these nuclear foci represent unprocessed pri-miRNAs, which contain the same sequences that hybridize to the LNA probes used in the tyramide amplification protocol and should be ISH targets of similar fidelity. Indeed, RT-PCR for pri- and pre-miRNAs at these time points show an increase in pri-mIR-34 levels at the relevant time points (Figure 2.3D), consistent with p53-dependent *de novo* transcription and processing of canonical miR-34 after IR. While levels of pre-miR-34 trended higher 3h after IR in wildtype cells (a fold change of 3.29 and 2.18, respectively), this result did not reach statistical significance (p=0.11). Similarly, other miRNAs investigated in this study do not show IR-dependent *de novo* transcription, and likewise do not show an increase in nuclear foci formation after IR (Figure 2.5B).

Discussion

In this work, we demonstrate that the nuclear localization and radiation-responsive activity of miR-34a at early time points after irradiation is dependent on nuclear paraspeckles. While most mature miRNAs are stabilized by binding to Ago2 concomitant with pre-miRNA processing [35, 36], unphosphorylated miRNAs are not Ago2-associated[13], consistent with Ago2 binding directly to the 5' phosphate[3]. Accordingly, localization of fully processed, unphosphorylated miR-34 within nuclear paraspeckles offers an alternative hypothesis to maintain the stability of the unphosphorylated pool before IR-mediated activation. Mass spectrometry performed on eluates from biotinylated miRNA mimics showed significant enrichment of paraspeckle proteins interacting with 5'OH miR-34a, leading to a hypothesis that nuclear paraspeckles interacted with unphosphorylated miR-34a *in vitro.* We have demonstrated that early activity of miR-34a but not other miRNAs after IR is dependent on nuclear paraspeckles, consistent with prior reports that early miR-34a activity is mediated by

rapid phosphorylation of an unphosphorylated pool. We have also demonstrated that miR-34a forms punctate nuclear localization in wildtype cells, but not in cells lacking nuclear paraspeckles, demonstrating that the localization of unphosphorylated miR-34a is mediated by paraspeckle formation.

While this work provides important preliminary information on the localization and stabilization of unphosphorylated miRNAs, further characterization of the mechanism and function of unphosphorylated miR-34 would be valuable. Most notably, while previous work[13] has demonstrated that phosphorylation of the unphosphorylated pool is dependent on the master DNA repair kinase ATM and the nucleotide kinase hClp1, neither protein has been previously shown to interact directly with nuclear paraspeckles. While hClp1 localization is complicated by its lack of punctate nuclear localization both before and after IR (Data not shown) ATM is known to rapidly change localization after DNA damage[37]- studies combining live-cell fluorescence for a paraspeckle marker protein[38] and tagged ATM[39] could reveal ATM-dependent chemistry at the surface of the paraspeckle, which would provide important mechanistic insights not only into activation of unphosphorylated miR-34, but also of stimulus-specific responses mediated by paraspeckles. To our knowledge, FUS is the only direct ATM target protein resident in nuclear paraspeckles- future studies of the phosphorylation of paraspeckle-resident FUS by ATM after IR could give important insight into how paraspeckles regulate stress responses.

To date, miR-34a is the only miRNA known to maintain an unphosphorylated pool. Given that paraspeckles have been shown to regulate unphosphorylated mIR-34, studies investigating whole miRNA levels in WT and DTH cells could reveal populations of miRNAs with variable 5’

phosphorylation status. In particular, small RNA sequencing in cells with and without paraspeckles could reveal different populations of small RNAs sensitive to ligation using 5' adapters, which require 5' phosphates [40, 41]. Further studies into shared features in sequence, structure, or interacting partners of other unphosphorylated miRNAs could lead to important insights on how unphosphorylated miRNAs are synthesized or transported to paraspeckles. Additionally, since paraspeckles have been shown to coordinate multiple stress responses [20-22], it is plausible that unphosphorylated miRNAs similarly respond to different stresses. While we have not yet investigated these other stresses, it would be interesting to see if IR activates other unphosphorylated miRNAs, or if paraspeckles maintain distinct cargoes to respond to distinct stimuli.

Present data also do not outline a clear hypothesis for the synthesis of unphosphorylated miR-34a. While prior work has shown that paraspeckles can regulate processing of specific miRNA species by recruiting the Microprocessor complex[42], the population of miRNAs described in that work does not include miR-34a, and other species described in that work (e.g. miR-17) do not appear to have unphosphorylated pools, implying that the unphosphorylated pool is not exclusively produced by paraspeckle-associated Microprocessor. Indeed, siRNA-mediated knockdown of Drosha and Dicer shows accumulation of pri- and pre-miRNAs, respectively, but irradiated WT A549s still show increased miR-34a activity relative to unirradiated controls 36h after IR, implying that the unphosphorylated pool is either stable for a prolonged period after transcription or is produced independent of canonical miRNA processing[13].

The localization of enzymes implicated in miRNA processing relative to the unphosphorylated pool also poses an interesting question- canonically, pri-miRNAs are moved to the cytoplasm by Xpo5 after cleavage by DROSHA, and both pre- and mature miRNAs are cytoplasmic. Both this work and prior study of unphosphorylated miR-34[13] agree that the unphosphorylated pool is nuclear and fully processed- future investigations into the synthesis of the unphosphorylated pool might benefit from controlling the localization of Dicer, which does sometimes localize to the nucleus, where it complexes with ADAR2, which is responsible for deaminating adenines on mRNAs and has been implicated in transporting inosine-modified transcripts to the paraspeckle. Alternatively, unphosphorylated miRNAs may be synthesized by an entirely novel process- further investigation into the synthesis rate of unphosphorylated miRNAs, paired with siRNA-mediated inhibition of canonical processing factors, could further reveal if the unphosphorylated pool is synthesized by similar mechanisms used by other miRNAs.

This work represents an important mechanistic step in studying unphosphorylated miRNAs- modulating nuclear paraspeckle formation is phenotypically mild, but may coordinate diverse cellular stress responses *via* maintenance of stress-responsive unphosphorylated miRNA pools. Paraspeckle formation is responsible for the early radiation-responsive activity and punctate nuclear localization of unphosphorylated miR-34, and future studies of paraspeckle-associated miRNAs may unveil broader stress responses sharing similar mechanisms.

Figures

Oligonucleotides		
gRNA oligos:	**Sequence 5'->3'**	**Notes**
NEAT1 ΔTH Fwd	GGTGGCACGTCCAGCACGGC	For deletion of the NEAT1_2 triple helix motif
NEAT1 ΔTH Rev	CAAAACCTGAGTGCGGCCAT	
SFPQ Promoter Fwd	CACCGCTTGACCACAGACATGTCTC	For Cas9 editing of the SFPQ promoter. From Li et al., RNA 2017
SFPQ Promoter Rev	AAACGAGACATGTCTGTGGTCAAGC	
Rbm3	N/A	Santa Cruz Biotechnology Cat# sc-406296
NUDT21	N/A	Santa Cruz Biotechnology Cat# sc-402082

Sequencing oligos:	**Sequence 5'->3'**	**Notes**
NEAT1 ΔTH Fwd	GACTGTGCCTCGTGTTCAGT	For sequencing cells with Cas9 editing of NEAT1 triple helix
NEAT1 ΔTH Rev	CACGTCCCCTGCTGTATTCC	For sequencing cells with Cas9 editing of NEAT1 triple helix
SFPQ Promoter Inside Fwd	GACGTAAACGGCCACAAGTTC	For sequencing GFP-SFPQ edited cells. Sequence is inside eGFP.
SFPQ Promoter Inside Rev	CTCAGGTAGTGGTTGTCGGG	For sequencing GFP-SFPQ edited cells. Sequence is inside eGFP.
SFPQ Promoter Outside Fwd	ATTGGAGCTGTCGATCGTGG	For sequencing GFP-SFPQ edited cells. Sequence flanks the edited region.
SFPQ Promoter Outside Rev	GAGAACGGAAGTCGTGGAGG	For sequencing GFP-SFPQ edited cells.

		Sequence flanks the edited region.
PsiCHECK Fwd	CGTGCTGAAGAACGAGCAGT	For sequencing PsiCHECK2 plasmids
PsiCHECK Rev	CAAACCCCCGCCTCCACGG	For sequencing PsiCHECK2 plasmids

Synthetic RNAs	**Sequence 5'->3'**	**Notes**
miR-34- Mass Spec	UGGCAGUGUCUUAGCUGGUUGU	3' biotin, 5' OH or 5' phosphate.
miR-34 Scramble - Mass Spec	UCCGUCACACUUAGCUGGUUGU	Synthesized with 5' OH.
miR-34a ISH	UGGCAGUGUCUUAGCUGGUUGU	5' phosphate , 3' digoxigenin
let-7a ISH	UGAGGUAGUAGGUUGUAUAGUU	5' phosphate , 3' digoxigenin
miR-17 ISH	CAAAGUGCUUACAGUGCAGGUAG	5' phosphate , 3' digoxigenin
Scramble ISH	GTGTAACACGTCTATACGCCCA	5' phosphate , 3' digoxigenin
U6 ISH	CACGAATTTGCGTGTCATCCTT	5' phosphate, 3' digoxigenin
NEAT1_m-CAL Fluor Red 610	Nucleotides 3800-11700 of NR_131012.1	Stellaris #VSMF-2249-5.
GAPDH-CAL Fluor Red 610	Nucleotides 175-1182 of NM_002046.4	Stellaris VSMF-2149-5.
eGFP-CAL Fluor Red 610	Nucleotides 289-1005 of U76561	Stellaris VSMF-1013-5.

PsiCHECK Plasmids	**Sequence 5'->3'**	**Notes**
PsiCHECK2 backbone	Sequences cloned into Xho1 and Not1 restriction sites	Promega #C8021
PsiCHECK2-miR-34-WT	TCGAGTCAACCAGCTAAGACACTGCCAGC	Addgene #78258
PsiCHECK2-miR-34-MUT	TCGAGACAACCAGCTATCACACACGGAGC	Addgene #78259
PsiCHECK2-let-7-WT	TCGAGAACTATACAACCTACTACCTCAGC	Addgene #78260
PsiCHECK2-let-7-MUT	TCGAGAACTATACAACGAACTAGGAGAGC	Addgene #78261

PsiCHECK2-miR-17-WT	TCGAGCCCGGGAATTCGTTTAAACCTAGAGC	Addgene #78262
PsiCHECK2-miR-17-MUT	TCGAGCCCGGGAATTCGTTTAAACCTAGAGC	Addgene #78263

RT-PCR Primers	Catalogue Number	Assay ID
miR-34a	4440887	000426
let-7	4440887	002307
miR-17	4440887	002308
U6	4440887	001973
Pri-miR-34	4427012	Hs03302884_pri
Pre-miR-34	4427012	Hs04333908
NEAT1 Total	4331182	Hs03453534_s1
NEAT1_2	4331182	Hs03924655_s1
GAPD	4331182	Hs02758991
Cdk4	4331182	Hs00364847
Bcl2	4331182	Hs04986394

Antibodies
For Immunofluorescence

Target	Conc.	Block	Manufacturer	Catalogue #	Species	Secondary Conc.
PSF	1:50	N/A	Sigma-Aldrich	P2860	Mouse	1:150

For Western Blotting

Target	Conc.	Block	Manufacturer	Catalogue #	Species	Secondary Conc.
Tubulin	1:1000	5% milk/TBST	Abcam	ab15246	Rabbit	1:1000
Bcl2	1:1000	5% milk/TBST	CST	15071	Mouse	1:1000
Cdk4	1:1000	5% milk/TBST	CST	12790	Rabbit	1:1000
Lamin	1:1000	5% milk/TBST	Abcam	ab229025	Rabbit	1:1000
FUS	1:1500	5% milk/TBST	Thermo Fisher	60160	Mouse	1:1000
Rbm3	1:300	5% milk/TBST	Santa Cruz	sc-390139	Mouse	1:1000
DAZAP	1:500	5% milk/TBST	Abcam	ab106851	Rabbit	1:1000
NONO	1:500	5% milk/TBST	Novus	NB100-1556	Rabbit	1:1000
NUDT21	1:150	5% milk/TBST	Abcam	ab221994	Rabbit	1:1000

Table 2.1- Oligonucleotides, synthetic RNAs, plasmids, probes, and antibodies used in these studies. Catalogue numbers are provided for oligonucleotides without publicly available sequences.

miR-34 5'OH

Accession	Score	Mass	emPAI
P09651	4028	38837	21.03
P22626	2707	37464	10.49
P04406	2290	36201	77.35
Q96AE4	1739	67690	2.93
Q92945	1652	73355	1.61
P00352	1429	55454	5.64
P29401	1120	68519	2.69
P04075	1101	39851	4.3
Q9BUJ2	1053	96250	1.08
P68104	999	50451	1.27
O14979	992	46580	2.41
O60218	933	36225	4.72
P52272	884	77749	1.47
P00558	864	44985	1.5
P51991	853	39799	3.52
P42330	836	37229	5.48
P31943	836	49484	1.98
Q14103	809	38581	3.73
P62937	798	18229	11.67
P19338	788	76625	1.03
P60709	764	42052	2.09
P26599	750	57357	2.21
P07355	724	38808	4.09
Q96EP5	700	43584	1.77
Q92879	682	52429	2.37
Q96I24	673	61944	1.53
P40926	653	35937	2.42
P06733	625	47481	1.38
P04083	584	38918	1.87
P09429	582	25049	4.71
P05783	580	48029	2.51
P23284	578	23785	6.16
P23528	547	18719	2.73
P35637	536	53622	0.81
P13645	530	59020	0.63
P26038	511	67892	1.44
P10809	481	61187	1.3
P68363	468	50804	1.4
P63241	456	17049	9.35
Q01130	452	25461	1.09
P52895	441	37111	2.59
P52597	434	45985	0.86

miR-34 5'P

Accession	Score	Mass	emPAI
P09651	1691	38837	5.5
P04406	1614	36201	12.69
P04264	1317	66170	2.18
P13645	1181	59020	2.11
P22626	899	37464	2.54
P00352	899	55454	2.74
P04075	680	39851	2.04
Q96AE4	624	67690	1.13
O60218	571	36225	2.39
P29401	517	68519	0.83
P35527	477	62255	0.85
P68104	446	50451	0.65
O14979	393	46580	0.98
P26599	380	57357	0.47
Q9BUJ2	367	96250	0.49
P42330	358	37229	0.97
P40926	346	35937	1.2
P07355	344	38808	1.08
P31943	331	49484	0.9
Q04828	317	37221	1.34
P09429	316	25049	2.47
P51991	300	39799	0.74
P06733	290	47481	0.49
Q96EP5	287	43584	0.66
Q92945	284	73355	0.3
P10809	252	61187	0.52
P61978	235	51230	0.75
P05783	227	48029	0.49
P30838	227	50762	0.46
P63241	225	17049	3.21
P35908	223	65678	0.4
P63261	223	42108	0.83
P23284	221	23785	1.51
P08238	214	83554	0.17
P62937	214	18229	2.27
Q14103	203	38581	0.92
P14866	203	64720	0.28
P07900	200	85006	0.16
A0A2R8Y7X9	200	18466	0.18
P52597	188	45985	0.23
P52272	174	77749	0.18
Q12906	173	95678	0.14

P61978	428	51230	1.24
P08238	416	83554	0.52
P05787	400	53671	1.43
P04264	400	66170	0.7
Q15056	378	27425	2.94
P07900	368	85006	0.57
P68032	362	42334	0.57
P14866	352	64720	0.41
Q06830	339	22324	5.12
P15311	336	69484	0.9
Q7KZF4	321	102618	0.6
Q99729	315	36316	1.01
P07437	311	50095	0.46
P30838	308	50762	0.65
P11142	308	71082	0.79
P13639	301	96246	0.54
P04350	295	50010	0.37
O95994	294	20024	3.71
P06744	290	63335	0.5
P15121	279	36230	0.84
P02545	279	74380	0.54
P98179	276	17160	2.49
P54819	266	26689	0.8
P11940	263	70854	0.5
P11021	261	72402	0.36
P00338	257	36950	1.56
Q01844	256	68721	0.38
P14618	249	58470	0.63
P63220	248	9220	1.61
Q14011	246	18637	1.29
P06576	239	56525	0.48
Q14847	231	30097	1.08
Q16881	231	71832	0.43
Q00839	231	91269	0.15
P35241	225	68635	0.75
P61604	224	10925	2.95
P60174	222	31057	0.66
P07195	217	36900	0.53
Q13310	217	71080	0.37
P25705	213	59828	0.24
P52209	207	53619	0.35
Q8NC51	200	44995	0.53
Q8N257	199	13900	1.4
P02768	199	71317	0.37
P54819	172	26689	0.6
P69905	170	15305	7.97
Q8NC51	165	44995	0.42
Q96I24	161	61944	0.43
P07814	160	172080	0.06
Q92879	158	52429	0.73
Q06830	157	22324	2.05
P05787	136	53671	0.43
Q8WUH6	136	11741	0.67
P61604	136	10925	1.28
P26038	135	67892	0.21
P23528	125	18719	1.28
Q00839	123	91269	0.15
Q13442	121	20618	0.35
P15121	120	36230	0.3
P52209	118	53619	0.19
O75390	115	51908	0.2
P39019	113	16051	0.77
P00338	112	36950	0.41
P02768	110	71317	0.2
Q99729	106	36316	0.42
Q9BQE3	104	50548	0.29
P04083	103	38918	0.28
P62328	103	5050	0.73
Q14847	98	30097	0.52
P0C7P4	97	31081	0.11
P13639	96	96246	0.18
P62263	94	16434	0.75
P23588	93	69167	0.05
Q99497	93	20050	0.85
P38646	92	73920	0.09
P06744	92	63335	0.22
P35637	92	53622	0.19
P60174	91	31057	0.5
Q12849	91	53606	0.06
P68032	88	42334	0.35
P62979	86	18296	0.96
P07998	85	18089	6.72
P11142	85	71082	0.2
P22392	85	17401	0.7
Q01130	84	25461	0.28
P62424	83	30148	0.68
O43809	83	26268	0.27
Q01105	83	33469	0.1

O43809	195	26268	1.04
P53396	191	121674	0.27
Q09666	184	629213	0.05
P63244	182	35511	0.7
Q92804	180	62021	0.43
Q12906	179	95678	0.14
P10599	176	12015	1.73
Q96DH6	176	35345	0.43
Q13442	175	20618	0.82
P16989	174	40066	0.17
Q13011	172	36136	0.55
P55795	172	49517	0.57
Q15046	172	68461	0.32
P35221	169	100693	0.17
Q9NTZ6	167	97561	0.3
P35527	160	62255	0.23
P23588	160	69167	0.15
P22392	159	17401	1.88
A0A2R8Y7X9	155	18466	0.18
Q15717	155	36240	0.42
P07814	155	172080	0.06
P38646	154	73920	0.14
A0A0U1RRH7	153	18541	0.95
Q00688	153	25218	1.38
P0DP23	151	16827	1.48
P00505	151	47886	0.49
P67809	148	35903	0.19
P07737	143	15216	2.34
Q13151	142	30993	0.5
P31942	141	36960	0.41
P14625	140	92696	0.19
P62979	139	18296	0.66
P07237	139	57480	0.39
P37837	137	37688	0.18
P39019	136	16051	1.14
P31483	130	43278	0.34
P55145	129	21143	1.09
O75390	128	51908	0.2
P08195	128	68180	0.45
O43776	126	63758	0.35
Q04837	125	17249	0.43
P26368	125	53809	0.19
P53999	124	14386	0.52
P0DMV8	119	70294	0.2
O60701	83	55674	0.19
P63220	81	9220	0.38
P02545	81	74380	0.14
P21291	80	21409	0.54
P09211	79	23569	0.3
P63313	76	5023	0.73
A0A0A6YYL6	75	26698	0.79
Q86V81	75	26872	0.26
P55145	75	21143	0.8
A0A087X1C1	72	9188	0.38
P23193	71	34404	0.2
P31025	71	19409	0.17
P13804	71	35400	0.09
P30101	70	57146	0.06
P26368	67	53809	0.06
P00505	65	47886	0.14
Q13509	63	50856	0.28
P15311	62	69484	0.15
P11940	62	70854	0.05
Q14CN4	61	56470	0.18
Q13011	61	36136	0.09
P10599	61	12015	0.65
Q8NHM4	60	27090	0.26
P15559	58	30905	0.5
P30405	57	22368	0.15
Q13177	57	58291	0.12
P11413	56	59675	0.05
O60814	55	13882	0.93
P11021	55	72402	0.14
P62304	54	10854	0.32
Q14011	54	18637	0.39
B4DLN1	53	48582	0.07
P06703	53	10230	0.34
P36542	52	33032	0.21
P81605	52	11391	0.3
P31942	51	36960	0.09
P61626	51	16982	0.2
P62753	51	28834	0.11
Q13409	51	71811	0.05
O60869	51	16359	0.76
Q9UQ80	51	44101	0.15
P60842	50	46353	0.07
P26885	50	15810	0.79
P00558	50	44985	0.07

P15559	118	30905	0.5
P45880	117	32060	0.48
P11413	116	59675	0.24
P62318	113	14021	1.38
P69905	112	15305	2.31
Q07021	112	31742	0.22
P08729	110	51411	0.36
P12956	109	70084	0.2
P81605	107	11391	0.69
O60701	107	55674	0.19
O14602	105	16546	0.45
P06703	103	10230	0.79
P60842	103	46353	0.23
A0A087X1C1	102	9188	0.38
P09936	100	25151	0.45
Q15365	100	37987	0.52
P43490	97	55772	0.19
Q8WUH6	96	11741	1.15
P21796	96	30868	0.23
P30101	96	57146	0.18
P62328	94	5050	0.73
P26583	94	24190	0.47
P38117	94	28054	0.25
P62263	93	16434	0.45
P05165	92	80635	0.22
O75369	92	280157	0.05
P23246	91	76216	0.13
P55072	91	89950	0.15
P07998	90	18089	6.72
P46782	90	23033	0.14
P21333	90	283301	0.07
O60869	89	16359	1.12
O60506	89	69788	0.26
P26885	86	15810	0.79
O15347	86	23137	0.71
P16152	86	30641	0.36
Q01105	86	33469	0.21
P31948	86	63227	0.16
P41567	85	12839	2.23
P63313	83	5023	0.73
P62805	83	11360	1.21
P51572	79	28031	0.12
P35908	79	65678	0.21
P62258	78	29326	0.11
P12956	49	70084	0.05
P02533	48	51872	0.2
Q5JTJ3	48	14449	0.23
Q15056	48	27425	0.26
O95994	47	20024	0.17
Q9P2E9	46	152764	0.04
O43175	46	57356	0.06
A0A075B6Z2	45	2220	1.8
P51572	44	28031	0.25
P08195	43	68180	0.15
P05023	42	114135	0.03
P15880	42	31590	0.22
P30044	41	22301	0.15
P06576	41	56525	0.12
P07477	40	27111	0.41
Q9UMS4	40	55603	0.06
P51884	40	38747	0.09
Q96DH6	39	35345	0.09
P07195	39	36900	0.29
P21796	39	30868	0.11
P26583	38	24190	0.29
Q96HC4	38	65102	0.05
Q15427	38	44414	0.07
Q07955	37	27842	0.12
P84103	36	19546	0.17
P25398	36	14905	0.51
P22314	35	118858	0.06
Q01085	35	41906	0.08
Q05682	34	93232	0.03
Q93088	34	45426	0.07
Q02790	34	52057	0.06
P67936	34	28619	0.12
Q9P258	33	56790	0.06
P99999	33	11855	0.29
P45880	33	32060	0.22
Q01518	33	52325	0.2
P0DMV8	33	70294	0.15
O75347	32	12904	0.26
P20774	32	34243	0.1
P54577	32	59448	0.06
Q5T749	32	67172	0.05
P62888	30	12947	0.26
Q9UHR5	30	33964	0.1
P18206	29	124292	0.03

Q16698	78	36330	0.09
P09211	77	23569	0.3
B4DLN1	77	48582	0.14
P60903	76	11310	1.21
P63104	76	27899	0.4
P13804	76	35400	0.2
Q15019	76	41689	0.26
P38159	76	42306	0.08
P25398	75	14905	0.51
Q86V81	75	26872	0.12
Q15084	75	48490	0.07
Q08257	74	35356	0.31
P0C7P4	73	31081	0.11
P35030	73	33306	0.21
Q12849	73	53606	0.19
O95202	73	83986	0.08
P21291	72	21409	1.06
P30048	72	28017	0.4
Q92928	71	22231	0.32
P61158	71	47797	0.22
P27797	71	48283	0.14
Q14697	70	107263	0.16
P13693	69	19697	0.37
Q12905	69	43263	0.16
A0A0A6YYL6	68	26698	0.79
Q99497	67	20050	0.36
P23193	67	34404	0.2
O00151	67	36505	0.19
Q02790	67	52057	0.28
Q9P258	67	56790	0.06
P27816	67	121443	0.03
P05387	66	11658	0.67
Q9BYD6	65	37113	0.19
P09382	64	15048	0.5
Q13177	64	58291	0.12
P49458	63	10219	0.34
Q9HB71	62	26308	0.43
P30040	62	29032	0.38
P06748	62	32726	0.21
P50395	62	51087	0.13
P42704	62	159003	0.04
Q02878	61	32765	0.21
P31040	61	73672	0.09
Q9P2E9	61	152764	0.07
Q13573	29	61514	0.05
P62917	28	28235	0.25
Q01844	27	68721	0.05
Q8N9F7	27	36429	0.09
O75027	26	82874	0.04
Q15365	26	37987	0.09
P43034	26	47178	0.07
P04844	25	69355	0.05
Q9NZ45	25	12362	0.28
Q9UIU6	25	83168	0.12
O95490	25	165468	0.02
P04843	24	68641	0.05
P62906	24	24987	0.28
P14927	24	13522	0.25
P37837	23	37688	0.09
Q9Y5G8	23	101329	0.07
Q8IZH2	23	195524	0.02
Q14204	23	534809	0.01
Q9GZN7	23	32462	0.1
Q96L46	22	27814	0.12
Q9Y4I1	22	216979	0.01
P07737	22	15216	0.22
Q9NTZ6	22	97561	0.03
O60603	22	90920	0.07
P63244	21	35511	0.09
Q9HCM1	21	196561	0.02

P35579	61	227646	0.01
O15511	60	16367	0.21
O75347	58	12904	0.26
P12004	55	29092	0.11
Q9ULV4	55	53899	0.06
P33240	55	61035	0.05
Q15427	54	44414	0.07
Q16851	54	57076	0.06
O43175	54	57356	0.12
Q16891	54	84026	0.16
P36542	53	33032	0.1
O96008	53	38211	0.09
Q16555	53	62711	0.11
P62310	52	11838	0.29
P60981	52	18950	0.63
Q86U42	52	32843	0.1
P51884	52	38747	0.09
O43570	52	39711	0.08
P50991	52	58401	0.12
P30041	51	25133	0.13
P07858	51	38766	0.18
Q99798	51	86113	0.04
Q9GZT3	50	12398	0.62
Q8TEA8	50	23580	0.14
Q13148	50	45053	0.07
Q16719	50	52831	0.13
P04843	50	68641	0.15
P31949	49	11847	0.29
P30084	49	31823	0.34
P06753	49	32987	0.21
P42765	49	42354	0.35
P26641	49	50429	0.13
P49321	49	85471	0.04
Q9BRA2	48	14217	0.24
Q5JTJ3	48	14449	0.23
P62424	48	30148	0.52
Q01518	48	52325	0.06
Q15459	47	88888	0.04
Q9NUP9	46	21935	0.15
P09012	46	31259	0.22
Q86XP3	46	103197	0.03
A0A075B6Z2	45	2220	1.8
Q13409	45	71811	0.05
P62906	44	24987	0.13

Q16630	44	59344	0.06
O94826	44	68096	0.05
P04844	44	69355	0.1
Q15181	43	33095	0.1
O14745	43	39130	0.08
Q01085	43	41906	0.46
P08670	43	53676	0.13
E9PL57	42	19581	0.17
P14927	41	13522	0.25
P35613	41	42573	0.08
Q99873	41	43061	0.16
P05091	41	56859	0.12
Q92896	41	138341	0.05
Q07666	40	48311	0.07
P13797	40	71279	0.05
P18206	40	124292	0.05
Q8N684	39	52189	0.06
P50990	39	60153	0.05
P05556	39	91664	0.07
O43707	39	105245	0.06
P49773	38	13907	0.24
P18669	38	28900	0.39
P40925	38	36631	0.19
Q96HC4	38	65102	0.05
P98088	38	601963	0.01
Q9NQ39	37	20279	0.36
P09525	37	36088	0.09
Q15599	37	37619	0.18
P28482	37	41762	0.08
Q15233	37	54311	0.06
P49368	37	61066	0.05
Q12797	37	86266	0.04
P14174	36	12639	0.27
O75828	36	31230	0.11
Q9NR56	36	42531	0.25
Q16836	35	34329	0.1
P29558	35	44705	0.07
Q9Y383	35	46942	0.07
A6NCN2	34	29555	0.11
Q13283	34	52189	0.2
Q92499	34	83349	0.08
Q9H910	33	20108	0.17
P82979	33	23713	0.14
P99999	32	11855	1.14

P59998	32	19768	0.17
Q13242	32	25640	0.13
Q9P0L0	32	28103	0.25
Q00059	32	29306	0.11
P08758	32	35971	0.09
Q9NR45	32	40738	0.08
P61160	32	45017	0.15
Q93088	32	45426	0.07
Q96I99	32	46824	0.07
Q14498	32	59628	0.05
Q14157	32	114579	0.03
P63167	31	10530	0.33
P84103	31	19546	0.17
P23396	31	26842	0.12
P27348	31	28032	0.4
P12268	31	56226	0.06
Q92900	31	125578	0.03
P62273	30	6900	0.52
Q16695	30	15613	0.22
P30049	30	17479	0.19
Q16629	30	27578	0.26
P36873	30	37701	0.09
Q9UQ80	30	44101	0.15
P22234	30	47790	0.22
Q9UHD8	30	65646	0.05
Q9BVC6	29	26194	0.13
P15880	29	31590	0.22
P49411	29	49852	0.07
P10606	28	13915	0.24
P62750	28	17684	0.19
Q13185	28	20969	0.16
Q92688	28	28941	0.11
P20774	28	34243	0.1
Q15293	28	38866	0.08
P14314	28	60357	0.05
P49588	28	107484	0.03
P05023	28	114135	0.03
Q07955	27	27842	0.12
Q15691	27	30151	0.11
K7ERQ8	27	31771	0.1
Q8TCT9	27	41747	0.08
Q13435	27	100279	0.03
Q9H098	26	15548	0.48
P30044	26	22301	0.32

Q14696	26	26231	0.27
P36578	26	47953	0.07
Q8ND56	26	50727	0.06
Q9UIU6	26	83168	0.08
Q13263	26	90261	0.04
O94979	26	133900	0.02
P30405	25	22368	0.15
Q92522	25	22474	0.15
Q9NX63	25	26421	0.13
P47756	25	31616	0.1
P31930	25	53297	0.06
P78395	25	58650	0.06
Q92841	25	80906	0.04
O75027	25	82874	0.04
Q9HCM1	25	196561	0.02
Q15363	24	22860	0.15
Q96N11	24	50642	0.13
Q9Y3I0	24	55688	0.06
O75083	24	66836	0.05
P51659	24	80092	0.04
Q9HCG8	24	105972	0.03
Q9H0D6	24	109426	0.03
P22314	24	118858	0.06
P11498	24	130293	0.02
Q15149	24	533462	0.01
P62277	23	17212	0.2
P08134	23	22334	0.15
P48047	23	23377	0.14
P23919	23	23976	0.14
Q6P1N9	23	34150	0.1
O15143	23	41722	0.16
P31153	23	43975	0.07
Q969S9	23	87401	0.04
P07711	22	37996	0.09
P07099	22	53143	0.06
Q9UMS4	22	55603	0.06
Q14247	22	61720	0.05
Q9NZI8	22	63783	0.05
O94925	22	74269	0.04
Q9Y5G8	22	101329	0.03
P30050	21	17979	0.19
P16401	21	22566	0.15
Q96L46	21	27814	0.12
Q9BT09	21	31128	0.11

Q92890	21	34763	0.2
O43684	21	37587	0.09
Q16658	21	55123	0.06
O60603	21	90920	0.04
Q9NQC3	21	130250	0.02

No RNA

Accession	Score	Mass	emPAI
P13645	951	59020	1.13
P04264	717	66170	1.06
P05783	414	48029	0.59
P35527	320	62255	0.43
P29401	311	68519	0.32
P04083	306	38918	0.38
P04406	281	36201	0.3
P08670	221	53676	0.27
P07355	186	38808	0.5
P35579	173	227646	0.03
P68371	169	50255	0.07
P27348	158	28032	0.4
P10809	147	61187	0.11
P06733	144	47481	0.14
Q5QNW6	127	13912	0.55
P00352	123	55454	0.19
P09651	121	38837	0.18
P61978	113	51230	0.06
P06703	99	10230	0.79
P54819	95	26689	0.12
P05787	94	53671	0.19
P08727	93	44079	0.07
P63261	91	42108	0.16
Q9Y490	89	271766	0.01
P00338	84	36950	0.19
P68104	83	50451	0.13
A0A140TA62	83	50806	0.06
P20700	83	66653	0.05
P49588	82	107484	0.03
P61604	81	10925	0.32
Q01105	79	33469	0.1
P16104	77	15135	0.22
P15311	77	69484	0.1

Scramble 5'OH

Accession	Score	Mass	emPAI
P13645	1217	59020	3.07
P04264	1199	66170	3.05
P00352	848	55454	2.15
P35527	548	62255	1.16
P04075	511	39851	1.39
P04406	501	36201	1.39
P29401	365	68519	0.92
O60218	319	36225	1.19
P35908	308	65678	0.88
P09651	305	38837	1.45
P22626	259	37464	0.52
P68104	259	50451	0.55
Q04828	252	37221	0.81
P42330	240	37229	0.66
P09429	225	25049	1.39
P40926	219	35937	0.69
P62937	214	18229	0.97
A0A2R8Y7X9	198	18466	0.18
P07355	197	38808	0.63
P11021	172	72402	0.19
P07814	164	172080	0.06
P04083	162	38918	0.63
P06733	160	47481	0.31
P23284	156	23785	0.69
P10809	153	61187	0.3
P69905	152	15305	3.04
Q06830	145	22324	1.31
P62987	140	15004	0.84
Q96AE4	131	67690	0.21
M0QYT0	130	36392	0.41
P15121	129	36230	0.19
P30838	128	50762	0.21
P02768	116	71317	0.43

P04350	76	50010	0.07
P43490	76	55772	0.06
P23246	76	76216	0.04
P22626	75	37464	0.09
P52209	75	53619	0.06
P37802	73	22548	0.15
P13639	71	96246	0.07
P18206	71	124292	0.05
P49327	71	275877	0.01
P63241	70	17049	0.2
O60218	70	36225	0.3
P19338	68	76625	0.04
Q6P2Q9	64	274738	0.01
P31151	62	11578	0.3
P13804	61	35400	0.09
Q9BQE3	57	50548	0.06
P04259	57	60315	0.11
P31946	55	28179	0.12
P35606	55	103278	0.03
Q9C0K3	53	23925	0.14
O00303	53	37654	0.09
Q00839	53	91269	0.04
H0YIN7	52	17553	0.19
P31949	51	11847	0.29
Q14974	51	98420	0.03
P55060	51	111145	0.03
Q00610	48	193260	0.02
A0A075B6Z2	45	2220	1.8
P55957	45	22152	0.15
Q99832	43	59842	0.05
O43707	39	105245	0.03
Q15149	38	533462	0.01
P61981	37	28456	0.12
Q9P2E9	37	152764	0.02
O95994	33	20024	0.17
P69905	31	15305	0.22
P04075	30	39851	0.08
P14174	28	12639	0.27
O43399	28	22281	0.15
Q15363	25	22860	0.15
Q9UL46	25	27555	0.12
P63104	25	27899	0.12
P16152	23	30641	0.11
Q13576	23	181036	0.02
P62424	114	30148	0.87
Q8NC51	112	44995	0.33
Q01105	111	33469	0.21
P06744	110	63335	0.16
Q8N257	105	13900	1.4
Q8WUH6	104	11741	0.67
Q12906	104	95678	0.11
A0A0A6YYL6	99	26698	1.02
P68032	98	42334	0.35
P61604	97	10925	0.73
Q00839	92	91269	0.07
P23528	89	18719	0.93
P62263	87	16434	0.75
P0C7P4	86	31081	0.11
P60174	85	31057	0.35
P05455	85	46979	0.07
P81605	83	11391	0.3
Q13442	83	20618	0.35
Q13011	81	36136	0.19
P07737	79	15216	0.49
P52209	79	53619	0.13
P62328	78	5050	0.73
Q9P2E9	77	152764	0.11
P11940	75	70854	0.09
Q13177	73	58291	0.12
P38646	73	73920	0.14
P05787	72	53671	0.19
P26038	72	67892	0.15
P07998	69	18089	4.49
P51884	69	38747	0.18
P05783	69	48029	0.39
P02533	69	51872	0.36
P04259	68	60315	0.3
P63313	67	5023	0.73
P10599	66	12015	0.65
O60869	66	16359	0.76
Q14103	66	38581	0.18
P07205	66	45166	0.07
Q92945	66	73355	0.04
P35030	64	33306	0.33
P55145	63	21143	0.34
Q5JTJ3	58	14449	0.23
P51991	58	39799	0.17
P22392	57	17401	0.7

P39019	22	16051	0.21
P07998	22	18089	0.19
Q96L46	22	27814	0.12
Q01518	22	52325	0.06
Q9C005	20	11243	0.31
A0A2R8Y7X9	20	18466	0.18
Q96N11	20	50642	0.06

P0CG34	55	5283	0.68
Q96EP5	55	43584	0.16
P00505	55	47886	0.07
P11142	55	71082	0.09
Q99497	54	20050	0.59
P15311	54	69484	0.15
P39019	52	16051	0.46
P08729	50	51411	0.13
Q96HC4	48	65102	0.05
P08195	48	68180	0.21
P02545	48	74380	0.14
O14979	47	46580	0.07
Q01518	46	52325	0.13
P23193	45	34404	0.1
O43175	45	57356	0.06
P21291	44	21409	0.16
P84103	43	19546	0.17
Q13409	43	71811	0.05
P36542	42	33032	0.1
P19338	42	76625	0.04
P35900	38	48514	0.22
P09211	36	23569	0.3
Q14847	36	30097	0.23
Q93088	36	45426	0.07
Q9NQ39	35	20279	0.36
P30041	35	25133	0.13
P54819	35	26689	0.12
Q14568	35	39454	0.08
P11413	35	59675	0.05
P99999	34	11855	0.29
P25398	34	14905	0.23
P26885	34	15810	0.47
Q00688	33	25218	0.13
P09382	32	15048	0.22
P51572	32	28031	0.12
P09012	32	31259	0.11
P05023	32	114135	0.03
O75027	31	82874	0.08
P14625	31	92696	0.04
P62753	30	28834	0.11
Q15365	30	37987	0.09
P30044	29	22301	0.15
P62857	28	7893	0.45
P20774	28	34243	0.1

P37837	28	37688	0.09
P61978	27	51230	0.13
Q14204	27	534809	0.01
P13639	26	96246	0.03
P30405	25	22368	0.15
Q9GZN7	25	32462	0.1
Q8NC01	25	32559	0.1
P53396	25	121674	0.03
Q96L46	24	27814	0.12
P07195	24	36900	0.09
Q96N11	24	50642	0.06
P06576	24	56525	0.06
Q13573	24	61514	0.05
Q96AV8	24	100283	0.03
P15880	23	31590	0.22
Q9UIU6	23	83168	0.12
Q9Y5G8	23	101329	0.07
P62888	22	12947	0.26
Q9Y2V2	22	16110	0.46
P30049	22	17479	0.19
P42765	22	42354	0.08
Q92804	21	62021	0.05
O60603	21	90920	0.04
Q16719	20	52831	0.06

Table 2.2- Mass spectrometry hits isolated in each of the conditions described, sorted by score. UniProt accession numbers, mass of the total protein, and emPAI values calculated from detected fragments are listed for each protein identified. Peptides with scores lower than 20 were removed from each data set. This list includes all proteins isolated in each set, including samples shared between sets.

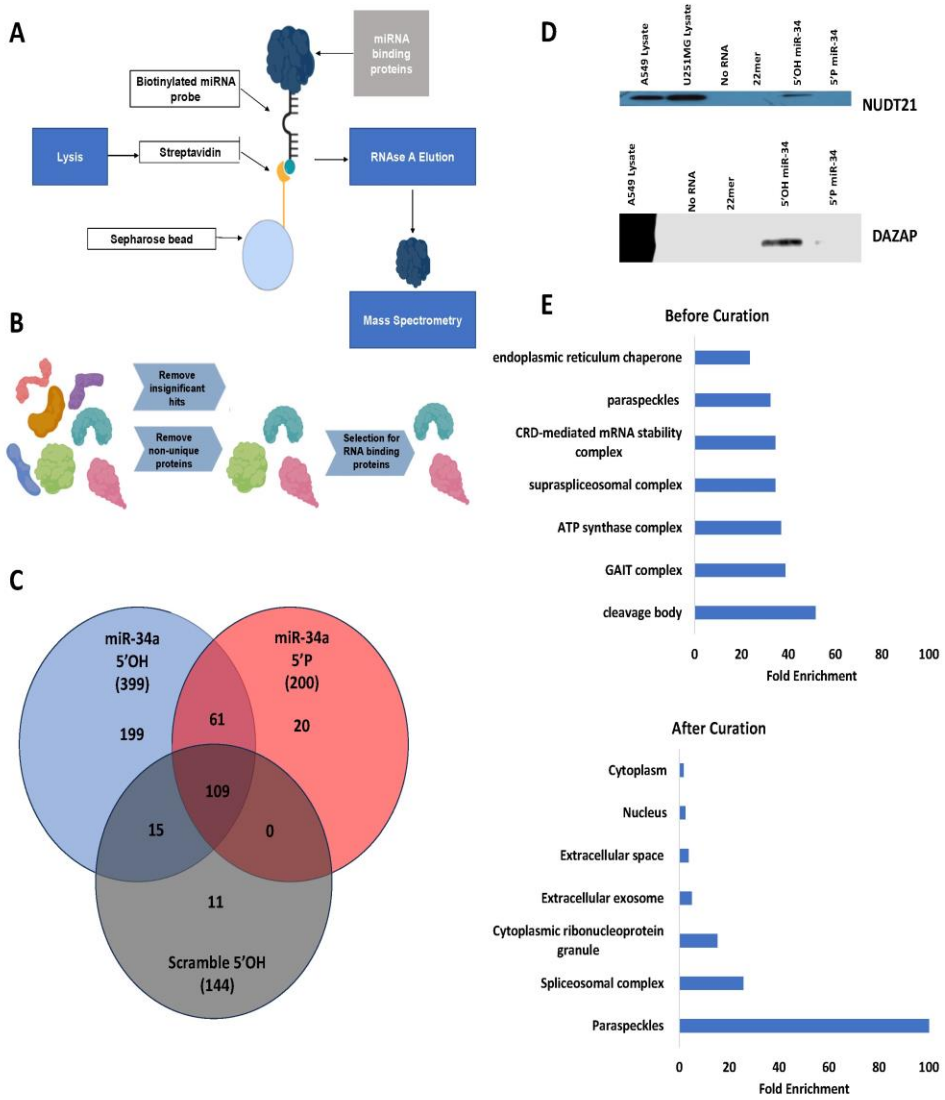

Figure 2.1- Mass spectrometry identifies nuclear paraspeckles as interacting partners of unphosphorylated miR-34 probes. A) Workflow of sample isolation for mass spectrometry. Streptavidin sepharose beads were incubated with biotinylated miRNA mimics and mixed with sonicated whole-cell lysates. Samples were eluted by RNAse A treatment. B) Curation of mass spectrometry hits. Candidate proteins were identified by significance, uniqueness to the 5'OH miR-34a probe, and presence of known RNA binding activity. C) Characterization of isolated proteins. Total number of proteins isolated binding to the indicated probe are shown in parentheses, with the number of proteins unique to that sample or overlapping with other samples shown in the Venn diagram. D) Pulldown of paraspeckle marker proteins from mass spectrometry eluates. Eluates were prepared as above and Western blotted to detect known paraspeckle proteins. E) Gene Ontogeny (GO) curation for Cellular Compartments performed on proteins identified in the 5'OH miR-34a eluates before and after curation.

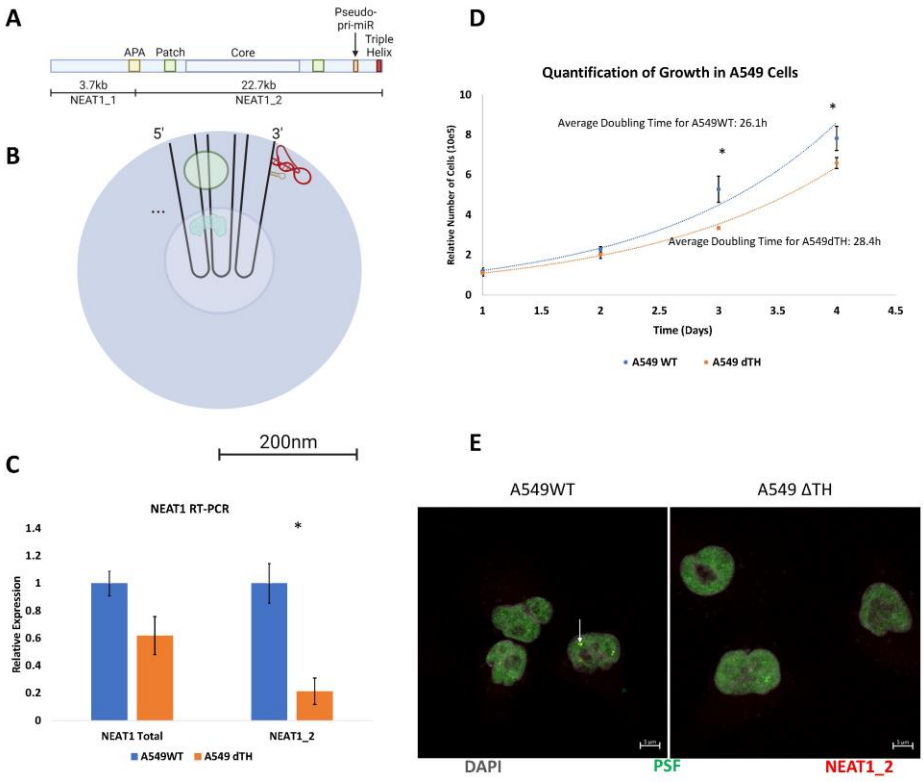

Figure 2.2- Characterization of a Cas9-mediated deletion of the NEAT1_2 triple helix domain. A) Structure of the NEAT1 lncRNA, including the shorter NEAT1_1 isoform and its alternative polyadenylation site. Regions of the lncRNA sequence colocalizing with the paraspeckle patch, core, pseudo-miRNA, and triple helix motif are highlighted. B) Structure of a nuclear paraspeckle. NEAT1_2 organizes its 3' and 5' ends on the exterior of the paraspeckle. Constituent proteins organize into distinct internal domains. Stability of both paraspeckles and NEAT1_2 are dependent on the triple helix domain (red) in lieu of polyadenylation. C) RT-PCR against sequences in NEAT1_1 (NEAT1 Total) and NEAT1_2 in wildtype and triple helix-deleted cells. D) Cell counts over time of cultured wildtype and dTH cells. Doubling time was calculated by exponential regression. *=$p<0.05$ by two-tailed paired Student's *t*-test. E) Paired immunofluorescence and *in situ* hybridization for the paraspeckle marker protein PSF and a region in the middle of NEAT1_2. Colocalization is indicated with white arrows.

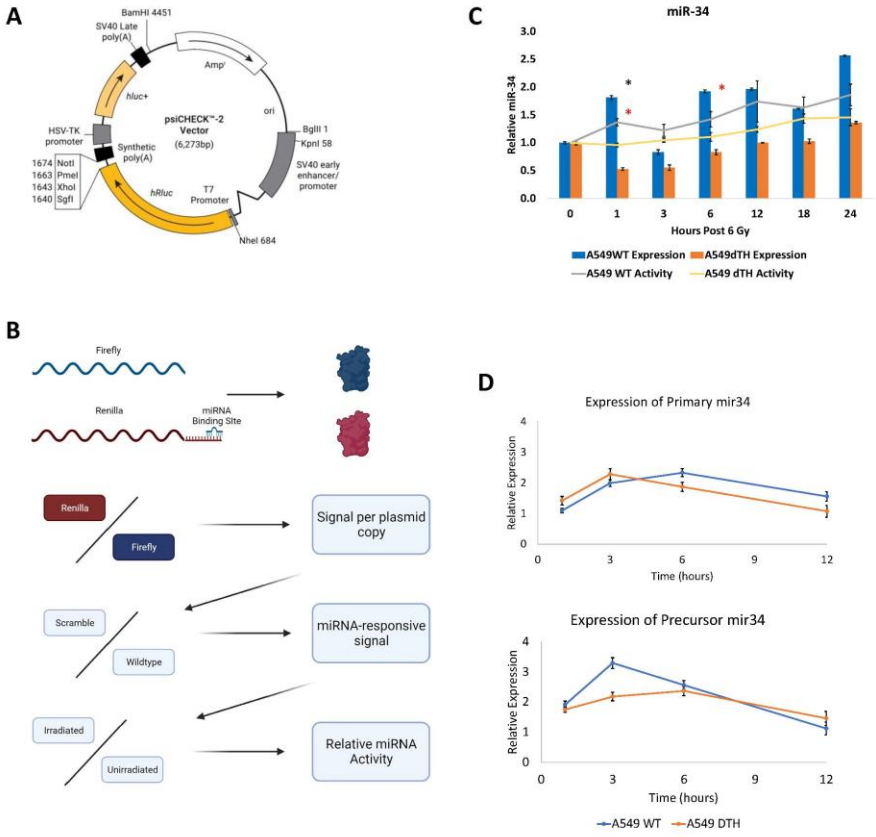

Figure 2.3 – Paraspeckles are required for the early radiation-responsive activity of unphosphorylated miR-34. A) Structure of the PsiCHECK-2 backbone used to quantify miRNA activity. Sequences specific to target miRNAs were cloned into the XhoI and NotI restriction sites. B) Workflow for analysis of miRNA activity using PsiCHECK-2 dual luciferase reporters. Cells were lysed and analyzed for Firefly and Renilla luciferase activity. Luciferase activity per plasmid copy was calculated by normalizing to constitutive Firefly activity. Activity due to the target miRNA was calculated by comparing this value measured in plasmids cloned with wildtype sequences to plasmids cloned with scrambled sequences. Values were then normalized to unirradiated controls. C) Activity (lines) and expression (bars) of miR-34. Activity was calculated by dual luciferase assay and expression by qRT-PCR. Data represents the mean of three biological repeats, each containing three technical repeats. * = $p<0.05$ by unpaired Student's t-test. D) qRT-PCR for miR-34a primary (top) and precursor (bottom) sequences.

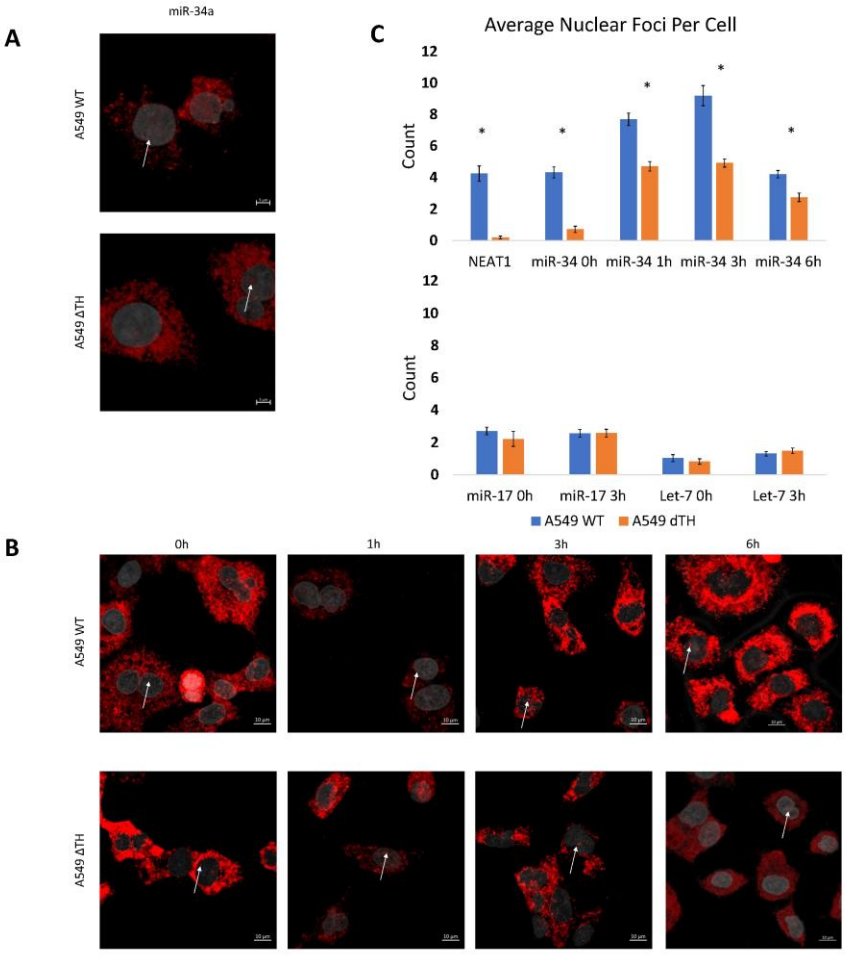

Figure 2.4 – Paraspeckles coordinate punctate nuclear localization of miR-34. A) Single molecule ISH for miR-34 in wildtype (top) and dTH (bottom) cells. Nuclear foci not explained by nearby cytoplasmic signal are indicated by white arrows. B) ISH in the above cells over time following a single 6 Gy dose. C) Quantification of detected nuclear foci for miR-34 (top) or control miRNAs (bottom) in both cell lines over time. *=$p<0.05$ by unpaired two-tailed Student's *t*-test.

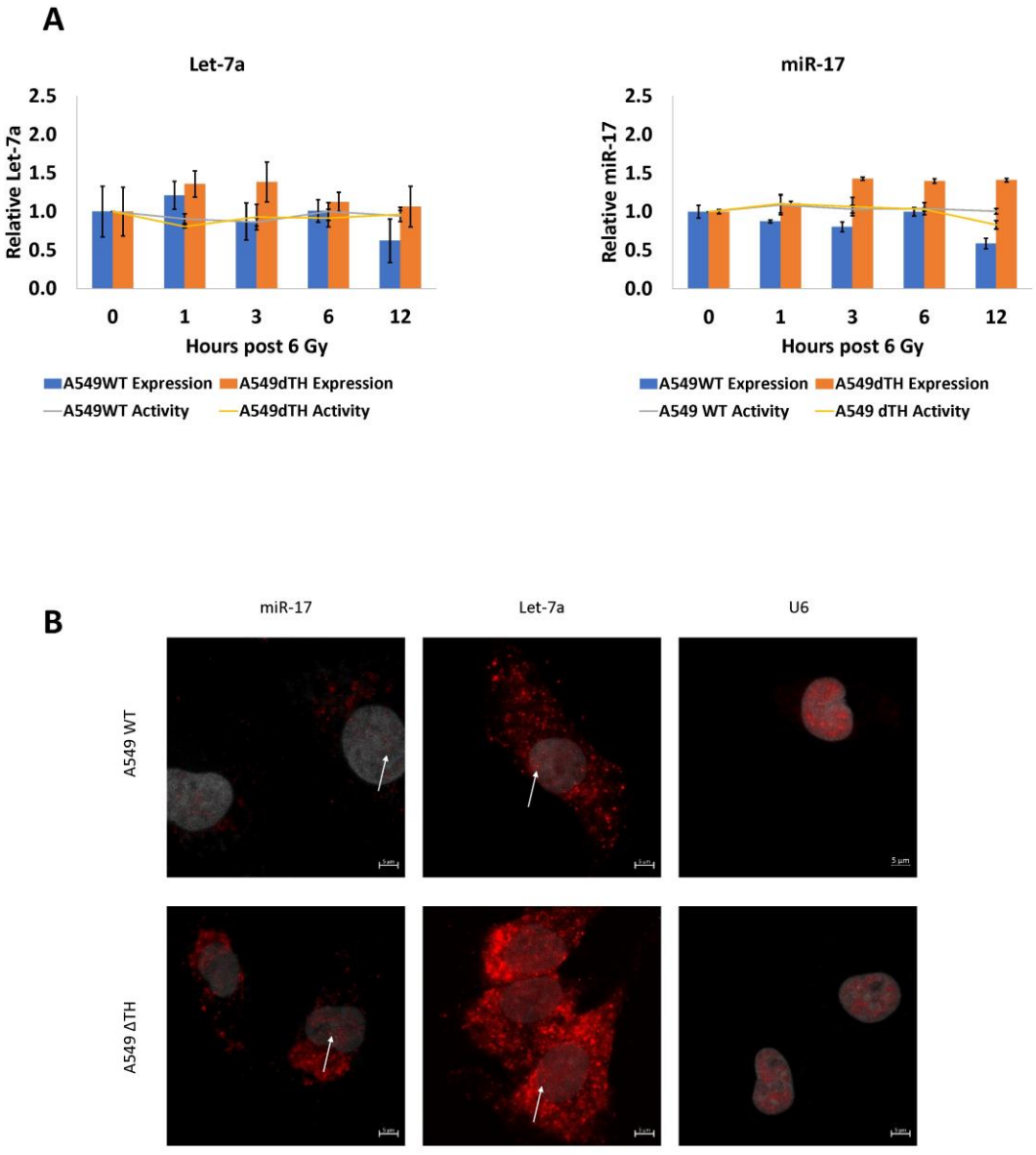

Figure 2.5- Control samples for previous experiments. A) Paired qRT-PCR and luciferase miRNA activity assay for Let-7a (left) and miR-17 (right), as in Figure 2.3C. B) Tyramide-amplified single molecule ISH for miR-17, Let-7a, and U6, as described in Figure 2.4.

References

1. Krol, J., I. Loedige, and W. Filipowicz, *The widespread regulation of microRNA biogenesis, function and decay.* Nat Rev Genet, 2010. **11**(9): p. 597-610.
2. Newman, M.A. and S.M. Hammond, *Emerging paradigms of regulated microRNA processing.* Genes & development, 2010. **24**(11): p. 1086-1092.
3. Elkayam, E., et al., *The Structure of Human Argonaute-2 in Complex with miR-20a.* Cell, 2012. **150**(1): p. 100-110.
4. Hermeking, H., *The miR-34 family in cancer and apoptosis.* Cell Death Differ, 2010. **17**(2): p. 193-9.
5. Lacombe, J. and F. Zenhausern, *Emergence of miR-34a in radiation therapy.* Crit Rev Oncol Hematol, 2017. **109**: p. 69-78.
6. Adams, B.D., C. Parsons, and F.J. Slack, *The tumor-suppressive and potential therapeutic functions of miR-34a in epithelial carcinomas.* Expert Opin Ther Targets, 2016. **20**(6): p. 737-53.
7. Zhang, L., Y. Liao, and L. Tang, *MicroRNA-34 family: a potential tumor suppressor and therapeutic candidate in cancer.* Journal of experimental & clinical cancer research : CR, 2019. **38**(1): p. 53-53.
8. Serviss, J.T., et al., *An antisense RNA capable of modulating the expression of the tumor suppressor microRNA-34a.* Cell death & disease, 2018. **9**(7): p. 736-736.
9. Beg, M.S., et al., *Phase I study of MRX34, a liposomal miR-34a mimic, administered twice weekly in patients with advanced solid tumors.* Invest New Drugs, 2017. **35**(2): p. 180-188.
10. Hong, D.S., et al., *Phase 1 study of MRX34, a liposomal miR-34a mimic, in patients with advanced solid tumours.* Br J Cancer, 2020. **122**(11): p. 1630-1637.
11. He, L., et al., *A microRNA component of the p53 tumour suppressor network.* Nature, 2007. **447**(7148): p. 1130-4.

12. Kato, M., et al., *The mir-34 microRNA is required for the DNA damage response in vivo in C. elegans and in vitro in human breast cancer cells.* Oncogene, 2009. **28**(25): p. 2419-2424.

13. Salzman, D.W., et al., *miR-34 activity is modulated through 5'-end phosphorylation in response to DNA damage.* Nat Commun, 2016. **7**: p. 10954.

14. Fox, A.H. and A.I. Lamond, *Paraspeckles.* Cold Spring Harbor perspectives in biology, 2010. **2**(7): p. a000687-a000687.

15. Modic, M., et al., *Cross-Regulation between TDP-43 and Paraspeckles Promotes Pluripotency-Differentiation Transition.* Molecular Cell.

16. Wilusz, J.E., et al., *A triple helix stabilizes the 3' ends of long noncoding RNAs that lack poly(A) tails.* Genes Dev, 2012. **26**(21): p. 2392-407.

17. Brown, J.A., et al., *Formation of triple-helical structures by the 3'-end sequences of MALAT1 and MENβ noncoding RNAs.* Proceedings of the National Academy of Sciences, 2012. **109**(47): p. 19202-19207.

18. Mittag, T. and R.V. Pappu, *A conceptual framework for understanding phase separation and addressing open questions and challenges.* Molecular Cell, 2022. **82**(12): p. 2201-2214.

19. Ripin, N. and R. Parker, *Formation, function, and pathology of RNP granules.* Cell, 2023. **186**(22): p. 4737-4756.

20. Choudhry, H., et al., *Tumor hypoxia induces nuclear paraspeckle formation through HIF-2alpha dependent transcriptional activation of NEAT1 leading to cancer cell survival.* Oncogene, 2015. **34**(34): p. 4482-90.

21. Imamura, K., et al., *Long noncoding RNA NEAT1-dependent SFPQ relocation from promoter region to paraspeckle mediates IL8 expression upon immune stimuli.* Mol Cell, 2014. **53**(3): p. 393-406.

22. Hirose, T., et al., *NEAT1 long noncoding RNA regulates transcription via protein sequestration within subnuclear bodies.* Molecular Biology of the Cell, 2013. **25**(1): p. 169-183.

23. Phatak, P. and J.M. Donahue, *Biotinylated Micro-RNA Pull Down Assay for Identifying miRNA Targets.* Bio Protoc, 2017. **7**(9): p. e2253.

24. Cook, K.B., et al., *RBPDB: a database of RNA-binding specificities.* Nucleic Acids Res, 2011. **39**(Database issue): p. D301-8.

25. Ashburner, M., et al., *Gene ontology: tool for the unification of biology. The Gene Ontology Consortium.* Nat Genet, 2000. **25**(1): p. 25-9.

26. *The Gene Ontology resource: enriching a GOld mine.* Nucleic Acids Res, 2021. **49**(D1): p. D325-d334.

27. Landthaler, M., A. Yalcin, and T. Tuschl, *The human DiGeorge syndrome critical region gene 8 and Its D. melanogaster homolog are required for miRNA biogenesis.* Curr Biol, 2004. **14**(23): p. 2162-7.

28. Griffiths-Jones, S., et al., *miRBase: microRNA sequences, targets and gene nomenclature.* Nucleic Acids Res, 2006. **34**(Database issue): p. D140-4.

29. Kasai, A., et al., *Double In situ Hybridization for MicroRNAs and mRNAs in Brain Tissues.* Front Mol Neurosci, 2016. **9**: p. 126.

30. Orjalo, A., H.E. Johansson, and J.L. Ruth, *Stellaris™ fluorescence in situ hybridization (FISH) probes: a powerful tool for mRNA detection.* Nature Methods, 2011. **8**(10): p. i-ii.

31. Marzi, M.J., et al., *Degradation dynamics of microRNAs revealed by a novel pulse-chase approach.* Genome Research, 2016. **26**(4): p. 554-565.

32. Phatak, P., et al., *Overexpression of miR-214-3p in esophageal squamous cancer cells enhances sensitivity to cisplatin by targeting survivin directly and indirectly through CUG-BP1.* Oncogene, 2016. **35**(16): p. 2087-97.

33. Naganuma, T., et al., *Alternative 3'-end processing of long noncoding RNA initiates construction of nuclear paraspeckles.* The EMBO journal, 2012. **31**(20): p. 4020-4034.

34. Sasaki, Y.T., et al., *MENepsilon/beta noncoding RNAs are essential for structural integrity of nuclear paraspeckles.* Proc Natl Acad Sci U S A, 2009. **106**(8): p. 2525-30.

35. Zamudio, J.R., T.J. Kelly, and P.A. Sharp, *Argonaute-bound small RNAs from promoter-proximal RNA polymerase II.* Cell, 2014. **156**(5): p. 920-934.

36. Rivas, F.V., et al., *Purified Argonaute2 and an siRNA form recombinant human RISC.* Nat Struct Mol Biol, 2005. **12**(4): p. 340-9.

37. Alexander, A. and C.L. Walker, *Differential localization of ATM is correlated with activation of distinct downstream signaling pathways.* Cell Cycle, 2010. **9**(18): p. 3685-6.

38. Widagdo, J., et al., *Familial ALS-associated SFPQ variants promote the formation of SFPQ cytoplasmic aggregates in primary neurons.* Open Biol, 2022. **12**(9): p. 220187.

39. Davis, A.J., et al., *Imaging of Fluorescently Tagged ATM Kinase at the Sites of DNA Double Strand Breaks.* Methods Mol Biol, 2017. **1599**: p. 277-285.

40. Lama, L., et al., *Small RNA-seq: The RNA 5'-end adapter ligation problem and how to circumvent it.* J Biol Methods, 2019. **6**(1).

41. Hafner, M., et al., *Identification of microRNAs and other small regulatory RNAs using cDNA library sequencing.* Methods, 2008. **44**(1): p. 3-12.

42. Jiang, L., et al., *NEAT1 scaffolds RNA-binding proteins and the Microprocessor to globally enhance pri-miRNA processing.* Nature structural & molecular biology, 2017. **24**(10): p. 816-824.

Chapter 3:

Alternative Interpretations and Approaches

Chapter 3:

Alternative Interpretations and Approaches

Given that little literature exists concerning the existence or activity of 5'OH miRNAs, initial approaches taken during the course of this project investigated several alternative mechanisms before evidence produced the paraspeckle-dependent mechanism described in the previous chapters. In this chapter, alternative theories that were considered for preservation and activation of the unphosphorylated pool will be explained. Additionally, several approaches concerning modulation of the paraspeckle-associated pool were attempted before being discarded or replaced by more practical methods- those initial approaches are also described below.

Interpretation of the mass spectrometry dataset

Initial interpretation of the mass spectrometry dataset described previously (Figure 2.1) assumed that interactions between 5'OH miRNAs and the factors responsible for their protection would be protein-based and likely direct. Cytoplasmic miRNA stability is highly dependent on Ago2 binding to the 5' phosphate [1], which, paired with the documented nuclear localization of 5'OH miR-34a, implied a different mechanism for stabilizing 5'OH miRNAs. We initially assumed a somewhat similar mechanism, in which binding to a specific protein would stabilize miRNAs by preventing interactions with cellular RNAses, similar to Ago2-mediated miRNA protection[2, 3].

Notably, phosphorylated miRNAs are stabilized through interactions on the termini of the sequence, enabling a single protein to bind miRNAs independent of their sequence[4]. By contrast, previous work has already demonstrated that not every miRNA species exists as 5'OH pools in steady-state A549 lung adenocarcinomas, implying sequence-specific mechanisms are involved in either the processing or stabilization of 5'OH miRNAs[5]. Since the literature currently contains no explanations of the mechanisms involved in 5'OH miRNA production, our initial approach could not assume sequence or structural specificity to the proteins hypothesized to protect 5'OH miRNAs.

Accordingly, analysis of candidate proteins that could stabilize 5'OH miRNAs was screened as previously described (Figure 2.1B)**.** Candidate proteins were then analyzed for known interaction with the proteins already demonstrated to be important to the activation of 5'OH miR-34a. This approach led to identification of three candidate proteins- Rbm3, NUDT21, and HNRNPA2B1. HNRNPA2B1 was not studied significantly- although it was the single most enriched protein isolated from the 5'OH miR-34a mass spectrometry, it was also significantly present in the 5'P miR-34a pulldown, implying a lack of specificity towards the phosphorylation status of miR-34a.

Alternative Methods for Mass Spectrometry

The mass spectrometry protocol described in this work presumes stable interactions between unphosphorylated miR-34 and the factors responsible for its protection in the cell- the protocol does not include a crosslinking step, and is performed on whole-cell lysates rather than transfection into living cells. Two approaches were performed to address both of these

concerns- transfection of biotinylated miRNA mimics into cultured cells and addition of formaldehyde-based crosslinking. Additionally, Coomassie staining of samples collected by all three protocols were analyzed to identify individual proteins with high signal.

Transfection of miRNA mimics into live cells was performed as previously described[6, 7]. Briefly, cells were grown to near confluence in 10cm plates. 2nmol of miRNA mimic was transfected into cells and let sit a variable amount of time. At the indicated time points, cells were washed with PBS and fixed in 1% formaldehyde for 10 minutes before neutralization with glycine. Fixed and crosslinked cells were scraped into cold PBS, resuspended in RIPA buffer, sonicated, clarified, and processed as described above. While this method reliably isolated protein detectable by BCA assay, it failed to isolate proteins by pulldown of biotin moieties conjugated to the RNA probes at any time point after transfection (4h-24h post), which may imply loss of biotinylated probes prior to fixation.

Samples isolated by each of the above methods were run on SDS-PAGE gels to confirm the presence of specific protein isolation prior to mass spectrometry. While RNAse A was strongly isolated in every protein sample, some samples also showed strong specific bands without an obvious candidate in the final mass spectrometry dataset. To identify these strongly-enriched proteins, we excised Coomassie stained bands from gels prior to transfer, dissolved the SDS-PAGE gel, desalted the sample, and performed ESI-FT-MS/MS as previously described. This approach uniformly caused a loss of specifically isolated proteins, including RNAse A, indicating a loss of sample at some point in the isolation process.

Hypotheses for the Utility of Rbm3 and NUDT21

Aside from their enrichment and specificity to the 5'OH miR-34a mass spectrometry data set, Rbm3 and NUDT21 both presented mechanistic rationales that made interaction with 5'OH miR-34 plausible.

NUDT21 is a member of the CFIm splicing factor complex, which is responsible for processing 3' end formation, responsible for establishing alternative polyadenylation sites in 3' UTRs of splicing pre-mRNAs [8-10]. Importantly, the CFIm complex also recruits Clp1 to phosphorylate newly-spliced transcripts [11], showing a direct mechanism linking a protein from the 5'OH miR-34a mass spectrometry dataset and a protein known to be involved in 5'OH miR-34a activation [5]. Other members of the CFIm complex were isolated in the mass spec data set, though Clp1 was not- this may be simply because the protocol did not include a crosslinking step, biasing towards more stable binding interactions, or that Clp1 is unable to access the site of NUDT21 binding until after activation.

Theories for the mechanistic relevance of NUDT21 in 5'OH miR-34a production or protection were not without their issues, however. While previous work demonstrated that siRNA-mediated knockdown of the miRNA processing factors DROSHA and Dicer allowed cells to retain some radiation-responsive miR-34a activation from the unphosphorylated pool, it is difficult to conclude from this observation that the unphosphorylated pool is produced in a manner independent of canonical processing. While similar splicing mechanisms have been implicated in the non-canonical processing of intronic miRNAs [1, 12], we did not have evidence to support a mechanism assuming that miR-34a was cleaved into a mature-length, sequence-

accurate 5'OH miR-34a in an NUDT21-dependent manner. Additionally, NUDT21 binds to UGUA motifs [11, 13], which are not present on the mature or unprocessed miR-34a sequences. Importantly, given that nuclear paraspeckles localize proximal to splicing-associated nuclear speckles [14], NUDT21 is itself a nuclear paraspeckle protein[15, 16].

The other candidate protein, Rbm3, is a cold shock-inducible RNA binding protein that has been implicated in cancer cell radiosensitivity [17, 18]. Rbm3 is known to interact with Dicer [19, 20], and its dysregulation affects signaling of several miRNAs [21]. Rbm3 is also known to interact with hnRNPA2B1, the single most abundant protein isolated in the mass spectrometry dataset. Notably, hnRNPA2B1 was also detected at a lower level in the 5'P miR-34 pulldown, while Rbm3 was unique to the 5'OH miR-34 pulldown. Rbm3 is also a known paraspeckle protein[15, 16].

Cas9-mediated Knockdown of Candidate Proteins

To investigate the role of NUDT21 and Rbm3 on production and protection of the unphosphorylated pool, we generated Cas9-mediated knockdowns of both proteins and introduced these deletions into A549 cells. Since the proprietary Cas9 platform used in these experiments (Santa Cruz Biotechnology) did not provide sequencing templates to confirm genetic loss, confirmation of Cas9 deletion was performed by Western blotting for the target proteins (data not shown).

Preliminary attempts to characterize interactions between these candidate proteins and the unphosphorylated pool focused on interactions between those proteins and factors implicated in 5'OH miR-34 activation- hClp1 and ATM. Immunoprecipitations performed on ATM

probing for the presence of NUDT21 and Rbm3 for all time points tested after IR, including multiple weights of NUDT21 (Figure 3.1). Interestingly, these IPs also detected interactions between Rbm3 and ATM before IR, which may be consistent with Rbm3's role in regulating several key downstream effectors of ATM signaling[22].

Further studies on the role of Rbm3 and NUDT21 in regulating unphosphorylated miR-34 were not performed due to the adoption of a hypothesis directed at nuclear paraspeckles. Notably, neither NUDT21 nor Rbm3 are required for paraspeckle formation[15], implying that loss of these factors is unlikely to have a significant effect on the unphosphorylated pool.

Other Methods of Paraspeckle Ablation

While the Cas9-mediated deletion of NEAT1 reliably eliminated nuclear paraspeckles, this approach also destabilized the NEAT1_2 transcript, since the Cas9 triple helix motif is necessary for stabilizing NEAT1 in lieu of polyadenylation [23](Figure 2.2A). While some expression of NEAT1_2 is maintained (Figure 2.2C), this reduction in overall NEAT1_2 transcript levels confounds our interpretation of stabilization of unphosphorylated miR-34 because it also affects mechanisms relying on direct base-pairing between miR-34 and NEAT1. Indeed, such sponging interactions are common among lncRNAs [24-26] and have been previously reported between NEAT1 and miR-34, whose expression levels inversely correlate[27]. Interestingly, the miR-34 binding site proposed in these works differs from those proposed by miRanda, which screens for Ago2 binding sites[28]. Comparing these CLIP sites with CLIP for miRNA-related proteins shows some colocalization with DGCR8 binding sites along the NEAT1_2 sequence[29](Figure 3.2). While we did not attempt to edit other parts of the NEAT1_2

sequence, a hypothesis based on direct base pairing between miR-34 and NEAT1_2 could investigate if paraspeckle-dependent regulation of unphosphorylated miR-34 is dependent on the fidelity of these sequences.

Accordingly, several other methods for removing nuclear paraspeckles were tested in this study and should be investigated further in future studies. Notably, paraspeckle-mediated phase separation is maintained both by NEAT1_2 and by an array of necessary proteins [15], one of which (NONO) was downregulated by siRNAs during the course of this study. Several alternative methods for modulating paraspeckle formation have been characterized[30]- investigating broader methods for disrupting phase separation could be beneficial in ensuring that the observed phenotypes are due to the physical properties of paraspeckles rather than the sequence of NEAT1_2 or interactions with sequestered proteins.

Similarly, phase separations are typically maintained by numerous weak interactions generated by high concentrations of interactors in a compartment at a suitable temperature [31]**.** Planar molecules such as hexanediols have been shown to disaggregate phase separations broadly across the cell by intercalating between these weak interactions [32], including those that maintain nuclear paraspeckles [33]. Our studies investigated both 1,6-hexanediol, which disaggregates phase separations, and 2,5-hexanediol, which does not. Importantly, these chemicals disrupt phase separations broadly across the cell, and therefore introduce the confound of affecting many interactions unrelated to nuclear paraspeckles.

Studies using these hexanediols, both to eliminate paraspeckles and to test the phenotype of paraspeckle loss, proved challenging. Firstly, treatment at concentrations and

times shown to disrupt paraspeckles in the literature [33] did not fully eliminate punctate NEAT1 foci in ISH models. While further optimization could have reconciled this discrepancy, we simultaneously noticed that treatment with any hexanediols completely eliminated luciferase signal in cells transfected with the plasmids used to measure miR-34 activity (data not shown), implying that this application would have been impractical in downstream applications.

Similarly, siRNA-mediated knockdown of NONO expression was investigated- cells were treated with siRNAs, irradiated, and the activity of miR-34 was measured by luciferase assay as previously described. Results from this approach were inconsistent- while NONO levels were reliably decreased at all time points investigated (Figure 3.3A), miR-34 activity did not change significantly, and siNONO-treated cells failing to demonstrate p53-dependent *de novo* miR-34 transcription (Figure 3.3B).

Since our present data do not show direct colocalization between miR-34 and nuclear paraspeckles, it is plausible that paraspeckles or some component within them are more important in predicting the stability of unphosphorylated miR-34 than the paraspeckles themselves. Showing similar results following abrogation of paraspeckle formation independent of NEAT1_2 downregulation would give more evidence to the argument that miR-34 is protected by phase separation rather than interactions with either NEAT1 or proteins within the paraspeckle.

Optimization of *In Situ* Hybridization

Several important experiments in this study relied on *in situ* hybridization (ISH) for different RNA species, necessitating a range of technical approaches. To this end, several distinct methods were attempted to localize both the lncRNA NEAT1_2 and the miRNAs investigated in this study.

Briefly, ISH relies on base-pairing interactions between a target endogenous RNA species and a probe RNA with a relevant conjugate, typically on one of its termini[34]. This conjugate may be either a fluorophore[35], an enzyme, or a chemically-relevant moiety used for downstream chemistry[36]. Given the low signal strength of single probes, many ISH applications "tile" the target transcript, providing multiple distinct probes covering the length of the target transcript and enabling multiple conjugates to be affixed to a single target RNA[37, 38]. This approach is not feasible for miRNAs, which are too short to bind multiple probes efficiently[36].

In addition to the sequence of the probe, which is typically a near-perfect complement of the target sequence, chemical modifications may be made on the probe to facilitate its binding to the target. This study used locked nucleic acid (LNA) probes, which force the probe into the conformation adopted while binding the target sequence. Ensuring that binding only occurs in a favourable conformation both increases the affinity for the target sequence and decreases affinity for off-target sequences.

The simplest fluorescent *in situ* hybridization (FISH) conjugates a fluorophore to the probe RNA, which is then directly visualized by fluorescence microscopy[35]. Several ISH protocols were attempted during the course of this study- these varied significantly in their approach, especially with respect to fixation, permeabilization, blocking, and addition of enzymatic reactions intended to decrease background signal[36, 39-42]. A brief summary of these methods can be found in Table 3.1.

Colocalization of miR-34a and Nuclear Paraspeckles

Several approaches were attempted to investigate the colocalization of miR-34a and markers of nuclear paraspeckles, none of which yielded usable results. While miR-34 yields distinct, punctate, nuclear signal in WT A549s, but not cells harbouring deletion of the NEAT1_2 triple helix motif, current experimental data is unable to demonstrate that these nuclear miR-34a foci are actually associated directly with the paraspeckle- only that their localization is dependent on the presence of intact paraspeckles within the cell. Additionally, ISH methods used in this study rely on base pairing to the sequence of the miR-34 transcript, implying that such probes are not only unable to determine the phosphorylation status of the target, but also that they cannot distinguish the amount of processing present on the hybridized miRNA- pri- and pre-miRs should hybridize with comparable efficiency.

Notably, several approaches described earlier in this study managed to successfully localize nuclear paraspeckles, including direct FISH for sequences in the middle of the NEAT1_2 transcript (Stellaris) and immunofluorescence for the paraspeckle marker proteins PSF and NONO (Figure 2.2E). These methods determined a number of paraspeckles present in both

wildtype and NEAT1 DTH cells similar to the number of nuclear miR-34 foci at baseline- while it is possible that nuclear paraspeckles are responsible for the production of unphosphorylated miR-34 without sequestering it directly, we see this explanation as improbable given the similar number of nuclear miR-34 foci and NEAT1 foci in wildtype cells, confirmed interactions with 5'OH miR-34 mimics, and plausibility of phase separation as a means for protecting the unphosphorylated pool.

Colocalization of Other Known Interactors and Paraspeckles

Prior research has implicated two proteins in the IR-dependent activation of unphosphorylated miR-34- the master DNA damage response kinase ATM and the RNA-directed kinase hClp1 [5]. While neither of these proteins have been shown to associate with paraspeckles under ambient conditions [15], interactions between these proteins and paraspeckles or paraspeckle contents could be IR-dependent. To this end, we performed paired ISH against paraspeckle targets and immunofluorescence against these proteins in wildtype cells shortly after a single 6 Gy dose.

To visualize IR-responsive colocalization of these factors and nuclear paraspeckles, immunofluorescence against both Clp1 and ATM was attempted in conjunction with ISH for NEAT1_2. Several rounds of optimization with and without irradiation failed to recover punctate localization of Clp1 at any time point (Data not shown), indicating that Clp1 may not concentrate in sufficient quantities to generate nuclear foci, but rather shows diffuse signal throughout the nucleus. Similar methods were able to recover punctate ATM foci consistent with prior reports of IR-dependent ATM localization and simultaneously localize paraspeckles consistent with

other data presented here, but did not demonstrate consistent colocalization with NEAT1_2 (Figure 3.4)- immunofluorescence for ATM paired with ISH for NEAT1_2 showed punctate localization of both, but the foci did not co-localize. Additionally, co-immunoprecipitation between ATM and the paraspeckle resident proteins Rbm3 and NUDT21, neither of which is required for paraspeckle formation, was attempted, but failed to yield conclusive results since ATM precipitated both proteins at all time points tested after IR (Figure 3.1).

Since ATM interactions with paraspeckles may be transient, we proposed but did not attempt a method to enable live-cell imaging of both paraspeckles and ATM, allowing localization of both proteins dynamically after IR. Paraspeckle localization could be accomplished by GFP tagging the paraspeckle marker protein SFPQ [43], paired with plasmid transfection of fluorescently-tagged ATM[44]. Alternatively, immunoprecipitation between paraspeckle marker proteins and ATM could be attempted after IR in both wildtype and NEAT1 dTH cells- our present data show interactions between ATM and some paraspeckle proteins after IR (Figure 3.1), but do not confirm that these interactions happen within the context of the paraspeckle.

Several attempts to clone GFP-SFPQ edited A549WT and NEAT1_2 dTH cells were made- briefly, cells were transfected with Cas9-sgRNA plasmids and an SFPQ HR donor as previously described [43] and sorted into clonal colonies by either FACS or serial dilution. In both cases, cells were selected for clonicity, screened for GFP fluorescence, and confirmed for editing by both Western blotting and sequencing using PCR probes amplifying regions flanking the GFP insertion site and within the GFP locus itself. Several cell lines were found to have successfully incorporated GFP immediately after the SFPQ promoter, but failed to show significant punctate

nuclear fluorescence characteristic of SFPQ's role as a paraspeckle marker protein. Since sequencing showed the expected results, it is plausible that the introduction of GFP by this method interacts negatively with sequence differences between A549 and the cell lines tested in the literature- future approaches should attempt similar fluorescent tagging methods aimed at different paraspeckle marker proteins.

Phenotypic Consequences of Paraspeckle Loss on miR-34a

Given the importance of miR-34 in radiation response and the time dynamics of DNA repair, we hypothesized that depletion of the unphosphorylated pool by elimination of paraspeckle formation would radiosensitize affected cancer cells and change the expression of downstream miR-34 target genes. To this end, we performed clonogenic assays, RT-PCRs, and Western blots to determine the phenotypic consequences of loss of the unphosphorylated pool.

Briefly, since radiation induces cell death and senescence by distinct mechanisms operating on different time scales [45, 46], traditional assays for cell viability do not sufficiently capture radiation-induced cell death. Clonogenic assays account for all mechanisms leading to cell death and senescence by measuring the capacity for treated cells to form clonal colonies over a two-week span following treatment[47]. In the context of radiation biology, the Dose Modifying Factor (DMF) of a given treatment in a particular cell line is represented as the ratio of radiation doses required to reduce clonogenic colony formation to 10% of the rate seen in unirradiated cells given identical other treatments.

We performed clonogenic assays using radiation doses ranging from 2-8Gy on WT and NEAT1_2 dTH A549s. While previous work has demonstrated that ablation of paraspeckles is

phenotypically mild, we hypothesized that early activation of the unphosphorylated pool would aid in DNA repair shortly after ionizing radiation, causing cells lacking nuclear paraspeckles to be more radiosensitive. However, NEAT1 dTH cells did not show significant radiosensitivity relative to A549 wildtype cells (Figure 3.5).

These clonogenic assays were paired with Western blots and RT-PCR for the miR-34 target proteins Cdk4 and Bcl2, which are implicated in cell cycle exit from G1 phase in cells lacking DNA damage and apoptosis, respectively [48, 49]. While both of these proteins are known to be significantly influenced by IR [48, 50], we hypothesized that the loss of unphosphorylated miR-34 would cause an increase in expression of both proteins on a short and moderate time scale after IR in cells lacking nuclear paraspeckles. Instead, we found no significant change in expression of either protein (Figure 3.6).

Together, these results indicate a general lack of detectable radiation-responsive phenotype downstream of unphosphorylated miR-34. This may indicate that the pool of unphosphorylated miR-34 is too small at baseline in A549s to elicit significant phenotypes, or may point to participation within redundant mechanisms that are adequately compensated by other means- for example, *de novo* transcription and processing of canonical miR-34 at later time points may be sufficient to prevent radiosensitivity derived from low miR-34 levels. Investigation into cooperation between unphosphorylated miR-34 and other radiation-responsive pathways, especially those hypothesized to interact with paraspeckles (e.g. ATM) could show broader phenotypic consequences to the unphosphorylated pool. Additionally, given the interplay between *de novo* miR-34 transcription and p53 [51, 52], the

unphosphorylated pool may comprise a more significant part of cellular radiation response in p53-mutant cancer cells.

Materials and Methods

Cell culture

All A549 cell lines, including Cas9 edited lines, were cultured in F12K media as described in Chapter 2. H1299 lines were maintained in the same incubator (5% CO_2, 37^oC) and cultured in RPMI-1640 (Gibco) supplemented with 10% fetal bovine serum and 1% penicillin/streptomycin.

Cas9 editing

Cas9 editing of Rbm3 and NUDT21 was performed according to manufacturer's specifications (Santa Cruz Biotechnology). Briefly, cells were seeded onto 6-well tissue culture plates in antibiotic-free media to 80% confluency, then transfected with 1ug of Double Nickase plasmid DNA and incubated for 20 minutes at room temperature with 5uL UltraCruz Transfection Reagent. This mixture was added dropwise to cells and cultured overnight, then selected for transfectants by screening for GFP-positive cells by fluorescence-activated cell sorting.

Due to the low viability of FACS-sorted cells under this protocol, separate lines were also kept using serial dilution- cells were counted and diluted to a concentration of one cell per 200uL, then transferred to 96 well plates. Single-cell clones were then assessed for GFP fluorescence and grown to confluency.

Candidate clones isolated by either protocol were tested for loss of protein expression via Western blotting.

Clonogenic Assays

To assess cellular survival after IR, 100,000 cells were plated onto 10cm plates and let settle for 24h before irradiation at 0,2,4,6, or 8 Gy. 24h after IR, plates were trypsinized, counted, and a known number of cells were plated in triplicate onto 60 mm tissue culture dishes and incubated for two weeks. Colonies were fixed and stained in 1:20 crystal violet in methanol. Colonies containing more than 50 cells were counted. The Dose Modifying Factor (DMF) for N=3 biological replicates was calculated as the ratio of the estimated radiation doses required to elicit a 1 log unit reduction in cellular viability between two conditions. Two-tailed Student's *t*-test was used to calculate significant differences in mean relative survival at each dose of radiation between encapsulated and monolayer cells.

Immunoprecipitation

To assess interactions between candidate proteins, clarified and sonicated lysates were incubated with 25-250ug of antibody for the target protein and mixed with 100uL of Protein G agarose slurry overnight at 4^{o}C. Beads were washed and pelleted in IP buffer (25mM Tris, 150mM NaCl, pH 7.2). After washing, beads were washed with water and resuspended in 1x Laemmli buffer, boiled and loaded into an SDS-PAGE gel directly.

Western blot samples were run at 100V and transferred onto nitrocellulose membranes. Membranes were washed, blocked in 5% nonfat dry milk in 1x TBST, and incubated overnight in primary antibody followed by HRP-conjugated secondary antibody. Luminescent signal was

detected by incubating membranes with chemiluminescent substrate (Thermo-Fisher) and either exposing on X-ray paper or visualizing on a Licor Odyssey imager.

Fluorescence Microscopy

Glass coverslips were sterilized with 70% ethanol, air dried, and coated with poly(L)-lysine for 30 minutes at room temperature in a 6-well plate. Cells were cultured onto coated slides at 50% confluency and let settle overnight. Fluorescent staining was performed using multiple different protocols, summarized in SECTION X.

Fluorescent imaging was performed on either a Keyence BZ-9000 or Zeiss LSM-700 microscope. Laser gain and power were matched for all samples stained for the same targets imaged using the LSM-700 platform. Images represent maximum intensity projections of z-stacked confocal images spanning the height of the nucleus. Quantification of nuclear foci was performed on individual z-stacks, omitting foci contiguous with cytoplasmic signal from nearby cells.

Quantification of mRNA and Protein Expression

Subconfluent 10cm plates were cultured and irradiated as described previously. At the indicated time points, cells were washed twice in PBS and scraped into cold PBS. Scraped cells were split into two equal tubes, pelleted, and resuspended in ice-cold RIPA buffer for protein extraction or QiaZOL buffer for RNA extraction.

Protein samples were sonicated, incubated on ice, and clarified by centrifugation. Samples were quantified by BCA assay and equal masses of protein were diluted into 1x

Laemmli buffer, boiled, and loaded into precast 4-20% SDS-PAGE gels. Gels were run at 100V for approximately two hours and transferred overnight to nitrocellulose membranes. Membranes were blocked with 5% nonfat dry milk in TBST and incubated in primary and secondary antibodies as described in TABLE X. Proteins were visualized with ECL solution, with luminescence detected either by X-ray paper or a Licor Odyssey. Relative quantification of protein levels in non-IP samples was performed by normalizing signal in each sample to loading controls from the same lane.

RNA samples were purified into ultrapure water as previously described [53]. Purified RNA was diluted to 2ng/uL stocks. cDNA for mRNA or lncRNA transcripts and their controls were synthesized using random hexamer primers, while cDNA for miRNA targets and their controls were synthesized using individual 3' hairpin primers as described in TABLE X. Composite RNA expression shown represents the average of three repeats, where each repeat consists of three technical replicates normalized to U6 snRNA expression calculated from the same sample.

Discussion

This project demonstrates well the importance of maintaining ideological flexibility during scientific research- while the initial ideas of the project were sound and followed norms that were well established in the scientific literature, the project largely failed to return experimentally interesting results until the main hypothesis was not just reoriented, but fundamentally changed. In the course of designing this project, we applied to several funding mechanisms and were ultimately awarded two- in both cases, the reviewers felt confident that

the design of the project and scope of the preliminary data was flexible enough to ensure a successful approach, even if our hypothesized outcome proved false. Thankfully, this was approximately correct- the datasets and general design did contain sufficient information to design a novel approach to the project that proved fruitful, but doing so required changing lines of thought significantly.

Most notably, we benefitted from moving away from simple models of RNA-protein interactions. The design and initial interpretation of the mass spectrometry dataset relied on an assumption that stabilization of the unphosphorylated pool would look similar to stabilization of phosphorylated miRNAs- that is to say, a protein with known RNA binding activity would interact with predictable motifs of the miRNA (presumably on the 5' and 3' end, though our lack of information regarding other unphosphorylated species meant we couldn't eliminate the possibility of interactions with the miR-34 sequence).

As such, our initial analysis of the mass spectrometry dataset focused on proteins themselves, rather than characteristics shared between those proteins. Our investigation of NUDT21 and RBM3 fit the mold of traditional analysis of mass spectrometry datasets well- these proteins were unique to the experimental condition, strongly enriched, had known RNA binding activity, and, in the case of NUDT21, had known interactions with proteins implicated in activation of the unphosphorylated pool, hinting at a mechanistic connection between the two. We never found a "smoking gun" protein in these sets- a protein unique to the unphosphorylated pool whose interactions were specific enough to uniquely bind unphosphorylated miR-34, and whose other interacting partners included known activators of the unphosphorylated pool.

Thankfully, we moved away from a model presuming direct interaction between stabilizing proteins and unphosphorylated miRNAs before spending significant time ablating individual proteins in the dataset and looking for phenotypic effects individually. While paraspeckles were described previously [54-56], mechanistic descriptions of biomolecular condensates and wider properties of liquid-liquid phase separation were not well described until 2017 [57, 58]. The mass spectrometry dataset contained a remarkable enrichment of paraspeckle proteins (Figure 2.1E), implying organization by a broader network of regulatory factors- but even this model only made sense in the context of compartmentalization driven by paraspeckles. Phosphorylated miRNAs are stabilized by Ago2 preventing interactions between the miRNA and degradatory enzymes [1, 2, 4]- similarly, unphosphorylated miRNAs may be protected by compartmentalization within paraspeckles, away from those same enzymes.

While the phenotypic differences in pathways thought to be impacted by the unphosphorylated pool were minor, it is difficult to draw conclusions about the functional relevance of unphosphorylated miRNAs based on these data for several reasons. Firstly, miRNAs are only one factor in complex regulatory networks involved in stress responses, and any effects of miR-34 must be taken in the context of the broader radiation response, which we do not expect to be significantly different in cells lacking nuclear paraspeckles. Additionally, the unphosphorylated pool does not represent the entire population of miR-34 in unirradiated cells, and *de novo* transcription begins rapidly after IR- it is plausible that the radiation response engendered by miR-34 activity after IR is still active to a lesser degree due to activity of phosphorylated miR-34 either transcribed prior to IR or as a result of IR-induced upregulation. Alternatively, the lack of detectable phenotype in radiation response could be due to the

significant redundancy in these pathways [59, 60]- while miR-34 knockout cells are generally more radiosensitive, it is plausible that alternative radiation response pathways adequately manage the radiation response in the cell lines investigated in this study. Future studies either investigation phenotypic consequences in other cell lines or combining paraspeckle knockdown with pharmaceutical inhibition of these alternative pathways may reveal synergistic effects that could not be detected due to the design of this study.

Figures

Protocol Name	PMID	Fixation Concentration	Fixation Duration	Permeabilization Concentration	Permeabilization Duration	Blocking Agent	Blocking Duration	ISH Probe	Other Treatments	Hybridization Concentration	Detection Method
Chaumeil	23407477	2% Paraformaldehyde	10 minutes	0.4% Triton X-100	5 minutes	2.5% bovine serum albumin, 10% normal goat serum, 0.1% Tween-20	30 minutes	biotin-miRNA mimic	0.1ug/uL RNAse A 1h		Fluorescent secondary antibody after anti-DIG primary
Vautrot	33792873	4% Paraformaldehyde	10 minutes	Ethanol dehydration	20 minutes-12h		None	3'Biotin LNA miRNA	Liquid nitrogen freezing	20-40nmol	Texas Red-Streptavidin
Saul	30922080	1% formaldehyde	10 minutes	0.5% Triton X-100	20 minutes	2% BSA	30 Minutes	Double-DIG miRNA	NA	1nm	Anti-DIG fluorophore
Kasai	27920667	4% Paraformaldehyde	10 minutes	None	None	1% Roche Blocking Reagent in TN Buffer	1h	3'DIG LNA miRNA	Proteinase K, Acetylation	2pmol	Tyramide Amplification
Modified Kasai	This work	4% Paraformaldehyde	10 minutes	None	None	1% Roche Blocking Reagent in TN Buffer	1h	3'DIG LNA miRNA	NA	2pmol	Tyramide Amplification
Pandya-Jones	25915022	4% Paraformaldehyde	10 minutes	0.5% Triton X-100	10 minutes	Ethanol dehydration series	variable	Directly conjugated	Ethanol dehydration, RNAse A treatment	Variable	Directly conjugated

Table 3.1- *In situ* hybridization protocols attempted in this study to localize miRNAs. Methods varied significantly in their fixation, permeabilization, blocking, and identity of the probe. Data shown in this work use an adaptation of the method shown by Kasai and colleagues (Kasai, 2016 #551) with the modifications described above.

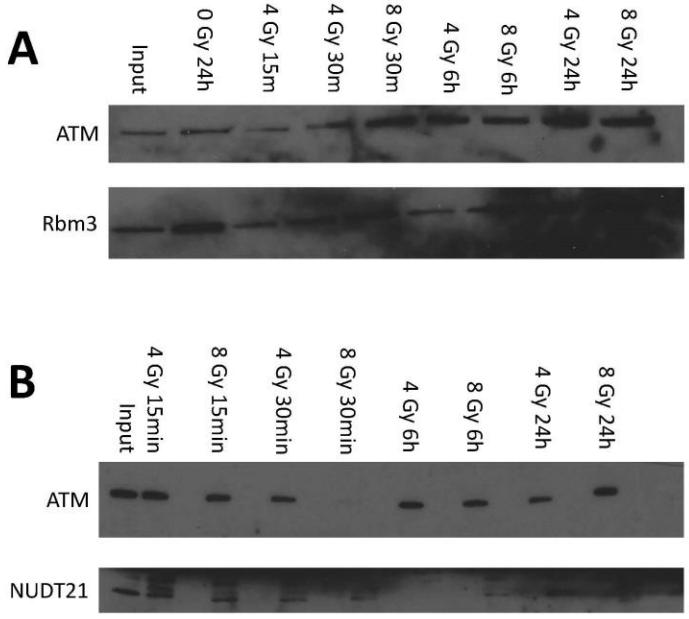

Figure 3.1- Immunoprecipitations pulling down ATM, which is required for activation of unphosphorylated miR-34. A) Immunoprecipitation of ATM and Western blots for both ATM and Rbm3, which was significantly isolated in the mass spectrometry dataset. Cells were treated with a single 4 Gy or 8 Gy dose. Lysates were mixed with Protein G Agarose beads conjugated with anti-ATM antibody. B) Immunoprecipitation as above and Western blotting for ATM and NUDT21.

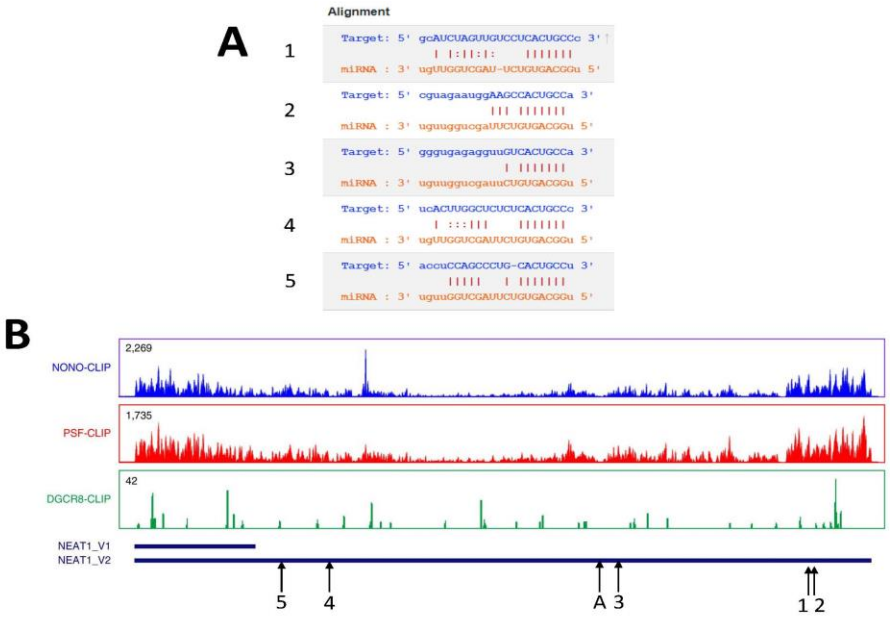

Figure 3.2- miRanda CLIP for miR-34 binding sites along the sequence of NEAT1_2. A) Sequence of predicted miR-34 binding sites along NEAT1_2. B) Location of the above miR-34 binding sites along the sequence of NEAT1_2, paired with CLIP for key proteins generated by Jiang and colleagues[29]. Binding site A was determined by Ji and colleagues[27].

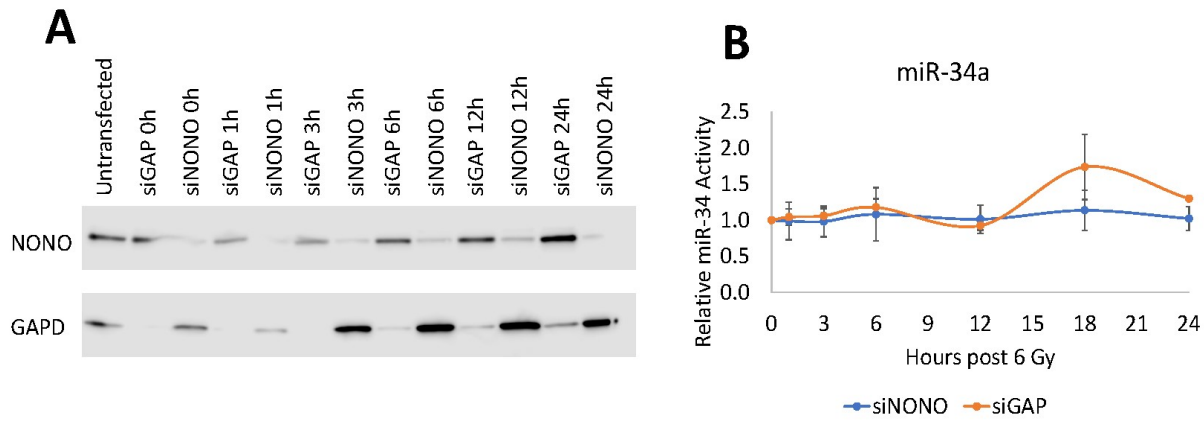

Figure 3.3- siRNA-mediated knockdown of NONO and its effects on unphosphorylated miR-34a. A) Western blots of lysates drawn from siRNA-treated cells. Cells were transfected with 25nM siRNA for 24h before treatment with a single 6 Gy dose. Lysates were drawn at the indicated time points after IR. B) Luciferase assay for miR-34a activity of siNONO and control transfected cells. Error bars represent standard error of the mean of three repeats.

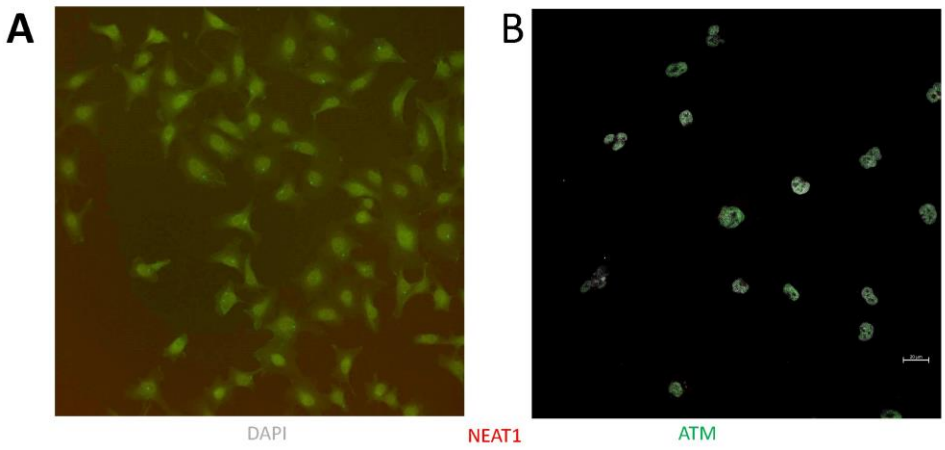

Figure 3.4- Paired immunofluorescence for ATM and *in situ* hybridization for a sequence in the middle of NEAT1_2 A) before and B) 1h after a single 6 Gy dose.

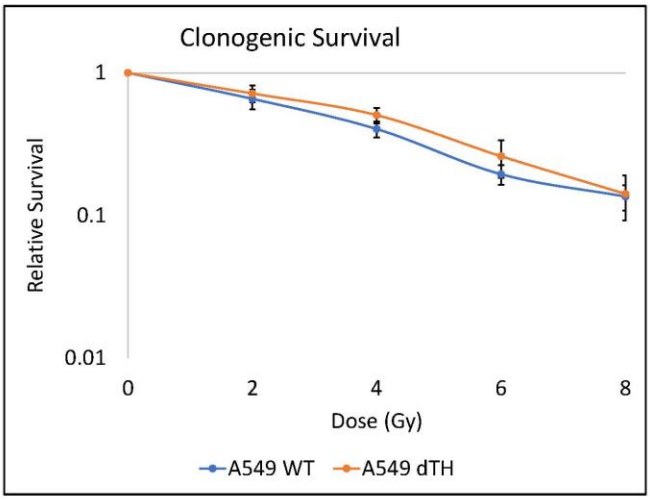

Figure 3.5- Clonogenic survival of irradiated wildtyle and dTH A549 cells. Plates were irradiated at the indicated doses and plated at known quantities in triplicate 24h later. Cells were fixed and stained with crystal violet 14 days later, and colonies of more than 50 cells were counted. Relative survival is calculated as a percentage of absolute survival at 0 Gy. Data points indicate average relative survival across three replicates. Error bars represent standard error of the mean.

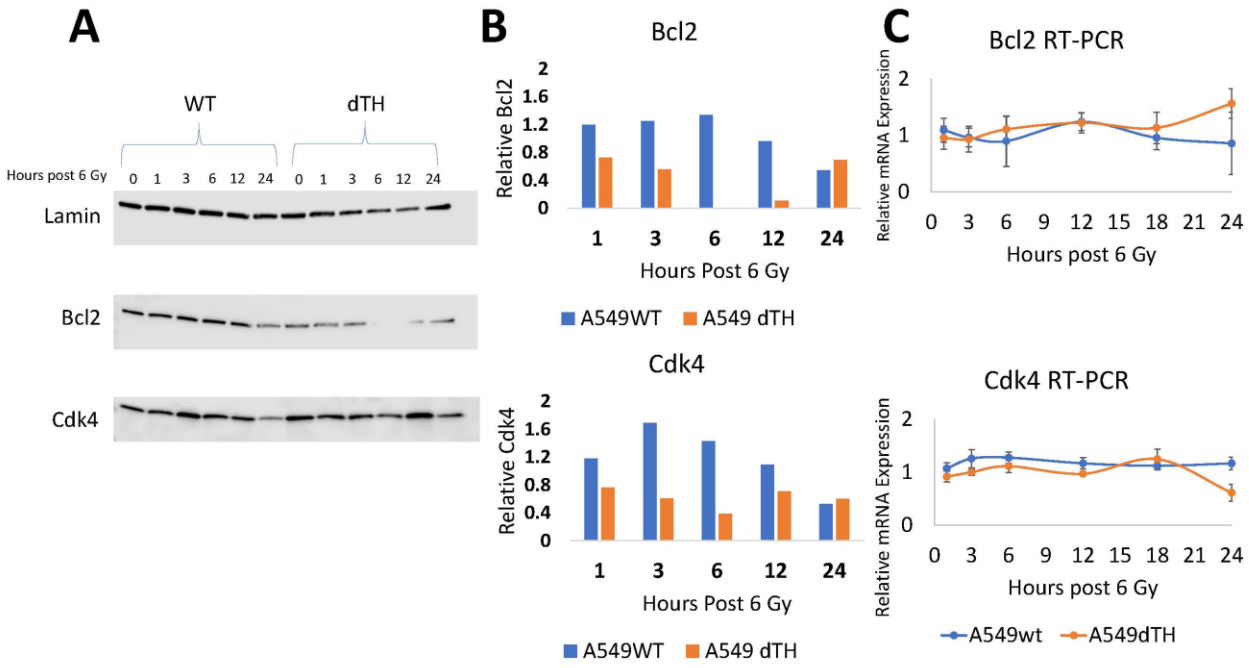

Figure 3.6- Differential expression of miR-34 target genes in wildtype and dTH cells. A) Western blot for the miRNA target proteins Bcl2 and Cdk4 over time after a single 6 Gy dose. B) Quantification of the Western blot shown in Panel A. C) Quantitative real-time PCR for Bcl2 and Cdk4. Error bars represent standard error of the mean of three biological repeats, each consisting of three technical repeats.

References

1. Zamudio, J.R., T.J. Kelly, and P.A. Sharp, *Argonaute-bound small RNAs from promoter-proximal RNA polymerase II.* Cell, 2014. **156**(5): p. 920-934.
2. Han, J. and J.T. Mendell, *MicroRNA turnover: a tale of tailing, trimming, and targets.* Trends in Biochemical Sciences, 2023. **48**(1): p. 26-39.
3. Han, J., et al., *A ubiquitin ligase mediates target-directed microRNA decay independently of tailing and trimming.* Science, 2020. **370**(6523).
4. Elkayam, E., et al., *The Structure of Human Argonaute-2 in Complex with miR-20a.* Cell, 2012. **150**(1): p. 100-110.
5. Salzman, D.W., et al., *miR-34 activity is modulated through 5'-end phosphorylation in response to DNA damage.* Nat Commun, 2016. **7**: p. 10954.
6. Imig, J., et al., *miR-CLIP capture of a miRNA targetome uncovers a lincRNA H19–miR-106a interaction.* Nature Chemical Biology, 2015. **11**(2): p. 107-114.
7. Phatak, P. and J.M. Donahue, *Biotinylated Micro-RNA Pull Down Assay for Identifying miRNA Targets.* Bio-protocol, 2017. **7**(9): p. e2253.
8. Cardinale, S., et al., *Subnuclear localization and dynamics of the Pre-mRNA 3' end processing factor mammalian cleavage factor I 68-kDa subunit.* Mol Biol Cell, 2007. **18**(4): p. 1282-92.
9. Zhang, Y., et al., *Structural Insights into the Human Pre-mRNA 3'-End Processing Machinery.* Mol Cell, 2020. **77**(4): p. 800-809.e6.
10. Brumbaugh, J., et al., *Nudt21 Controls Cell Fate by Connecting Alternative Polyadenylation to Chromatin Signaling.* Cell, 2018. **172**(1-2): p. 106-120.e21.
11. de Vries, H., et al., *Human pre-mRNA cleavage factor II(m) contains homologs of yeast proteins and bridges two other cleavage factors.* Embo j, 2000. **19**(21): p. 5895-904.

12. Okamura, K., et al., *The mirtron pathway generates microRNA-class regulatory RNAs in Drosophila.* Cell, 2007. **130**(1): p. 89-100.

13. Yang, Q., G.M. Gilmartin, and S. Doublié, *The structure of human cleavage factor I(m) hints at functions beyond UGUA-specific RNA binding: a role in alternative polyadenylation and a potential link to 5' capping and splicing.* RNA Biol, 2011. **8**(5): p. 748-53.

14. Fox, A.H., et al., *Paraspeckles: a novel nuclear domain.* Curr Biol, 2002. **12**(1): p. 13-25.

15. Naganuma, T., et al., *Alternative 3'-end processing of long noncoding RNA initiates construction of nuclear paraspeckles.* The EMBO journal, 2012. **31**(20): p. 4020-4034.

16. Yap, K., T.H. Chung, and E.V. Makeyev, *Hybridization-proximity labeling reveals spatially ordered interactions of nuclear RNA compartments.* Mol Cell, 2022. **82**(2): p. 463-478.e11.

17. Ma, R., et al., *RNA binding motif protein 3 (RBM3) drives radioresistance in nasopharyngeal carcinoma by reducing apoptosis via the PI3K/AKT/Bcl-2 signaling pathway.* Am J Transl Res, 2018. **10**(12): p. 4130-4140.

18. Ma, R., et al., *Inhibition of cell proliferation and radioresistance by miR-383-5p through targeting RNA binding protein motif (RBM3) in nasopharyngeal carcinoma.* Ann Transl Med, 2021. **9**(2): p. 123.

19. Pilotte, J., E.E. Dupont-Versteegden, and P.W. Vanderklish, *Widespread regulation of miRNA biogenesis at the Dicer step by the cold-inducible RNA-binding protein, RBM3.* PLoS One, 2011. **6**(12): p. e28446.

20. Bronisz, A., et al., *The nuclear DICER-circular RNA complex drives the deregulation of the glioblastoma cell microRNAome.* Sci Adv, 2020. **6**(51).

21. Dresios, J., et al., *Cold stress-induced protein Rbm3 binds 60S ribosomal subunits, alters microRNA levels, and enhances global protein synthesis.* Proc Natl Acad Sci U S A, 2005. **102**(6): p. 1865-70.

22. Ehlen, A., et al., *Expression of the RNA-binding protein RBM3 is associated with a favourable prognosis and cisplatin sensitivity in epithelial ovarian cancer.* J Transl Med, 2010. **8**: p. 78.

23. Wilusz, J.E., et al., *A triple helix stabilizes the 3' ends of long noncoding RNAs that lack poly(A) tails.* Genes Dev, 2012. **26**(21): p. 2392-407.

24. Ding, F., et al., *NEAT1/miR-23a-3p/KLF3: a novel regulatory axis in melanoma cancer progression.* Cancer Cell Int, 2019. **19**: p. 217.

25. Shao, T., et al., *The long noncoding RNA HOTAIR serves as a microRNA-34a-5p sponge to reduce nucleus pulposus cell apoptosis via a NOTCH1-mediated mechanism.* Gene, 2019. **715**: p. 144029.

26. Zhang, J., et al., *Identifying miRNA sponge modules using biclustering and regulatory scores.* BMC Bioinformatics, 2017. **18**(3): p. 44.

27. Ji, Y., et al., *The Long Noncoding RNA NEAT1 Targets miR-34a-5p and Drives Nasopharyngeal Carcinoma Progression via Wnt/β-Catenin Signaling.* Yonsei medical journal, 2019. **60**(4): p. 336-345.

28. Enright, A.J., et al., *MicroRNA targets in Drosophila.* Genome Biology, 2003. **5**(1): p. R1.

29. Jiang, L., et al., *NEAT1 scaffolds RNA-binding proteins and the Microprocessor to globally enhance pri-miRNA processing.* Nature structural & molecular biology, 2017. **24**(10): p. 816-824.

30. An, H., et al., *A toolkit for the identification of NEAT1_2/paraspeckle modulators.* Nucleic Acids Res, 2022. **50**(20): p. e119.

31. Mittag, T. and R.V. Pappu, *A conceptual framework for understanding phase separation and addressing open questions and challenges.* Molecular Cell, 2022. **82**(12): p. 2201-2214.

32. Düster, R., et al., *1,6-Hexanediol, commonly used to dissolve liquid–liquid phase separated condensates, directly impairs kinase and phosphatase activities.* Journal of Biological Chemistry, 2021. **296**.

33. Yamazaki, T., et al., *Functional Domains of NEAT1 Architectural lncRNA Induce Paraspeckle Assembly through Phase Separation.* Mol Cell, 2018. **70**(6): p. 1038-1053.e7.

34. John, H.A., M.L. Birnstiel, and K.W. Jones, *RNA-DNA hybrids at the cytological level.* Nature, 1969. **223**(5206): p. 582-7.

35. Shakoori, A.R., *Fluorescence In Situ Hybridization (FISH) and Its Applications*. Chromosome Structure and Aberrations. 2017 Feb 10:343-67. doi: 10.1007/978-81-322-3673-3_16.

36. Kasai, A., et al., *Double In situ Hybridization for MicroRNAs and mRNAs in Brain Tissues.* Front Mol Neurosci, 2016. **9**: p. 126.

37. Navin, N., et al., *PROBER: oligonucleotide FISH probe design software.* Bioinformatics, 2006. **22**(19): p. 2437-8.

38. Liu, G. and T. Zhang, *Single Copy Oligonucleotide Fluorescence In Situ Hybridization Probe Design Platforms: Development, Application and Evaluation.* Int J Mol Sci, 2021. **22**(13).

39. Chaumeil, J., M. Micsinai, and J.A. Skok, *Combined immunofluorescence and DNA FISH on 3D-preserved interphase nuclei to study changes in 3D nuclear organization.* J Vis Exp, 2013(72): p. e50087.

40. Vautrot, V., et al., *Fluorescence In Situ Hybridization of Small Non-Coding RNAs.* Methods Mol Biol, 2021. **2300**: p. 73-85.

41. McHugh, C.A., et al., *The Xist lncRNA interacts directly with SHARP to silence transcription through HDAC3.* Nature, 2015. **521**(7551): p. 232-6.

42. Saul, M.J., et al., *miR-574-5p as RNA decoy for CUGBP1 stimulates human lung tumor growth by mPGES-1 induction.* Faseb j, 2019. **33**(6): p. 6933-6947.

43. Li, R., et al., *Functional dissection of NEAT1 using genome editing reveals substantial localization of the NEAT1_1 isoform outside paraspeckles.* Rna, 2017. **23**(6): p. 872-881.

44. Canman, C.E., et al., *Activation of the ATM Kinase by Ionizing Radiation and Phosphorylation of p53.* Science, 1998. **281**(5383): p. 1677-1679.

45. Kochan, J.A., et al., *Meta-analysis of DNA double-strand break response kinetics.* Nucleic Acids Res, 2017. **45**(22): p. 12625-12637.

46. Shibata, A., et al., *Factors determining DNA double-strand break repair pathway choice in G2 phase.* Embo j, 2011. **30**(6): p. 1079-92.

47. Franken, N.A., et al., *Clonogenic assay of cells in vitro.* Nat Protoc, 2006. **1**(5): p. 2315-9.

48. Jo, G.H., et al., *Radiation-induced autophagy contributes to cell death and induces apoptosis partly in malignant glioma cells.* Cancer Res Treat, 2015. **47**(2): p. 221-41.

49. Baker, S.J., et al., *CDK4: a master regulator of the cell cycle and its role in cancer.* Genes Cancer, 2022. **13**: p. 21-45.

50. Hagen, K.R., et al., *Silencing CDK4 radiosensitizes breast cancer cells by promoting apoptosis.* Cell Div, 2013. **8**(1): p. 10.

51. Kato, M., et al., *The mir-34 microRNA is required for the DNA damage response in vivo in C. elegans and in vitro in human breast cancer cells.* Oncogene, 2009. **28**(25): p. 2419-24.

52. Li, W.J., et al., *MicroRNA-34a: Potent Tumor Suppressor, Cancer Stem Cell Inhibitor, and Potential Anticancer Therapeutic.* Front Cell Dev Biol, 2021. **9**: p. 640587.

53. Rio, D.C., et al., *Purification of RNA using TRIzol (TRI reagent).* Cold Spring Harb Protoc, 2010. **2010**(6): p. pdb.prot5439.

54. Andersen, J.S., et al., *Directed proteomic analysis of the human nucleolus.* Curr Biol, 2002. **12**(1): p. 1-11.

55. Fox, A.H., et al., *Paraspeckles: A Novel Nuclear Domain.* Current Biology, 2002. **12**(1): p. 13-25.

56. Sasaki, Y.T., et al., *MENepsilon/beta noncoding RNAs are essential for structural integrity of nuclear paraspeckles.* Proc Natl Acad Sci U S A, 2009. **106**(8): p. 2525-30.

57. Banani, S.F., et al., *Biomolecular condensates: organizers of cellular biochemistry.* Nat Rev Mol Cell Biol, 2017. **18**(5): p. 285-298.

58. Shin, Y. and C.P. Brangwynne, *Liquid phase condensation in cell physiology and disease.* Science, 2017. **357**(6357).

59. Stracker, T.H., T. Usui, and J.H. Petrini, *Taking the time to make important decisions: the checkpoint effector kinases Chk1 and Chk2 and the DNA damage response.* DNA Repair (Amst), 2009. **8**(9): p. 1047-54.

60. Darzynkiewicz, Z., *Redundancy in response to DNA damage: the key to protection of genome integrity.* Cell Cycle, 2011. **10**(20): p. 3425.

Conclusions:

Paraspeckles and Unphosphorylated miRNA

This work represents a critical early step in characterizing unphosphorylated miRNA pools- while previous work has demonstrated that unphosphorylated miR-34 exists and can be selectively phosphorylated in a radiation-dependent manner, further study of the characteristics, mechanisms, and utility of the unphosphorylated pool were limited by the inability to modulate the pool's activity. This work represents a significant advancement in this emergent field- demonstrating that nuclear paraspeckles are required for the early radiation-responsive activity of the unphosphorylated pool will allow new studies into the significance of unphosphorylated miR-34, as well as characterization of paraspeckle-dependent stress responses, the activity of other unphosphorylated miRNAs, and mechanisms involved in coordinating the above stress responses and synthesis of unphosphorylated miRNAs.

While significant attention has been paid to miR-34 in the context of both cancer and radiation biology [1-3], only a single paper has thus far demonstrated the activity of unphosphorylated miRNAs. That work showed that miR-34 is unique among currently-characterized miRNAs in that the activity of the miRNA increases prior to *de novo* transcription and processing after irradiation as a result of phosphorylation of an unphosphorylated, fully-processed reservoir of miR-34. That work additionally demonstrated that the activation of the unphosphorylated pool was connected to the cell's radiation response, as it was dependent on the master DNA damage kinase ATM *via* uncharacterized mechanisms. Even though this work demonstrated the existence of a novel form of miRNA regulation, the ability to study unphosphorylated miRNA more broadly was limited by the available tools- without knowledge of how the unphosphorylated pool was produced or maintained in the cell, it was difficult to design experiments with broader phenotypic or mechanistic consequences.

In this chapter, we will describe the immediate significance of this work, as well as the potential for new investigations into the regulation of unphosphorylated miRNAs that are newly available as a result of this work.

Paraspeckles regulate unphosphorylated miR-34

First, we performed mass spectrometry using biotinylated miRNA mimics to identify probable interacting partners of unphosphorylated miR-34. Briefly, sonicated whole-cell lysates were incubated with 3' biotinylated miR-34 with and without a 5' phosphate, as well as a 5'OH scrambled sequence and no-RNA controls(Figure 2.1A). Co-purified proteins were eluted and analyzed by ESI-FT-MS/MS, generating a list of proteins isolated under each condition. Analyzing proteins with known RNA binding capacity unique to the 5'OH miR-34 data set (Figure 2.1B) demonstrated a significant enrichment for nuclear paraspeckle proteins, leading to a hypothesis that paraspeckles were responsible for protecting endogenous 5'OH miR-34 by sequestering the miRNA away from cellular RNAses (Figure 2.1E). This result was also consistent with prior results- Salzman and colleagues performed RT-PCR on RNA drawn from different cellular compartments and argued that endogenous 5'OH miR-34 was nuclear, unlike phosphorylated miRNAs, which are typically cytoplasmic [4].

To test whether paraspeckles are responsible for maintaining unphosphorylated miR-34, we generated a Cas9-mediated deletion of the triple helix motif of the structural lncRNA NEAT1_2, resulting in loss of paraspeckle formation (Figure 2.2). Using this cell line, we demonstrated that cells lacking paraspeckles do not increase miR-34 activity immediately after

IR prior to *de novo* transcription, consistent with loss of the unphosphorylated pool(Figure 2.3). Similarly, we see that wildtype cells localize miR-34 into nuclear foci, which are abolished when paraspeckles are lost (Figure 2.4). Neither paraspeckle-dependent early activation nor nuclear localization were observed for other miRNAs known to lack an unphosphorylated pool, validating that the observed phenotypes were specific to unphosphorylated miR-34. Lastly, we observed that the number of nuclear miR-34 foci increased in both cell lines after IR, consistent with pri-miRNA formation connected to IR-dependent *de novo* transcription of miR-34(Figure 2.4C). These results demonstrate that nuclear paraspeckles are required for the activity and punctate nuclear localization of unphosphorylated miR-34, but may not be necessary for processing unphosphorylated miRNAs.

Future Directions

Implications for synthesis of unphosphorylated miRNAs

Unphosphorylated miR-34 is fully processed and localized to the nucleus- Northern blots show that it runs approximately 1 nucleotide heavier than 5'P miR-34, consistent with a charge difference imparted by the phosphate group[4]. While the lack of sequencing data from barcoded primers prevents broader statements on other modifications to the unphosphorylated pool, the pool has been shown to depend on activation of the nucleotide kinase Clp1 for its activation, which canonically phosphorylates the 5' ends of spliced transcripts [5, 6]. While we have not investigated the possibility of other modifications, the unphosphorylated pool appears to be the same length and degree of processing as Ago2-loaded 5'P miR-34- given the overall structural similarity, what mechanisms are responsible for synthesizing the unphosphorylated

pool as a distinct miRNA population? What cellular mechanisms are responsible for creating the unphosphorylated pool, and how is this pathway regulated?

While neither this work nor the existing literature offer direct mechanistic explanations for the synthesis of the unphosphorylated pool, observations here and in the wider literature can still offer reasonable hypotheses to guide future study of unphosphorylated miRNA synthesis. This section will review existing data on how canonical miRNA synthesis affects the unphosphorylated pool, paired with connections between the activity of miRNA processing enzymes and paraspeckle biology.

While 36h-long siRNA-mediated knockdown of DROSHA and Dicer do not abolish the activity of the unphosphorylated pool[4], it is difficult to conclude if this speaks to non-canonical processing of the unphosphorylated pool without knowledge of the half-life of either the pool itself or the paraspeckles responsible for its stability. Several known miRNAs are processed by mechanisms independent of the Microprocessor and Dicer [7, 8], though miR-34 has not been shown to share these mechanisms[9]. Our work does not demonstrate conclusively whether the unphosphorylated pool derives from pri-miRNAs processed at the surface of the paraspeckle-rates of pri- and pre-miRNA synthesis are roughly equal between wildtype and NEAT1_2 DTH cells, but it is difficult to conclude that this represents a difference in the unphosphorylated pool specifically without knowledge of how the unphosphorylated pool is made.

The localization of the unphosphorylated pool also poses a significant challenge to theories about its synthesis. Briefly, significant evidence has now demonstrated that the unphosphorylated pool is nuclear [4](Figure 2.4A). Canonical miRNA processing happens in

multiple compartments- the Microprocessor cleaves the pri-miR into a pre-miR in the nucleus, at which point is it exported by Xpo5 and further processed by cytoplasmic Dicer [10]. Given that the length of the unphosphorylated pool implies that it has already been cleaved by Dicer, canonical processing would assume both a distinct mechanism to remove the 5' phosphate and a mechanism to import the miRNA back into the nucleus.

A more parsimonious theory for the synthesis of the unphosphorylated pool could investigate the role of nuclear Dicer. While Dicer activity connected to miRNA synthesis is typically cytoplasmic, nuclear Dicer has been implicated in DNA damage responses[11] and processing of transcription start site miRNAs[8]. Notably, Dicer binds several coenzymes during its processing- in the nucleus, Dicer has been shown to associate with the adenine deaminase ADAR1[12], which is responsible for deaminating adenines into inosines [13]. Prior work has demonstrated that inosine-modified RNAs are sequestered by nuclear paraspeckles, and while our work did not investigate the presence of inosines in the unphosphorylated pool, broader screening projects have shown that miR-34 is deaminated at an adenine present in the mature sequence [13-15].

Given these observations, it is plausible that the unphosphorylated pool is processed by nuclear Dicer. Future studies investigating this mechanism could control the localization of Dicer by editing either the phosphorylation sites responsible for exposing its nuclear localization sequence (NLS) or editing the NLS itself[16]. Similar to the present study, we would expect cells with obligate cytoplasmic Dicer to maintain *de novo* transcription of miR-34, but lose both early activation and nuclear punctate localization of miR-34, consistent with specific loss of the unphosphorylated pool. Additionally, Dicer's nuclear association with ADAR enzymes[12]

presents an attractive mechanism for controlling paraspeckle loading- ISH probes that account for the hypothesized inosine modification or direct sequencing of nuclear miRNAs using a method sensitive to miRNA modifications could confirm if the unphosphorylated pool contains any modifications, which may lend extra credence to a synthesis mechanism involving nuclear Dicer and ADAR. Notably, this mechanism does not provide an explanation as to why the unphosphorylated pool lacks a terminal phosphate- given that the mass spectrometry data set did not recover known phosphatases, mechanistic studies of nuclear Dicer processing, with particular attention paid to the establishment of the 5' phosphate, could be productive.

miR-34 Localization Within Paraspeckles

Perhaps the largest limitation of the work presented in this study is its inability to show direct colocalization between miR-34 and paraspeckles. While this work demonstrates coordination between miR-34 and paraspeckle resident proteins and shows that paraspeckles are responsible for organizing punctate nuclear localization of miR-34, it is possible that paraspeckles are necessary for the synthesis of unphosphorylated miR-34 but do not physically contain the pool after synthesis.

Since tyramide amplification ISH of miR-34 does not appear amenable to co-imaging with other RNA ISH probes or immunofluorescent antibodies, we propose modification of the existing ISH protocol to incorporate electron microscopy-compatible gold moieties. Paraspeckles are more dense than the surrounding nucleoplasm, meaning they can be visualized within the interchromatin granule-associated zone without needing to stain for a marker protein or NEAT1[17]. The miR-34 ISH protocol in this work successfully binds DIG-conjugated LNA probes

to endogenous miR-34, and could be adapted to bind anti-DIG gold probes that can be visualized by electron microscopy[18].

This approach would not only allow for direct colocalization of miR-34 and nuclear paraspeckles, but would also provide important insights into how miR-34 is organized within the paraspeckle. Paraspeckles have distinct internal architecture, with different factors localizing specifically to the surface, core, or patches within the structure[19]- electron microscopy could show if miR-34 localizes to a specific region. Additionally, since the ISH approach detailed in this work offers resolution comparable to the size of the paraspeckle, we are currently unable to quantify how many copies of unphosphorylated miR-34 are maintained by a single paraspeckle- electron microscopy would allow for direct quantification. We propose that electron microscopy using anti-DIG immunogold would be technically feasible, validate direct colocalization between miR-34 and nuclear paraspeckles, and would provide important detail regarding the organization of miR-34 within the paraspeckle.

Identification of Other Unphosphorylated miRNAs

While miR-34 is currently the only miRNA known to harbour an unphosphorylated pool, we hypothesize that this mechanism extends to other miRNA species as well. Unphosphorylated miR-34 was identified primarily by its activation faster than *de novo* transcription and processing- an approach that requires several paired experiments iterated over multiple time points. Given that paraspeckles are responsible for protecting unphosphorylated miR-34, modulation of paraspeckle formation can be leveraged to identify other unphosphorylated miRNAs.

The most plausible method to rapidly screen for other unphosphorylated species could use small RNA sequencing, taking special care to adapt methods sensitive to the status of the 5' phosphate. Typical small RNA sequencing methods use T4 ligases to append adapters to both termini of the small RNA pool- since ligation of 5' adapters requires a 5' phosphate, this method will not identify unphosphorylated miRNAs. A sequencing approach comparing a pool derived from 3' adapters versus a pool derived from both 3' and 5' adapter ligation [20] could identify miRNAs that are not amenable to 5' adapter ligation, rapidly creating a list of plausibly unphosphorylated miRNAs.

An alternative approach to identification of paraspeckle-associated miRNAs could involve purification of paraspeckles directly [21], which could then be followed by sequencing methods described above or RT-PCR with 3' hairpin primers. This approach offers the significant advantage over paraspeckle knockdowns in that paraspeckles are also responsible for processing a subset of miRNAs[22], which would be depleted in NEAT1 dTH conditions despite not containing unphosphorylated pools. Purifying paraspeckles directly avoids this issue by ensuring that the sequenced RNAs interact physically with the paraspeckle.

Paraspeckles as Coordinators of Stress Responses

Several studies have characterized paraspeckles in diverse stress responses, typically related to their ability to sequester factors implicated in that stress response [23-25]. Prior investigation of the unphosphorylated pool demonstrated that activation of 5'OH mIR-34 is dependent on the master DNA damage response kinase ATM, which may imply a mechanistic link between paraspeckles and ATM.

While our work attempted to colocalize ATM and paraspeckle marker proteins, this approach proved inviable, possibly because interactions between ATM and paraspeckles are transient. Notably, one canonical ATM target [26] is required for paraspeckle formation. Likewise, both ATM and paraspeckles change localization shortly after genotoxic challenges, implying that colocalization between ATM and paraspeckles is possible.

To account for how these interactions may be transient, we propose live-cell imaging in cells tagged with fluorescent ATM and paraspeckle marker proteins. Both of these systems already exist in the literature- while implementation of GFP-tagged SFPQ proved inviable in our A549s, tagging of other paraspeckle marker proteins may prove viable. These cells could then be transfected with YFP-tagged ATM to enable real-time imaging of both proteins after irradiation. This approach would provide several important insights- firstly, it would demonstrate physical interactions between paraspeckles and ATM, consistent with ATM-dependent activation of the unphosphorylated pool[4]. This approach would also allow for precise quantification of the timing of this mechanism. Lastly, activation of similar RNA-based phase separations often results in complete dissolution of the phase separation- a live-cell imaging approach could show if activation of the unphosphorylated pool derives from a reconfiguration of the paraspeckle or its dissolution.

Since we are only aware of a single ATM target protein localized to nuclear paraspeckles, we hypothesize that ATM acts on paraspeckles by phosphorylating FUS. ATM has been shown to target FUS at multiple residues[27]- selective mutation of these phosphorylation sites could help both validate that FUS is an ATM target in the paraspeckle and demonstrate that specific FUS phosphorylations are responsible for maintaining paraspeckle structure or stability,

consistent with other studies demonstrating FUS is necessary to maintain phase separations[28]. To that end, Cas9-mediated mutation of one or multiple FUS phosphorylation sites could provide important insights into interactions between ATM and paraspeckles, demonstrating paraspeckles as a site of broader DNA damage responses and giving insight into regulation within the paraspeckle.

Nuclear Paraspeckle-Dependent Protection of Unphosphorylated miR-34

This work represents an important mechanistic characterization of the behaviour and mechanisms governing unphosphorylated miR-34, opening significant avenues for new study. Importantly, while previous work had characterized the existence and radiation dependence of unphosphorylated miR-34[4], it did not demonstrate phenotypic consequences or extend the existence of unphosphorylated miRNAs to other species, largely due to an inability to specifically modulate the activity of unphosphorylated miRNAs before IR.

Here, we have demonstrated that the activity and punctate nuclear localization of unphosphorylated miR-34 is dependent on phase separation coordinated by nuclear paraspeckles, particularly the lncRNA NEAT1_2. By deleting a domain necessary for the stability of NEAT1_2, we were able to create isogenic lines lacking paraspeckle formation. This deletion was phenotypically mild at baseline- similar deletions are similarly mild in animal models[29]. Loss of paraspeckles reduces early radiation-responsive miR-34 activity, consistent with loss of unphosphorylated miR-34, without eliminating pri-miRNA transcription or preventing global miRNA processing. Additionally, paraspeckles were shown to coordinate punctate nuclear localization of miR-34, but not other miRNAs, by ISH.

Given the tolerability of paraspeckle deletions in both cell culture and animal models, future studies of unphosphorylated miRNAs could benefit significantly from the newfound ability to control the activation and localization of unphosphorylated miRNAs. Radiation-responsive miR-34 is the only miRNA currently known to harbour an unphosphorylated pool- future studies of paraspeckle-depleted cells could uncover broader pathways of miRNA regulation, including novel methods of processing and activation that could imply more robust and rapid miRNA-related translational repression than would be possible through canonical stress-responsive transcription and processing.

References

1. Hermeking, H., *The miR-34 family in cancer and apoptosis.* Cell Death Differ, 2010. **17**(2): p. 193-9.
2. Lacombe, J. and F. Zenhausern, *Emergence of miR-34a in radiation therapy.* Crit Rev Oncol Hematol, 2017. **109**: p. 69-78.
3. Li, W.J., et al., *MicroRNA-34a: Potent Tumor Suppressor, Cancer Stem Cell Inhibitor, and Potential Anticancer Therapeutic.* Front Cell Dev Biol, 2021. **9**: p. 640587.
4. Salzman, D.W., et al., *miR-34 activity is modulated through 5'-end phosphorylation in response to DNA damage.* Nat Commun, 2016. **7**: p. 10954.
5. Weitzer, S. and J. Martinez, *The human RNA kinase hClp1 is active on 3' transfer RNA exons and short interfering RNAs.* Nature, 2007. **447**(7141): p. 222-6.
6. de Vries, H., et al., *Human pre-mRNA cleavage factor II(m) contains homologs of yeast proteins and bridges two other cleavage factors.* Embo j, 2000. **19**(21): p. 5895-904.
7. Okamura, K., et al., *The mirtron pathway generates microRNA-class regulatory RNAs in Drosophila.* Cell, 2007. **130**(1): p. 89-100.
8. Zamudio, J.R., T.J. Kelly, and P.A. Sharp, *Argonaute-bound small RNAs from promoter-proximal RNA polymerase II.* Cell, 2014. **156**(5): p. 920-934.
9. Titov, II and P.S. Vorozheykin, *Comparing miRNA structure of mirtrons and non-mirtrons.* BMC Genomics, 2018. **19**(Suppl 3): p. 114.
10. Bartel, D.P., *MicroRNAs: genomics, biogenesis, mechanism, and function.* Cell, 2004. **116**(2): p. 281-97.
11. Burger, K., et al., *Nuclear phosphorylated Dicer processes double-stranded RNA in response to DNA damage.* The Journal of Cell Biology, 2017. **216**(8): p. 2373-2389.

12. Ota, H., et al., *ADAR1 forms a complex with Dicer to promote microRNA processing and RNA-induced gene silencing.* Cell, 2013. **153**(3): p. 575-89.

13. Paul, D., et al., *A-to-I editing in human miRNAs is enriched in seed sequence, influenced by sequence contexts and significantly hypoedited in glioblastoma multiforme.* Sci Rep, 2017. **7**(1): p. 2466.

14. Hirose, T., et al., *NEAT1 long noncoding RNA regulates transcription via protein sequestration within subnuclear bodies.* Molecular Biology of the Cell, 2013. **25**(1): p. 169-183.

15. Marceca, G.P., et al., *MiREDiBase, a manually curated database of validated and putative editing events in microRNAs.* Scientific Data, 2021. **8**(1): p. 199.

16. Bronisz, A., et al., *The nuclear DICER-circular RNA complex drives the deregulation of the glioblastoma cell microRNAome.* Sci Adv, 2020. **6**(51).

17. Souquere, S., et al., *Highly ordered spatial organization of the structural long noncoding NEAT1 RNAs within paraspeckle nuclear bodies.* Mol Biol Cell, 2010. **21**(22): p. 4020-7.

18. Morioka, H., et al., *Co-localization of HSV-1 DNA and ICP35 protein by in situ hybridization and immunocytochemistry.* J Electron Microsc (Tokyo), 1999. **48**(5): p. 621-8.

19. Naganuma, T. and T. Hirose, *Paraspeckle formation during the biogenesis of long non-coding RNAs.* RNA Biol, 2013. **10**(3): p. 456-61.

20. Hafner, M., et al., *Identification of microRNAs and other small regulatory RNAs using cDNA library sequencing.* Methods, 2008. **44**(1): p. 3-12.

21. Wang, Y.-L., et al., *DNA damage-induced paraspeckle formation enhances DNA repair and tumor radioresistance by recruiting ribosomal protein P0.* Cell Death & Disease, 2022. **13**(8): p. 709.

22. Jiang, L., et al., *NEAT1 scaffolds RNA-binding proteins and the Microprocessor to globally enhance pri-miRNA processing.* Nature structural & molecular biology, 2017. **24**(10): p. 816-824.

23. Choudhry, H., et al., *Tumor hypoxia induces nuclear paraspeckle formation through HIF-2alpha dependent transcriptional activation of NEAT1 leading to cancer cell survival.* Oncogene, 2015. **34**(34): p. 4482-90.

24. Imamura, K., et al., *Long noncoding RNA NEAT1-dependent SFPQ relocation from promoter region to paraspeckle mediates IL8 expression upon immune stimuli.* Mol Cell, 2014. **53**(3): p. 393-406.

25. Adriaens, C., et al., *p53 induces formation of NEAT1 lncRNA-containing paraspeckles that modulate replication stress response and chemosensitivity.* Nat Med, 2016. **22**(8): p. 861-8.

26. Ji, Y., et al., *The Long Noncoding RNA NEAT1 Targets miR-34a-5p and Drives Nasopharyngeal Carcinoma Progression via Wnt/β-Catenin Signaling.* Yonsei medical journal, 2019. **60**(4): p. 336-345.

27. Gardiner, M., et al., *Identification and characterization of FUS/TLS as a new target of ATM.* Biochemical Journal, 2008. **415**(2): p. 297-307.

28. Carey, J.L. and L. Guo, *Liquid-Liquid Phase Separation of TDP-43 and FUS in Physiology and Pathology of Neurodegenerative Diseases.* Front Mol Biosci, 2022. **9**: p. 826719.

29. Nakagawa, S., et al., *Paraspeckles are subpopulation-specific nuclear bodies that are not essential in mice.* The Journal of cell biology, 2011. **193**(1): p. 31-39.